

2009

Carmel Bay : oceanographic dynamics and nutrient transport in a small embayment of the central California coast

Dustin Carroll
California State University, Monterey Bay

Follow this and additional works at: https://digitalcommons.csumb.edu/caps_thes

Recommended Citation

Carroll, Dustin, "Carmel Bay : oceanographic dynamics and nutrient transport in a small embayment of the central California coast" (2009). *Capstone Projects and Master's Theses*. 69.
https://digitalcommons.csumb.edu/caps_thes/69

This Master's Thesis is brought to you for free and open access by Digital Commons @ CSUMB. It has been accepted for inclusion in Capstone Projects and Master's Theses by an authorized administrator of Digital Commons @ CSUMB. Unless otherwise indicated, this project was conducted as practicum not subject to IRB review but conducted in keeping with applicable regulatory guidance for training purposes. For more information, please contact digitalcommons@csumb.edu.

**CARMEL BAY: OCEANOGRAPHIC DYNAMICS AND
NUTRIENT TRANSPORT IN A SMALL EMBAYMENT OF
THE CENTRAL CALIFORNIA COAST.**

A Thesis Presented to
The Faculty of Moss Landing Marine Laboratories
California State University Monterey Bay

In Partial Fulfillment
of the Requirements for the Degree
Master of Science

by
Dustin Carroll
March 2009

© 2009

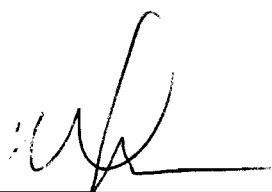
Dustin Carroll

ALL RIGHTS RESERVED

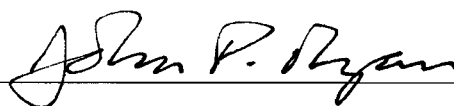
APPROVED FOR MOSS LANDING MARINE LABORATORIES



Dr. Erika McPhee-Shaw, Assistant Professor



Dr. Michael H. Graham, Associate Professor



Dr. John Ryan, Monterey Bay Aquarium Research Institute

ABSTRACT

CARMEL BAY: OCEANOGRAPHIC DYNAMICS AND NUTRIENT TRANSPORT IN A SMALL EMBAYMENT OF THE CENTRAL CALIFORNIA COAST.

By Dustin Carroll

Using an extensive mooring time series from the outer edge of Stillwater Cove, this study investigated the oceanographic dynamics and their contribution to nutrient delivery in Carmel Bay. Carmel Bay is small embayment located at the northern end of the Big Sur coast, and it is distinguished by having a submarine canyon within extremely close proximity to the beach. This embayment is open to open ocean coastal California Current conditions; however, it also provides a sheltered environment from wind and swell. No previous studies have been conducted on the circulation features of Carmel Bay and Stillwater Cove, and HF radar coverage does not extend into Carmel Bay. Point source mooring time series measurements were used to explain in great detail the temporal variability of hydrographic conditions and nutrient delivery to Stillwater Cove and Carmel Bay. A model was developed to estimate the annual nutrient delivery budget in Stillwater Cove due to internal waves, upwelling, and terrestrial sources. Consistent internal waves were observed in Stillwater Cove during stratified conditions, and vertical velocities due to internal tidal pumping in Carmel Canyon were 15 m/hr. The spatial variability of the internal tide at locations spanning the greater Monterey Bay was also examined. Locations within close proximity to submarine canyons had an additional source of nutrients via internal waves, while locations on the shelf lacked this mechanism and had to rely on upwelling alone.

ACKNOWLEDGEMENTS

I would like to thank my thesis committee members Dr. Erika McPhee-Shaw, Dr. Michael H. Graham, and Dr. John Ryan for their continuous support and expertise on this project. Sara Tanner and Craig Hunter provided invaluable support, instructing me on the analysis techniques for measuring phosphate and nitrate. I would also like to thank Luke Beatman for helping me with operating instrumentation during the cruises and processing the data. My sincere thanks also go to the crew of the R/V John H. Martin and R/V Sheila B for their expertise and patience during the cruises. Finally, I am indebted to the faculty and staff of Moss Landing Marine Laboratories, in particular Joan Parker and the IT ground.

TABLE OF CONTENTS

LIST OF TABLES.....	VII
LIST OF FIGURES.....	VIII
1. INTRODUCTION	1
<i>1.1 Carmel Bay</i>	<i>1</i>
<i>1.2 Background and Theory.....</i>	<i>7</i>
<i>1.3 Objectives</i>	<i>10</i>
2. OBSERVATIONS	11
<i>2.1 Stillwater Cove Study Site.....</i>	<i>11</i>
<i>2.2 Moored Physical Oceanographic Observations.....</i>	<i>13</i>
<i>2.3 Hydrographic Observations.....</i>	<i>16</i>
<i>2.4 Meteorological Data</i>	<i>18</i>
<i>2.5 Watershed Data.....</i>	<i>18</i>
<i>2.6 Summary of Data Collection</i>	<i>21</i>
<i>2.7 Spectral Analysis.....</i>	<i>23</i>
<i>2.8 Temperature Nitrate Relationships</i>	<i>24</i>
3. RESULTS	26
<i>3.1 Seasonal Description of Carmel Bay</i>	<i>26</i>
<i>3.2 Spectral Analysis.....</i>	<i>37</i>
<i>3.3 High Frequency Variability</i>	<i>39</i>
<i>3.4 Deep Response to Tides: Internal Waves between 0 and 100 m</i>	<i>41</i>
<i>3.5 Monterey Bay Spectral Results - Along Coast Distribution</i>	<i>46</i>
<i>3.6 Stillwater Cove Nutrient Model.....</i>	<i>61</i>
<i>3.6 Greater Monterey Bay Nutrient Model and Budget</i>	<i>68</i>
4. DISCUSSION	80
4.1 Preamble	80
<i>4.1.1 Stillwater Cove Annual Nutrient Budget</i>	<i>83</i>
<i>4.1.2 Seasonal Currents</i>	<i>86</i>
<i>4.1.3 Tidal Currents</i>	<i>90</i>
<i>4.1.4 Synoptic Winter Mixing Events.....</i>	<i>97</i>
<i>4.1.5 Carmel Bay Upwelling.....</i>	<i>102</i>
4.2 Internal Tide in Carmel Bay	106
<i>4.2.1 Horizontal Advection.....</i>	<i>106</i>

4.2.2 Vertical Advection	111
4.2.3 Spatial Variability of the Internal Tide in Monterey Bay	115
4.3 Tidal Flushing and Stagnation in Stillwater Cove	122
4.4 Implications for Cross-Shelf Nutrient Transport in Monterey Bay.....	130
5. REFERENCES	134

LIST OF TABLES

1. Summary of terrestrial samples	62
2. Total estimated NO ₃ values	79
3. Total estimated NO ₃ contribution percentages	79
4. Stillwater Cove annual nutrient contributions	85

LIST OF FIGURES

1. Carmel Canyon System.....	1
2. Map of Stillwater Cove, California.....	13
3. PISCO and MLML mooring locations.....	15
4. Stillwater Cove terrestrial runoff locations.....	19
5. Date ranges of data collection.....	22
6. Carmel Bay bathymetry and rotated coordinate system.....	23
7. Temperature nitrate relationships for Monterey Bay.....	25
8. Year-long daily averaged temperature from Stillwater Cove and Monterey Bay.....	26
9. Temperature steps during upwelling relaxation.....	27
10. Upwelling events in the Stillwater Cove water column during July 2006.....	28
11. Distinct upwelling events in the Stillwater Cove column during September 2006.....	29
12. Upwelling events in the Stillwater Cove water column during October 2006.....	30
13. Winter conditions and storm events in Stillwater Cove.....	31
14. Average Stillwater Cove currents during summer.....	32
15. Average Stillwater Cove currents during winter	33
16. Average Stillwater Cove currents during spring	34
17. Progressive vector diagram of currents in Stillwater Cove.....	36
18. Spectral analysis of Stillwater Cove near-surface and bottom temperatures.....	37
19. Coherence of Stillwater Cove bottom temperatures and Monterey Bay tidal height.....	38
20. Internal waves in Stillwater Cove during two weeks of summer.....	40
21. Internal waves in Stillwater Cove during two weeks of summer (2).....	40
22. Repeated CTD casts in Carmel Bay on October 31st 2007.....	42
23. Internal waves in Stillwater Cove on October 31st 2007.....	43
24. Currents in Stillwater Cove during June 2006 (pseudocolor plot).....	45
25. Currents in Stillwater Cove during June 2006.....	45
26. Monterey Canyon head spectral results	47
27. Carmel Bay spectral results.....	48
28. Inner Monterey Shelf spectral results.....	50
29. Greater Monterey Bay spectral results.....	51
30. Monterey Canyon coherence results.....	53
31. Carmel Bay coherence results.....	54
32. Inner Monterey Shelf coherence results.....	56
33. Greater Monterey Bay coherence results.....	58
34. Diurnal power spectral density.....	59

35. Semi-diurnal power spectral density.....	60
36. MLML Weather Station rainfall 2007.....	63
37. Stillwater Cove summer nitrate model.....	65
38. Stillwater Cove winter nitrate model.....	66
39. Stillwater Cove estimated NO ₃ contributions from terrestrial runoff.....	67
40. MLML Seawater System nitrate model.....	69
41. Weston Beach nitrate model.....	70
42. Sunset Point nitrate model.....	71
43. Point Joe nitrate model.....	72
44. Lovers' Point nitrate model.....	73
45. Soquel Point nitrate model.....	74
46. Point Sur nitrate model.....	75
47. Wind band estimated NO ₃ budget.....	76
48. Diurnal tidal band estimated NO ₃ budget	77
49. Semi-diurnal tidal band estimated NO ₃ budget	78
50. Total estimated NO ₃ budget	78
51. Bottom depth sub-tidal and tidal progressive vector diagram.....	87
52. Tidal and sub-tidal daily path length.....	88
53. Bottom currents during the rising diurnal tide.....	91
54. Current direction during rising diurnal tide.....	92
55. Bottom currents during the falling diurnal tide.....	92
56. Current direction during falling diurnal tide.....	93
57. Mean currents 1 hour before peak diurnal high tide.....	95
58. Mean currents 1 hour after peak diurnal high tide.....	96
59. Winter mixing and warming events.....	100
60. Winter mixing and warming events.....	100
61. Monterey Bay SST during November 9th, 12th, 13th, and 15th 2007... ..	101
62. Carmel and Monterey Bay surface temperatures during upwelling and upwelling relaxation.....	104
63. Monterey Bay SST during July 2006. Contour lines are 1°C temperature intervals.....	105
64. Carmel Bay SST from August 8th 2008.....	109
65. Eight day composite SST for the week of August 1st 2008.....	110
66. Carmel Canyon CTD, May 18th 2006.....	111
67. Horizontal velocity component during the rising semi-diurnal tide.....	114
68. Diurnal phase between bottom temperature and Monterey Bay tidal height.....	119
69. Semi-diurnal phase between bottom temperature and Monterey Bay tidal height.....	119

70. Diurnal time lag between bottom temperature and Monterey Bay tidal height.....	120
71. Semi-diurnal time lag between bottom temperature and Monterey Bay tidal height.....	120
72. Mooring distance from the 500-m isobath.....	121
73. Stagnation scenario.....	124
74. Non-stagnation scenario.....	125
75. Stillwater Cove seasonal tidal excursion distances.....	126
76. Stillwater Cove seasonal sub-tidal excursion distances.....	127
77. Elapsed time before significant mixing would occur.....	129
78. Spatially interpolated estimated NO ₃ budget for the greater Monterey Bay.....	133

1.1 Carmel Bay

Carmel Bay is a small embayment located on the central coast of California. The mouth of the bay faces directly westward and is exposed to open ocean coastal California Current conditions; however, it is also possibly influenced by smaller scale topographic effects such as wind and wave sheltering (Figure 1). Carmel Bay also has a unique bathymetric gradient, as the Carmel Submarine Canyon is located within close proximity to the near-shore environment within the bay. At the south end of Carmel Bay, the 100-m isobath is located ~ 500 m from shore. Stillwater Cove is a small semi-enclosed basin located directly inside of Carmel Bay.

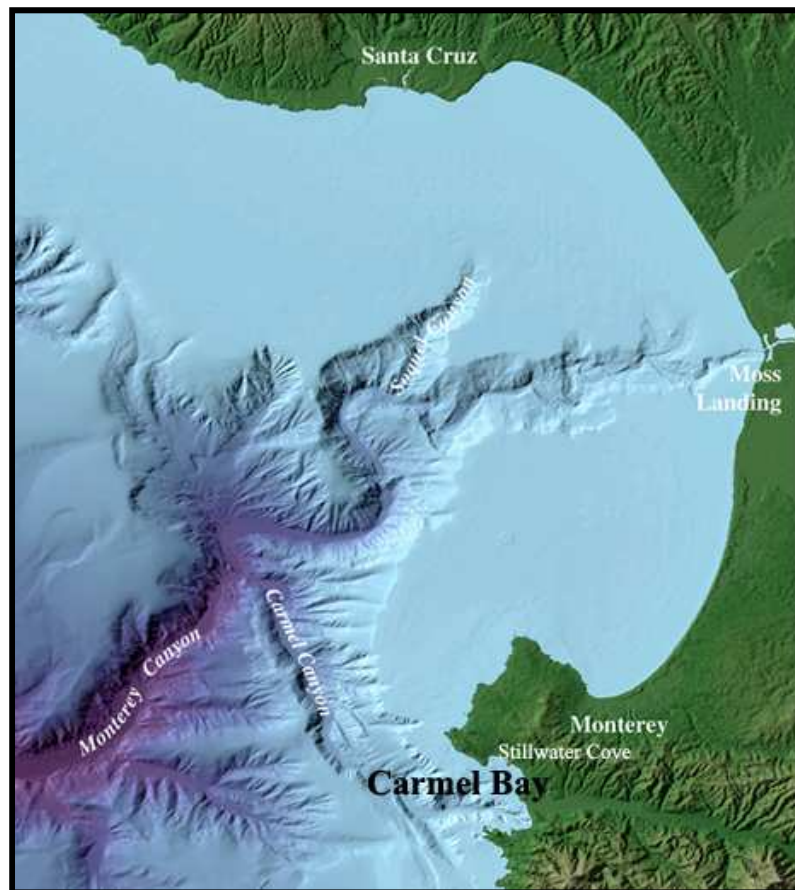


Figure 1: Monterey Bay and Canyon System, MBARI Image.

The coastal waters surrounding this region are frequently exposed to strong winds and large winter swells. Several large harbors along the coast provide shelter for watercraft; however, Stillwater Cove is one of the few non-manmade shelters along central California where mooring a boat is possible. Stillwater Cove also provides a habitat for a large Giant kelp population. The *Macrocystis pyrifera* canopy inside of Stillwater Cove exhibits unique temporal dynamics and has been found to have annually peaked and declined earlier than other nearby areas of central California, including nearby Carmel Point (Donnellan, 2004).

Stillwater Cove lies directly adjacent to the Pebble Beach golf course and housing community, which supplies a significant source of pollution and nutrients directly into the nearby cove via multiple terrestrial sources. In 2003-2004, Stillwater Cove and the Pebble Beach Tennis Club beach had the 6th worst dry-weather bacterial water quality of all sampled California beaches (Heal the Bay, 2004). From 1995 to 2002, the mean NO₃ concentrations in Pebble Beach watersheds ranged from 2.1 to 13.2 mg/l, with Stillwater Cove being the location of highest mean detection (Pebble Beach Company, 2004). This data suggests that terrestrial runoff from the Pebble Beach golf courses and residential development may be strongly contributing to nutrient loading in Stillwater Cove; however, Stillwater Cove has a tiny spatial scale compared to the California coast, and coastal oceanographic variability scales are likely much larger than the cove. The southward facing mouth of the cove is approximately 1 km wide, while the vertical length of the cove ranges from 400 to 700 m. Little is known about oceanographic variability on 1 km scales or coast wide along-coast variability in onshore transport of nutrients. No previous studies have been conducted on the circulation features of Carmel

Bay and Stillwater Cove. Monterey Bay has been the site of High-frequency (HF) radar measurements for a number of years, yet coverage does not extend into Carmel Bay. It is still not known how Stillwater Cove's behavior mimics the oceanographic dynamics of the Monterey Bay. Specifically, are there oceanographic similarities or does Carmel Bay have distinct oceanographic features?

In the coastal environment, nutrient exposure is a key factor in the growth of kelp and primary production. The transport of nutrients to shallow areas (< 20 m) is essential for the health of *M. pyrifera* (Jackson, 1977, Wheeler and North, 1980), with nitrate being the limiting nutrient in kelp growth (Jackson, 1977, Zimmerman and Kramer, 1984, Fram *et al.*, 2008). Onshore transport of deep water provides vital nutrients to the coastal ecosystem; however, little research has quantified the spatial variability of cross shelf nutrient transport to the near-shore ecosystem along the California coast and many questions still remain unanswered. What is the spatial variability of the nutrient field along the California Coast? How does the nutrient field vary across bathymetric gradients? How do the oceanographic dynamics that contribute to cross-shelf transport vary spatially and temporally?

Understanding nutrient exchange across the inner shelf is difficult because continental shelf dynamics (alongshelf currents and associated Ekman transport, fronts, internal waves, sub-mesoscale eddies, coastal trapped waves), near-shore dynamics (breaking surface waves and alongshore drift), and terrestrial runoff are all potentially important processes (McPhee-Shaw *et al.*, 2007). Due to the multitude of oceanographic dynamics that may contribute to cross-shelf transport, it is vital to construct a method that can isolate specific cross-shelf dynamics, and quantify their contribution to near-shore

nutrient delivery. Identifying and quantifying these cross-shelf transport mechanisms is essential to understanding near-shore ecosystems which heavily rely on deeper, offshore water for input of nutrients, larvae, and biogenic particles (Bassin *et al.*, 2005). This project sought to use the framework provided in Largier *et al.* (1993) to separate oceanographic dynamics into separate frequency bands. Largier *et al.* (1993) examined subtidal circulation over the Northern California shelf, and separated their respective time series into four distinct frequency bands: the tidal band (< 24 hrs), the wind band (days to weeks), the mesoscale band (weeks to months), and the annual band (year). Bassin *et al.* (2005) suggested that sub-mesoscale eddies are an important transport mechanism for nutrients and biogenic particles in Southern California within the wind and mesoscale frequency band. McPhee-Shaw *et al.* (2007) followed the approach in Largier *et al.* (1993) and investigated cross-shelf transport of nutrients to the kelp forests of the Santa Barbara Channel within the synoptic (2 to 10 days) and diurnal frequency bands (< 24 hrs). This study provided a first-order budget for the nutrient exposure to the inner-shelf kelp forests in the Santa Barbara region. Their study assessed that the primary method of nutrient delivery for the Santa Barbara inner-shelf was spring and summer upwelling of cold sub-nutricline water and “synoptic-scale” upwelling events during fall and winter. Internal waves during stratified summer conditions and terrestrial input during winter runoff events were 4th contributor sources of nutrients.

For the scope of this project, I was interested in identifying cross-shelf nutrient delivery to the near-shore ecosystem from the oceanographic dynamics associated with a wind and tidal band described in Largier *et al.* (1993). We used the same approach as McPhee-Shaw *et al.* (2007) in a spatial region along the California coast that has not been

previously studied. Although studies examining cross-shelf transport have been conducted in southern and northern California, little is known about the spatial variability of the nutrient field along the California coast. Recently deployed *in-situ* instrumentation in Stillwater Cove by the Center for Integrative Coastal Observation, Research, and Education (CICORE), provided the opportunity to study nutrient delivery to the near-shore environment. This study was first motivated by attempting to identify and describe hydrographic conditions that lead to transport of oceanographic nutrients into the Stillwater Cove ecosystem. The near-shore physical environment is responsible for both long and short-term effects on the dynamics of the inner-shelf ecosystem. Understanding these oceanographic processes can provide a key insight to the factors that control ecosystem variability and drive the complex near-shore environment. Specifically this project focuses on understanding nutrient delivery to the *M. pyrifera* kelp population located inside the cove, whose dense strands provide habitats for numerous other species (Dayton, 1985).

Knowledge of the physical processes surrounding the kelp ecosystem is essential in order to accurately describe nutrient delivery, spore dispersal, and overall kelp population dynamics. The CICORE Stillwater Cove mooring provided a high resolution year-long time series of currents and vertical temperature profiles. This dataset allowed for the analysis and interpretation of the seasonal and intra-seasonal oceanographic variability of the cove and Carmel Bay. A thorough investigation of near-shore circulation, barotropic and baroclinic currents, upwelling, and internal waves was undertaken. Once the primary oceanographic dynamics and corresponding frequency bands were identified, this project sought to understand how both oceanographic and

terrestrial processes deliver nutrients into the unique Stillwater Cove ecosystem. This project compared oceanographic nutrient inputs to estimates of nutrient supply from terrestrial sources. The seasonal variability in both oceanographic and terrestrial nutrient sources was assessed. Using multiple sources of *in-situ* oceanographic and terrestrial data from Stillwater Cove, several questions were investigated: 1.) What are the general oceanographic dynamics of Stillwater Cove, and how do these processes contribute to nutrient delivery? 2.) How does terrestrial runoff from the Pebble Beach golf course and community contribute to nutrient loading in Stillwater Cove? 3.) How does the estimated oceanic nutrient delivery budget in Stillwater Cove compare with locations within the greater Monterey Bay and along the California Coast?

A major component of this study is also to understand the role of internal waves / tides in transporting nutrients to near-shore coastal ecosystems, specifically in shallow regions (< 20 m). Recently developed numerical models have suggested that the nearby Carmel Submarine Canyon may also be a strong location for internal tide generation (Jachec *et. al.*, 2006). Internal waves propagating directly from the Carmel Submarine Canyon or from further offshore may transport nutrient-rich water into Stillwater Cove during stratified summer conditions. Shea and Broenkow (1982) also demonstrated that the interaction of the internal tide with a submarine canyon can cause an overspill of cold bottom water above the canyon rim. Transects normal to the Monterey Submarine Canyon showed a 20-m thick lens of 12 °C water moving northward out of the Canyon during high internal tide (Shea and Broenkow, 1982). The overspill from the interaction of the internal tide and Carmel Canyon may also be a possible mechanism of nutrient delivery into Stillwater Cove. Although numerous studies of internal waves have been

conducted in the Monterey Bay Submarine Canyon and on the Inner Monterey Shelf, the spatial variability of internal waves as a function of submarine canyon proximity has not been fully described. Motivated by the consistent presence of internal waves during stratified conditions in Stillwater Cove observed in the CICORE mooring data, this project sought to investigate and characterize the spatial variability of internal tides / waves in the greater Monterey Bay. Datasets from both Monterey and Carmel Submarine Canyons and locations on the Monterey Shelf were used. Specifically, this study focused on the relationship between internal tide generation, internal waves, and the proximity to submarine canyons. Using multiple sources of *in-situ* oceanographic data at locations that spanned the greater Monterey Bay, several questions were investigated: 1.) How does the presence of the internal tide and internal waves vary spatially at locations within close proximity to submarine canyons and at locations on the shelf? 2.) How does the strength of the diurnal and semi-diurnal tidal signal vary throughout the water column at these locations? 3.) Are the observed internal waves in phase with the diurnal and semi-diurnal tide, and does the phase vary with distance from submarine canyons?

1.2 *Background and Theory*

The continental shelf of California is characterized by a system of steep shelves with a very narrow width. The California Current System (CCS) is one of the most productive coastal ecosystems in the world (Barber and Smith, 1981). The CCS is an Eastern Boundary System of currents from Oregon to Baja California and extends up to 1000 km offshore. It is composed of the southward meandering California Current at the surface, a poleward California Undercurrent, and surface countercurrents including the

Davidson Current. The CCS has high biological productivity and is the major source of nutrient rich water that is upwelled to the coastal marine ecosystem. First, let us consider the primary mechanism of cross-shelf transport in the wind frequency band (days to weeks). Consider a hypothetical eastern boundary in the Northern Hemisphere under strong equatorward wind stress. Winds blowing parallel to the coast produce a surface Ekman layer within a timescale of $1/f$ (where f is the Coriolis factor $f=2\Omega \sin(\text{latitude})$) that causes transport 90° to the right of the wind and results in the offshore transport of surface water. This convergence of water offshore and the associated divergence at the coastal boundary results in a horizontal pressure gradient. Transport is towards the coast in the frictional Ekman boundary layer at the bottom. The onshore transport in the Ekman bottom boundary layer balances the offshore flow in the surface Ekman layer and results in cross-shelf transport of nutrient rich bottom water. Macronutrients such as nitrate, phosphate, and silicic acid essential to primary productivity are thus brought to the surface layer. Typically freshly upwelled waters in this region can have temperatures on the order of 8°C - 11°C , nitrate concentrations of $15\text{-}35\ \mu\text{M}$, phosphate concentrations of $1.3\text{--}2.6\ \mu\text{M}$, and silicic acid concentrations of $15\text{-}45\ \mu\text{M}$ (Bruland *et al.*, 2001). The most intense coastal upwelling along California is generally restricted to a relatively narrow band within 10 km of the coast and is enhanced south of prominent points of land such as Point Arena, Point Reyes, Año Nuevo and Point Sur (Huyer, 1983). This upwelling is a primary source of the nutrient-rich water that drives Monterey Bay's high biological productivity. During the spring and summer months, upwelling brings cool nutrient-enriched water from depth. Upwelling inside and around Monterey Bay may occur as: a result of coastal upwelling due to wind driven Ekman transport of coastal

surface water offshore, open ocean upwelling due to positive wind stress curl within the bay, or bathymetrically induced upwelling due to flow over the steep submarine canyon walls (Breaker and Broenkow, 1989; Graham and Largier, 1997). Moving on to the tidal frequency band (< 24 hrs), we will examine the effects of the barotropic tide on cross-shelf transport. The barotropic tide is a large-scale wave with a wavelength of ~ 6000 km that propagates around the ocean basins, forced by the gravitational forces of the moon and sun. Since barotropic tidal currents slosh back and forth, there is no significant net cross-shelf transport onshore or offshore. Barotropic tidal currents do not contribute to net cross-shelf transport; however, barotropic tidal flow across rough bottom topography can cause barotropic to baroclinic energy conversion. Energy from the barotropic tide is transformed into the displacement of isopycnal surfaces and forces oscillations in the density field. The most effective transmission of energy from the barotropic to baroclinic tide occurs in regions where the shelf topography is critical to the semi-diurnal internal tide. The critical angle occurs where the slope of the topography approximately equals the critical angle c determined by the semi-diurnal internal tide (Cacchione *et al.*, 2002). As a result, internal waves are radiated outward as inclined rays.

These generated internal waves are gravity waves that propagate within the ocean along strong density gradients. Internal waves of tidal frequency are termed internal tides. Internal waves can also be generated by atmospheric forcing (Hosegood and Van Haren, 2004), but the majority of internal wave energy is generated from the barotropic tides interaction with bottom topography. As internal waves propagate inshore, the thermocline is vertically displaced and cold nutrient rich water is advected upwards. This mechanism can bring vital nutrients up to the surface especially when coupled with

periods of upwelling. McPhee-Shaw et al. (2007) found that over the course of a two-year period in the Santa Barbara channel, 9-12% of the total nitrate delivery to the inner shelf was due to internal waves. Internal waves can be an important net source of nutrients for inner-shelf ecosystems such as kelp forests (Jackson 1998, Zimmerman and Kremer, 1984). Internal waves have been previously observed in the nearby Monterey Bay, with the majority of the studies focused on the Monterey Canyon at depths greater than 100m (Broenkow and McKain, 1972; Shea and Broenkow, 1981; Heard, 1992; Petruncio *et al.*, 1998; Kunze *et al.*, 2001, Cazenave, 2008). Observations in the Monterey Submarine Canyon head have shown the presence of strong internal tides along the axis of the canyon (Rosenfeld, 1999). Data from two shipboard experiments in 1994, designed to observe the semi-diurnal internal tide in Monterey Canyon, measured semi-diurnal currents an order of magnitude larger than the estimated barotropic tidal currents. These currents were caused by a highly energetic internal tide propagating up the canyon (Petruncio *et al.*, 1998). Several recent studies have focused on studying the dynamics of internal waves on the inner shelf region of Monterey Bay (Storlazzi *et al.*, 2003; Carter *et al.*, 2005; Cazenave, 2008).

1.3 Objectives

Carmel Bay is a embayment along the Central Coast of California, and it contains a unique environment constrained within a very small spatial scale. Located within the bay is Stillwater Cove, a small semi-enclosed basin that contains a large *M. Pyrifera* population. The near-shore environment within the bay is exposed to open ocean coastal California Current conditions, and due to the close proximity of Carmel Canyon it may be strongly influenced by submarine canyon dynamics and associated internal tides. Terrestrial runoff from the nearby Pebble Beach golf course may also be contributing to

nutrient loading to the near-shore ecosystem. No previous studies have been conducted on the circulation features of Carmel Bay and Stillwater Cove. It is still not known if Carmel Bay's behavior functions separately or mimics the oceanographic dynamics of the outer coast. I seek to understand how the oceanographic dynamics and nutrient field in Carmel Bay compares to surrounding regions. The primary objective of this project is to characterize the spatial variability of the nutrient field across the Monterey Bay by quantifying cross-shelf nutrient transport in the wind and tidal frequency bands.

An important goal of this project is to understand how nutrient contributions from the tidal frequency bands vary as a function of distance from submarine canyons.

Specifically, how do tidal band nutrient budgets compare from locations out on the shelf to locations within close proximity to submarine canyons? Is along-coast variability in the semi-diurnal internal tide set by the distance from a submarine canyon head?

2. OBSERVATIONS

2.1 Stillwater Cove Study Site

Stillwater Cove faces directly southward along the California coast, and is sheltered from winter swells and northwesterly winds. During summer conditions, south swells are blocked by nearby Point Lobos to the south. Due to the combined shadowing of both north and south swells by the cove's unique geographic location, only large winter northwest swells can refract around Pescadero Point and propagate into the cove's sheltered environment. The inside of the cove is protected by Pescadero Point to the west and Arrowhead Point to the east, with Pescadero rocks separating the cove in the center (Figure 1). The depth of the cove ranges from ~9 m to ~14 m, with a depth of ~12 m in

the region directly surrounding the Pescadero rocks. The California Coastal Commission has declared Stillwater Cove and Carmel Bay an “Area of Special Biological Significance” (ASBS) (Brown, 2001). The Carmel Bay ASBS lies entirely within the Monterey Bay National Marine Sanctuary, and contains the Carmel Bay State Marine Conservation Area. Carmel Bay has the second largest number of pollutant discharges of an ASBS in the state, a total of 348 direct discharges including polluted runoff from streets, highways, golf courses, and private homes (Brown, 2001). The location of Stillwater Cove also presents the unique opportunity to study the effects of submarine canyon dynamics on a sheltered near-shore environment. Located to the south of Stillwater Cove (< 1 km), the Carmel Submarine Canyon is a local source of nutrient-rich cold bottom water. Carmel Canyon is a relatively straight arm of the Monterey Canyon system and contains three distinct heads (Figure 2). Two of the Carmel Canyon heads are located inside Carmel Bay, one at the shoreline opposite San Jose Creek and the other offshore ~ 3 km from the mouth of the Carmel River (Green, 1977). The third head extends along-trend with the north-south oriented main canyon form, approximately 3km past the intersection of the two other heads (Green, 1977).



Figure 2: Map of Stillwater Cove, California.

2.2 Moored Physical Oceanographic Observations

A multitude of moored instruments provided a year-long time series of oceanographic and meteorological conditions in Stillwater Cove and the greater Monterey Bay region (Figure 3). The CICORE Stillwater Cove mooring is located at $36^{\circ} 33' 30'' \text{ N} / 121^{\circ} 56' 40'' \text{ W}$ in 20 m depth. This location is ~200 m directly south of Stillwater Cove, at the extreme north end of Carmel Bay. Geographically, this is an appealing location as the mooring is able to capture the oceanographic dynamics of Stillwater Cove and provides valuable insight to Carmel Bay. The mooring was deployed and maintained from June 2006 to February 2008. The CICORE mooring was equipped with a multi-beam bottom mounted acoustic Doppler current profiler (ADCP) (RD

Instruments, 600kHz) at ~20m depth. Data were averaged into 1-m vertical bins. Velocity profiles were measured at a 15-minute sampling rate, and then averaged to hourly records. The mooring was also equipped with SeaBird SBE 39 Thermistors located at 6 m, 9 m, 12 m, 15 m, and 18 m depths. This thermistor array was synchronized at a 2-minute sampling rate, and provided a high resolution time series of the vertical temperature gradient. Four additional high resolution SBE 39 thermistors were added to the mooring from October to December 2007 to provide further insight to vertical mixing and turbulence. These thermistors were deployed at 8 m, 11 m, 14 m, and 16 m depths with a 10-second sampling rate.

Additionally, eight near-shore moorings (< 30 m) that spanned the greater Monterey Bay were chosen for this study to provide a spatial comparison to Stillwater Cove (Figure 3). These moorings had a combined along-coast spatial scale of ~ 70 km. Seven of these long term moorings were deployed and maintained by the Partnership for Interdisciplinary Studies of Coastal Oceans (PISCO). The Moss Landing Marine Laboratories (MLML) Seawater System is located directly at the head of the Monterey Submarine Canyon at 36° 48' 9" N / 121° 47' 29.39" W in 20 m depth. Three of the moorings were located within close proximity (< 4 km) to a submarine canyon head: the MLML Seawater System, the PISCO moorings at Weston Beach and Sunset Point. Two of the moorings were located on the inner Monterey Shelf at a greater distance (> 7 km) from a submarine canyon: the PISCO moorings at Point Joe and Lovers' Point. The last two moorings were located on the shelf at a significant distance (> 14 km) from any major submarine canyons: the PISCO moorings at Point Sur and Soquel Point. The PISCO moorings were equipped with StowAway Tidbit and StowAway XTI Thermistors located

at four evenly spaced depths throughout the water column. For the purposed of this project, only thermistor data from near-surface and near-bottom depths were used. Six of the PISCO mooring thermistor arrays were synchronized at a 2-minute sampling rate, while one location (Lovers' Point) was synchronized at a 4-minute sampling rate. The MLML Seawater System is equipped with a Weed Instrument 5A00A1 temperature sensor, and an Oxyguard 840 dissolved oxygen sensor. Both instruments are synchronized at a 5-minute sampling rate. For this study, all PISCO and MLML temperature mooring data were re-gridded onto a 2-minute time interval.



Figure 3: PISCO, MLML, and MBARI mooring locations.

Data from the Monterey Bay Aquarium Research Institute (MBARI) M0, M1, and M2 moorings were used to compare the seasonal temperature variability of Monterey Bay to Stillwater Cove and the calculate temperature-nitrate relationships. The M1 and M0 moorings are located inside the Monterey Bay at $36^{\circ} 45' 0''$ N / $-122^{\circ} 1' 48''$ and $36^{\circ} 49' 47.9''$ N / $-121^{\circ} 54' 0''$ W, while the M2 mooring is located outside the Monterey Bay at $36^{\circ} 42' 0''$ N / $-122^{\circ} 23' 24''$ W. Preliminary work on the CICORE time series from summer 2006 showed that Stillwater Cove followed the same seasonal regime shifts in temperature and is subject to similar upwelling conditions as Monterey Bay. Year-long thermistor datasets from both 1-m and 20-m depths were used to examine the relationship between seasonal patterns, trends, and variability in Carmel Bay and the greater Monterey Bay. Temperature-nitrate relationships from the M0, M1, and M2 moorings were calculated over a year-long period, using surface temperature and nitrate data from the MBARI In-Situ Ultraviolet Spectrophotometer (ISUS). The National Data Buoy Center (NDBC) station 46042 located 27 nm west of Monterey Bay provided a time series of wave height and period. This dataset was used to correlate strong winter storms to vertical mixing in Stillwater Cove.

2.3 Hydrographic Observations

CTD (conductivity, temperature, and density) profiles and seawater samples for from Carmel Bay were collected during three cruises on the R/V John Martin. A single CTD profile was made on October 20th 2006 for a preliminary investigation of the Carmel Bay water column, and three separate CTD profiles along with seawater samples

from Niskin bottles at near-surface, 30 m, and 60 m depths were made on May 18th 2007. During October 31st 2007, CTD casts were conducted every hour over an eight-hour period from the peak semi-diurnal low tide to the peak diurnal high tide. This repeated CTD survey was conducted in order to observe the vertical excursion of the internal tide in Carmel Bay during the rising diurnal tide. At the end of the survey, seawater samples were taken at 60 m, 100m, and 180m depths. The CTD temperature data and nitrate concentrations from the May 18th 2007 and October 31st 2007 cruises were used to calculate a temperature-nitrate relationship for Carmel Bay. The seawater samples were analyzed for nitrate and phosphate concentrations using a LaChat Instruments QuickChem 8500 Series flow injection analyzer provided by California State University Monterey Bay (CSUMB). The auto sampler runs a measured portion of the sample through each channel, where it is then mixed with the corresponding reagent and heated to form a color reaction. The color was then measured photometrically to obtain a concentration of the analyte. Nitrate is quantitatively reduced to nitrite by passage of the sample through a copperized cadmium column. The nitrite was then determined by diazotizing with sulfanilamide followed by coupling with N-(1-naphthyl) ethylenediamine dihydrochloride. The resulting water-soluble dye has a magenta color which is read photometrically at 520 nm. The phosphate reacts with ammonium molybdate and antimony potassium tartrate under acidic conditions to form a complex. This complex is reduced with ascorbic acid to form a blue complex which absorbs light at 885 nm. The absorbance is proportional to the concentration of phosphate in the sample. In order for the QuickChem 8500 to detect the concentrations of the samples, standards with known concentration were made. The standards were then used to compare the

unknown concentration of the sample to the known concentration of the standard. In order to verify that the standards were correct, several quality check solutions with known concentrations were run through the QuickChem 8500.

2.4 Meteorological Data

The MLML weather station hourly wind dataset was used to correlate identified upwelling events in Stillwater Cove to strong periods of seasonal northwest winds in the Monterey Bay region. Terrestrial runoff events were identified by the MLML weather station daily rainfall dataset. National Oceanic and Atmospheric Administration (NOAA) hourly tidal height from Monterey Bay was used to correlate temperature and currents with tidal data.

2.5 Watershed Data

The proximity of Stillwater Cove to the Pebble Beach development presented a unique opportunity to study the effects of terrestrial nutrient runoff into a small semi-enclosed basin. Hydrological data on storm drain discharge and nutrient concentrations were used to calculate a daily wet / dry bulk terrestrial nutrient input into Stillwater Cove. To estimate the bulk terrestrial nutrient input into the cove, this project followed methods described in McPhee-Shaw *et al.* (2007). Terrestrial runoff discharges into Stillwater cove via the two stormwater drains near the Pebble Beach Club pier and Stillwater creek (Figure 4). The stormwater drains are ~ 30 inches in diameter and have an area of ~ 706 inches squared.



Figure 4: Stillwater Cove terrestrial runoff locations.

Both locations were sampled during the 2007 summer baseflow and winter stormflow during several significant rain storms during the winter season. A Global Water Instrumentation hand-held flow meter was used to directly measure the discharge rate and the mean water level in the storm drain was recorded. The recorded flow rates and nutrient concentrations of Stillwater creek were extremely low ($< 1.6 \mu M$) and the effects of nutrient input via the creek were ignored for this project. The winter hydrological dataset was averaged to provide a standard winter discharge rate for significant storm events. The measured discharge rates and nutrient concentrations were assumed to be constant for the entire day on which sampling is conducted. Manual samples of storm drain water were collected below the surface of the thalweg and analyzed for NO_3 and PO_4 concentrations. The storm drain samples were then analyzed

for nitrate and phosphate concentrations using the methods described in Strickland and Parsons (1972). A mixing reagent composed of 10 mL of 24 μM ammonium molybdate, 25 mL of 2.5 μM sulphuric acid, 10 mL of 0.3 μM ascorbic acid and 5 mL of 0.4 μM potassium antimonyl-tartrate solutions was used. Five standards ranging from 0.5 -3 μM phosphate and a blank were made. Ten milliliters of each seawater sample and standards were transferred into a glass beaker and 1mL of the mixing reagent was added. These samples were then left for 20 minutes. The absorbance for each standard and sample was analyzed at a wavelength of 885nm in a 10cm cell path. The seasonal wet and dry nutrient concentrations in Stillwater Cove due to terrestrial input were then estimated by assuming the terrestrial discharges are mixed evenly into the near-shore coastal waters. This calculation requires an estimate of the volume of seawater in which the terrestrial runoff initially mixes. This is often not well constrained; however, the enclosed nature of Stillwater Cove provides a convenient limit on the size of the mixing basin. Using ADCP data from the Stillwater Cove mooring mean flow during a 24-hour period was calculated to estimate the possible excursion distance of terrestrial runoff. For the purposes of this dataset, the currents were vertically averaged throughout the water column, and the time series ran from June 15, 2006 to May 18th, 2007. The mean 24-hour grid excursion distance was 500 x 500 m. The size of Stillwater Cove is ~ 1000 m x 500 m, far below the average excursion distance. We assume that the terrestrial discharge is mixed evenly into the entire Stillwater Cove area within the period of a day. Further, considering that vertical mixing in the ocean is very slow process when compared to horizontal mixing, we can further reduce the volume to a portion of the water column depth. Using an lower bound for open ocean eddy diffusivity of $1.3 \times 10^{-4} \text{m}^2/\text{s}$ (Munk, 1966) and a upper bound

of $10^{-3}\text{m}^2/\text{s}$ (MacKinnon and Gregg, 2002), we can estimate that the bounds of the vertical diffusion of the terrestrial runoff over a 24-hour period may range between 10 meters and 27.8 meters. This was estimated using an eddy diffusivity scale: $U = \frac{L}{T}$, (where U = velocity scale, L = length, and T = time). Using interpolated bathymetric data from the California Department of Fish and Game GIS dataset, we estimated the entire volume of Stillwater Cove to be approximately 183,970,000 liters. For our mixing model, a volume of 1000 m x 500 m x (3 variable depths) was chosen. This area represents the general size of Stillwater Cove, and is smaller than the average 24 hour excursion distance. Three separate volume depths of 3 m, 10 m, and 20 m were chosen to provide a range of estimates based on different rates of vertical mixing. The three volumes used in this model are: 1.5×10^9 liters, 5×10^9 liters, and 1×10^{10} liters respectively.

2.6 Summary of Data Collection

The available data from the multiple time series used in this project spanned both long and short data ranges (Figure 4). Data processing and analysis was conducted using Mathwork's Matlab, and All PISCO thermistor and NOAA Monterey Bay tidal height data was re-gridded onto a two minute sampling interval to be consistent with the resolution of the CICORE mooring. Currents were rotated into a coordinate system aligned with the depth-averaged axis of principal variance, calculated using empirical orthogonal functions. This was oriented approximately along-isobath: at 283° (clockwise from 0° north) for the Stillwater Cove mooring (Figure 6). A right-hand coordinate system is used for a viewer looking poleward with the coast on the right: The along-isobath component, v , is positive poleward (northwest towards Stillwater Cove), and the

cross-isobath component, u , is positive onshore (northeast towards Carmel Beach).

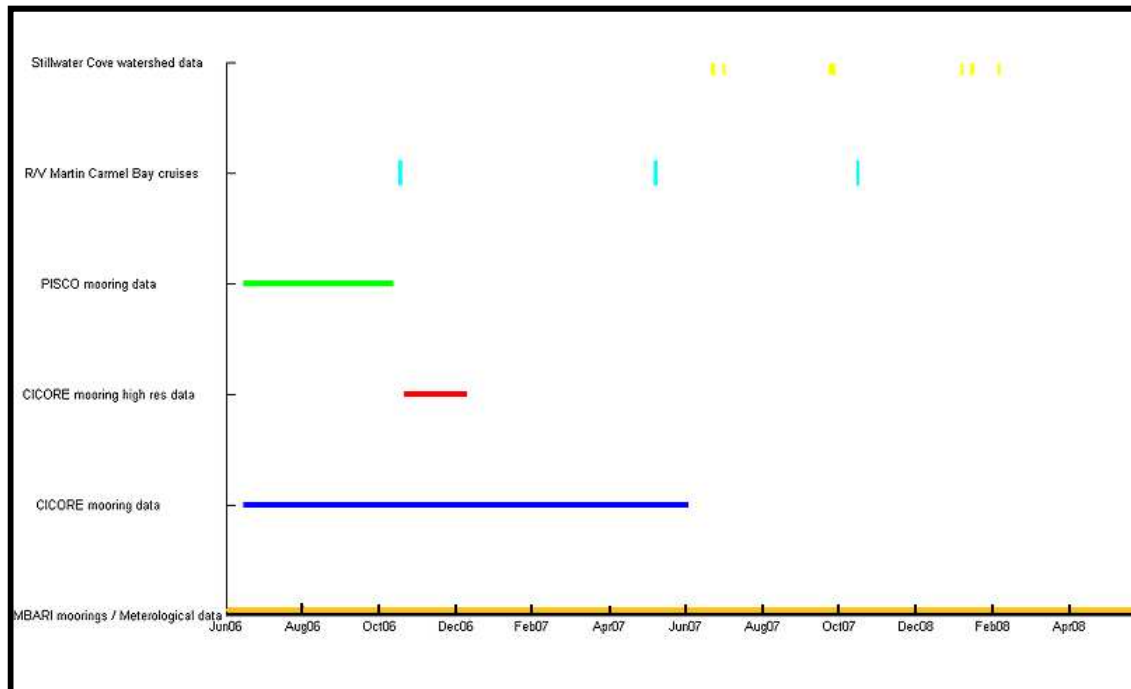


Figure 5: Date ranges of data collection.

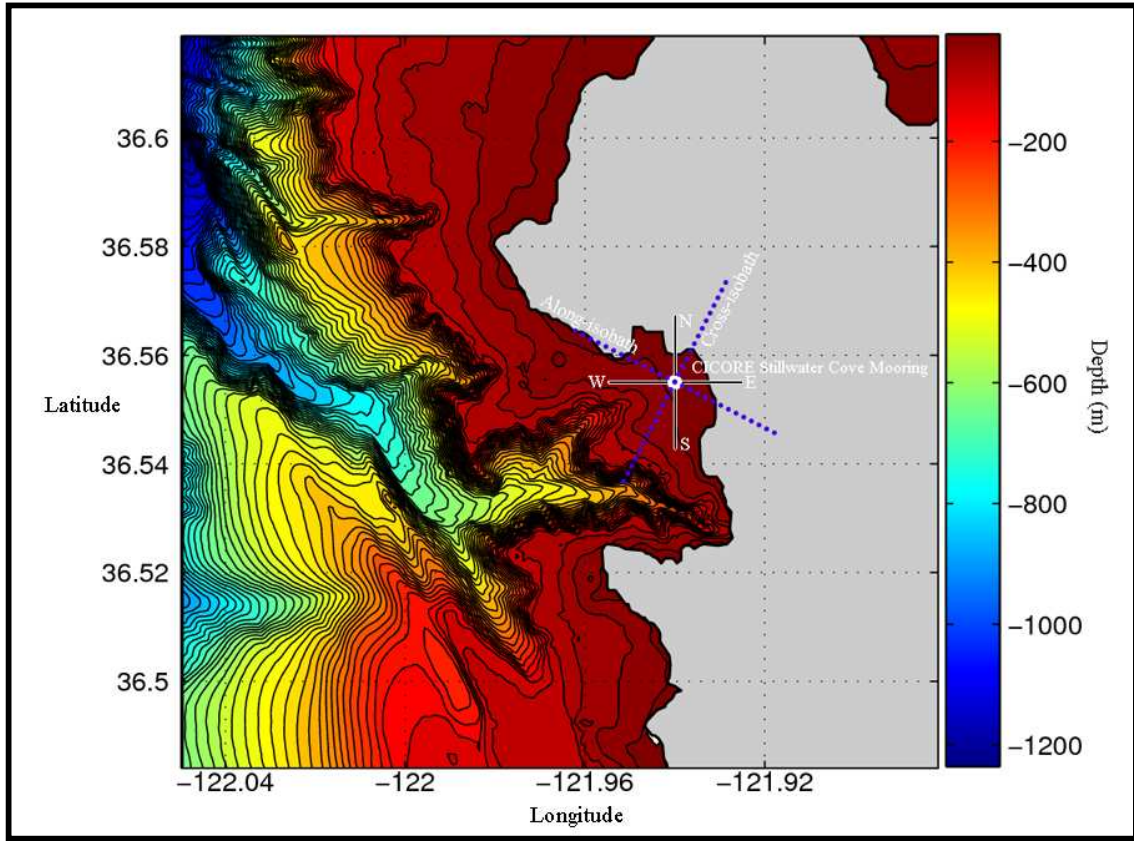


Figure 6: Carmel Bay bathymetry and rotated coordinate system.

2.7 Spectral Analysis

NOAA Monterey Bay tidal data was used to correlate the tide with observed internal waves at CICORE and PISCO mooring locations. A data range of 6/18/2006 to 10/10/2006 was chosen for the spectral and cross-spectral analysis. Continuous data from this time range was available from all the PISCO and CICORE mooring datasets, and the time series provided a seasonal transition from strongly stratified summer conditions to early fall. The raw thermistor and tidal height data was imported into Matlab, cropped to the desired data ranges, and then interpolated to a two minute sampling rate. Spectral analysis was used on the thermistor datasets to examine the strength of the diurnal and

semi-diurnal tidal signal throughout the water column at each mooring locations. The spectral power density was calculated using Welch's averaged, modified periodogram spectral estimation method. The thermistor time series were divided into 2^{12} sized data segments with no overlap, and the periodogram was calculated by computing the discrete fast Fourier transform, and then computing the squared magnitude of the result. The individual periodograms were then time-averaged. Cross-spectral analysis and coherence were then used to examine the correlation between temperature and tidal signals throughout the water column at each mooring locations. For the scope of this project, only the spectral results from the near-surface and near-bottom depths and coherence from the near-bottom depths will be presented.

2.8 Temperature-Nitrate Relationship

In-situ samples of nitrate concentrations in the Carmel Bay water column were limited to episodic cruises on the R/V Martin. Continuous *in-situ* nitrate observations were not available over the entire time series; however, a predictive relationship between temperature and nitrate allowed for the calculation of a “proxy” nitrate signal from the more complex temperature time series. The resulting continuous proxy time series was then used to examine spectral, seasonal, and event-scale features of near-shore nitrate concentrations. Temperature-nitrate relationships were derived from four distinct locations in the greater Monterey Bay: the MBARI M2 and M0 moorings, the MBARI Land/Ocean Biochemical Observatory (LOBO) mooring in northern Monterey Bay, and from multiple CTD casts taken in Carmel Bay (Figure 7). For the MBARI M0 mooring, a least-squares fit to a fourth order polynomial between nitrate ($\mu\text{M L}^{-1}$) and temperature ($^{\circ}\text{C}$) was $N_{m0}(T) = 0.00383T^4 - 0.2511T^3 + 6.5807T^2 - 79.986T + 373.32$. For the

MBARI M2 mooring, a least-squares fit to a fourth order polynomial between nitrate ($\mu\text{M L}^{-1}$) and temperature ($^{\circ}\text{C}$) was $N_{m2}(T) = -0.0315T^4 + 1.6845T^3 - 32.881T^2 + 274.86T - 814.21$. For the MBARI LOBO mooring, a least-squares fit to a fourth order polynomial between nitrate ($\mu\text{M L}^{-1}$) and temperature ($^{\circ}\text{C}$) was $N_{lobo}(T) = -0.1751T^4 + 8.0977T^3 - 138.99T^2 + 1045.1T - 2873.1$. For Carmel Bay, a linear fit was $N_{carmel}(T) = -0.16 \cdot x + 13$. The min error bound on $N_{m0}(T)$ was $2.74 \mu\text{M L}^{-1}$, and the max error bound was $2.8355 \mu\text{M L}^{-1}$. The min error bound on $N_{m2}(T)$ was $3.65 \mu\text{M L}^{-1}$, and the max error bound was $3.70 \mu\text{M L}^{-1}$. The min error bound on $N_{lobo}(T)$ was $1.88 \mu\text{M L}^{-1}$, and the max error bound was $2.37 \mu\text{M L}^{-1}$.

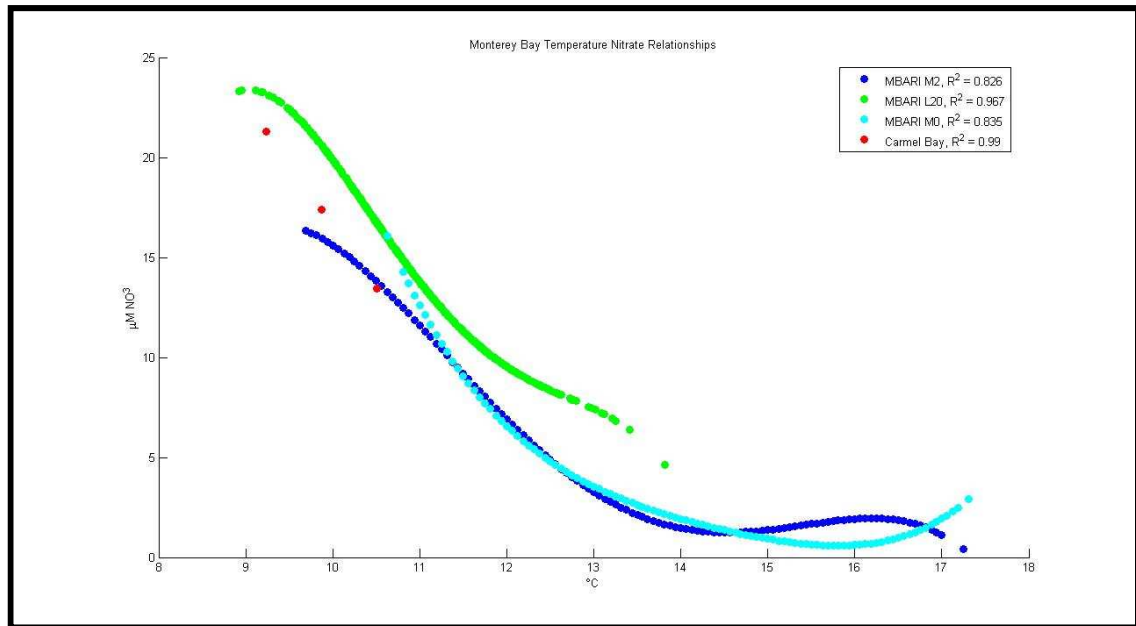


Figure 7: Temperature-Nitrate relationships for Carmel and Monterey Bay.

3. RESULTS

3.1 Seasonal Description of Carmel Bay

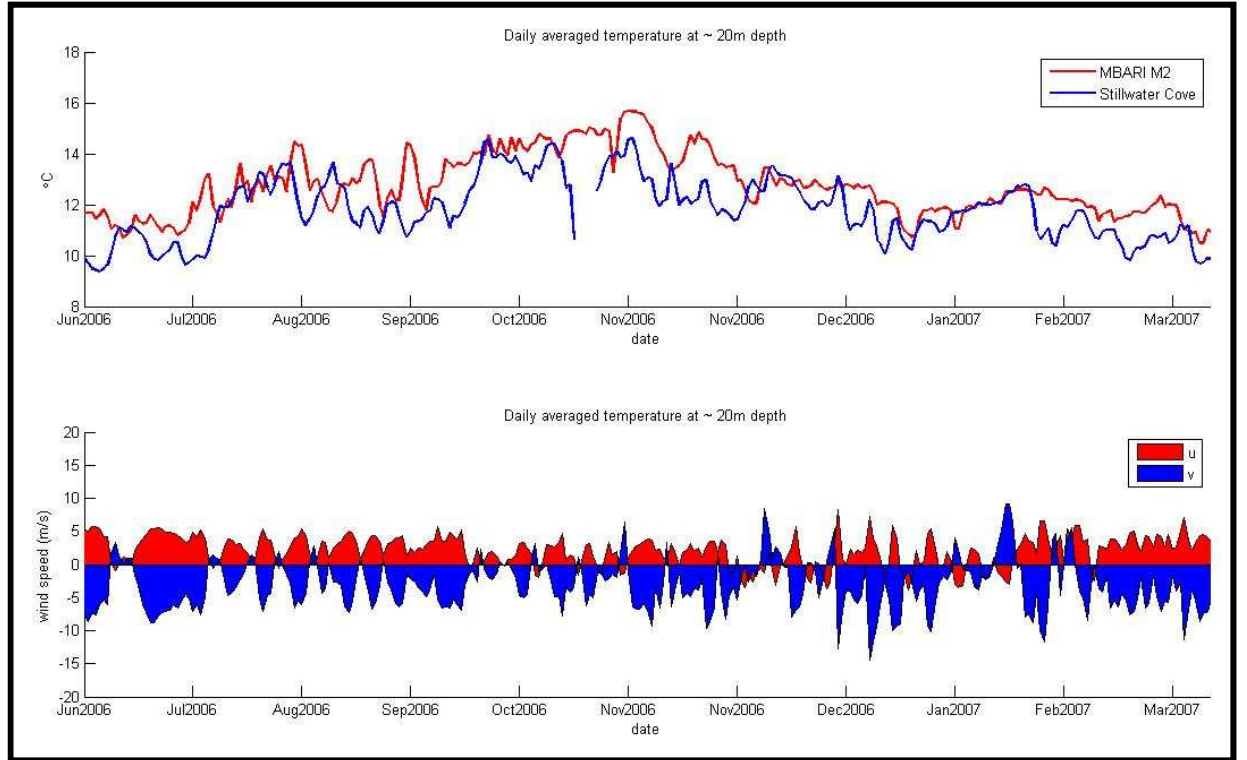


Figure 8: Year-long daily averaged temperature from Stillwater Cove and Monterey Bay.

For the seasonal analysis of the oceanographic dynamics in Stillwater Cove, a time series from June 15th 2006 to June 15th 2007 was chosen. A year-long time series of daily averaged temperature data from both the Stillwater Cove mooring and MBARI M2 moorings at ~20-m depths are presented in Figure 8. A striking feature is that the Stillwater Cove water column is colder year-round compared to the nearby Monterey Bay. Stillwater Cove temperatures at ~20 m are 0.90°C colder than the MBARI M2 mooring. The greatest temperature differences between Monterey and Carmel Bay are during stratified summer condition, whereas during winter conditions and periods of

strong vertical mixing, the temperature difference is greatly reduced. Three distinct temperature regimes were present in both the Stillwater Cove and Monterey Bay temperature records during summer conditions (Figure 9). These steps in the temperature time series are most apparent during periods of upwelling relaxation where northwesterly winds were reduced significantly. At each subsequent step, the average temperature increased $1.5^{\circ}\text{C} - 2^{\circ}\text{C}$ and until the next period of intense upwelling conditions.

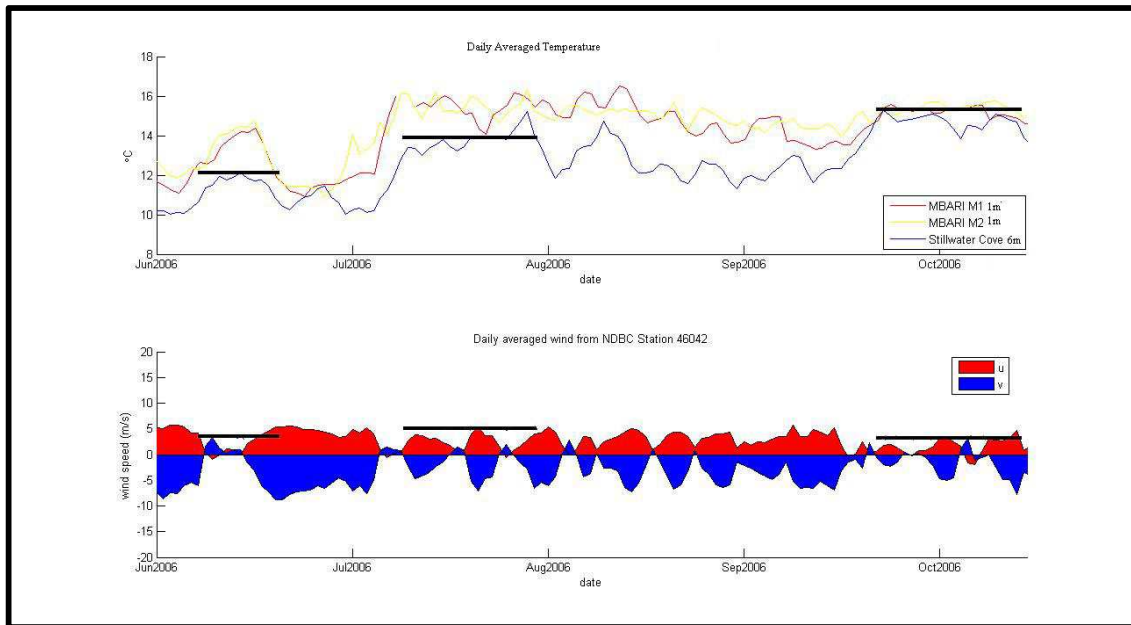


Figure 9: Distinct temperature steps during upwelling relaxation conditions present in both the Stillwater Cove and Monterey Bay temperature time series. Black lines represent periods of upwelling relaxation. When the u is positive and the v is negative, the winds are from the north-west indicating upwelling favorable conditions. Temperature time series was daily averaged and wind time series was bandpass filtered $[0\ 0.9]$ cycles per day.

Stillwater Cove is subject to strong upwelling events during spring and summer conditions, where cold upwelled water fills the near-shore water column. Upwelling favorable conditions occurred frequently from March to August. Typical summer

upwelling conditions lasted 5 – 7 days on average with the most sustained periods of strong northwesterly winds lasting up to two weeks. The average speed of the northwesterly winds conducive to upwelling conditions inside the cove was 5 - 7 m/s. Figure 10 shows an example of an upwelling event, where nutrient rich cold bottom water from offshore is upwelled to the surface of the near-shore water column. This upwelling event lasted for two weeks. Average background temperatures in the water column during this time period were 12.5°C, whereas the upwelled water was on average 10°C. The influx of cold upwelled water typically lagged the onset of the northwest winds by 3 – 4 days.

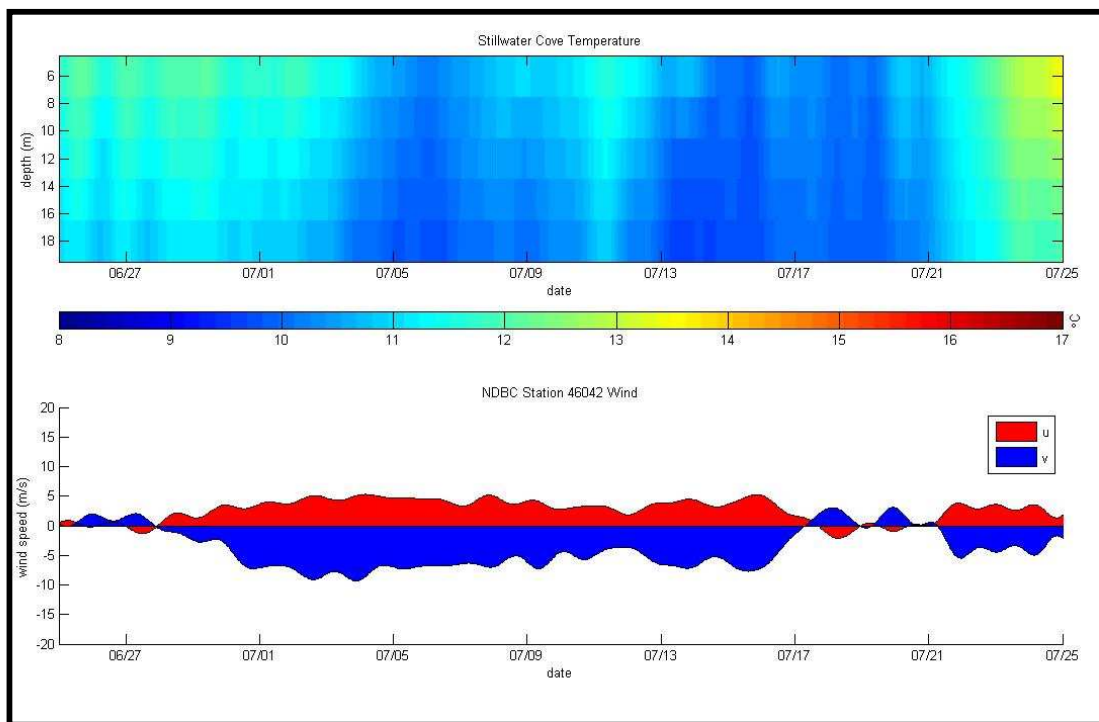


Figure 10: Upwelling event in the Stillwater Cove water column during July 2006. Temperature and wind time series were bandpass filtered [0 0.9] cycles per day.

Sporadic upwelling favorable conditions followed by relaxation events continued to occur throughout August and September. Figure 11 shows more sporadic upwelling conditions in Stillwater Cove during the later part of the summer. These upwelling conditions only lasted 3-4 days on average. Between these sporadic upwelling events, periods of light winds / wind reversal occurred along with upwelling relaxation.

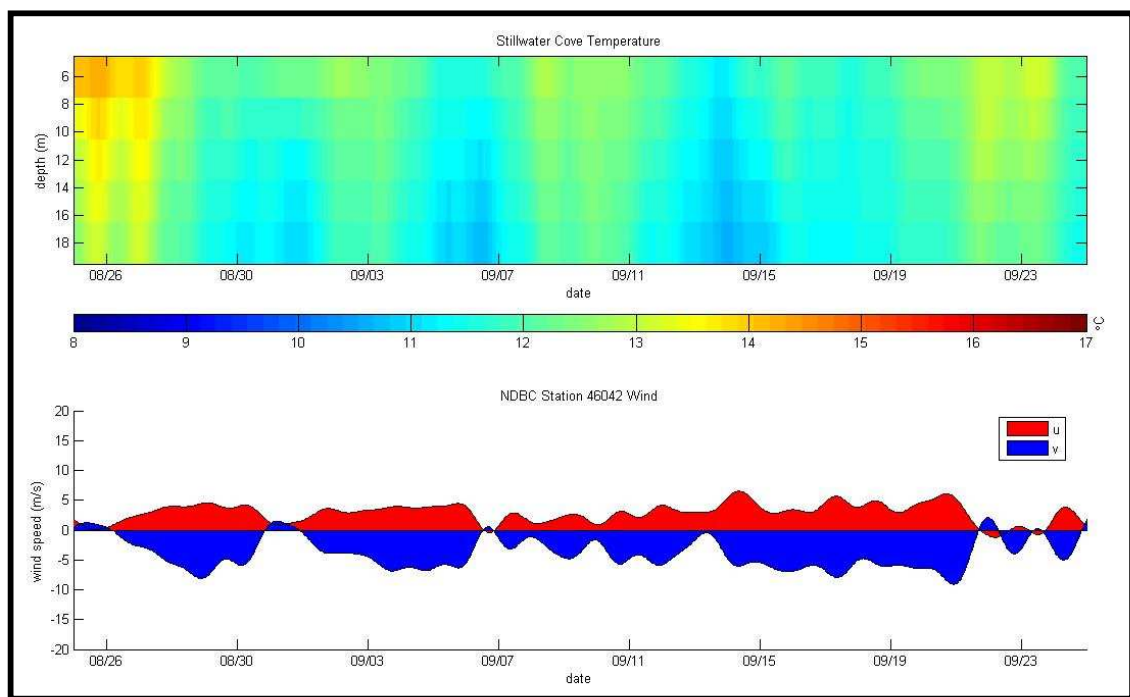


Figure 11: Distinct upwelling events in the Stillwater Cove water column during September 2006. Temperature and wind time series were bandpass filtered [0 0.9] cycles per day.

By early October upwelling has become even more sporadic and the Stillwater Cove water column had warmed significantly to an average water column temperature of 15°C (Figure 12). The strength and the duration of the northwesterly winds had subsided significantly and upwelling events lasted a few days on average.

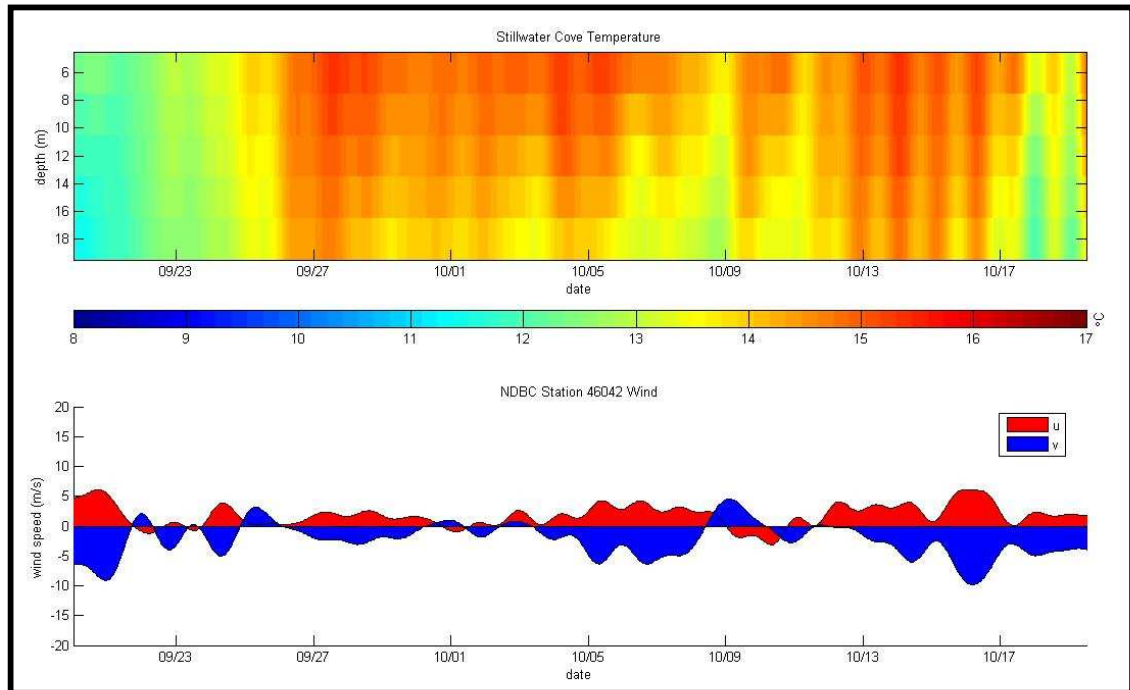


Figure 12: Upwelling events in the Stillwater Cove water column during October 2006. Temperature and wind time series were bandpass filtered [0 0.9] cycles per day.

Transitioning to winter conditions, Stillwater Cove experiences periods of intense vertical mixing and strong winter storms events (Figure 13). During this time of the year, the average wind field is governed by milder northwest / south winds. With the arrival of strong northwest swells from the Gulf of Alaska come increased periods of northwesterly winds. Figure 13 shows four distinct storm events arriving in Stillwater Cove during December / January 2006, with an average storm significant wave height of 6 m and swell duration of 3 days. During these storm events, the northwest winds had an average sustained wind speed of 8 m/s. Correlated with the arrival of these storm events, the water temperature in Stillwater Cove warmed by $\sim 2^{\circ}\text{C}$ and the entire water column became vertically mixed to a homogenous temperature. After the swell event subsided, the water column transitioned back to stratified conditions.

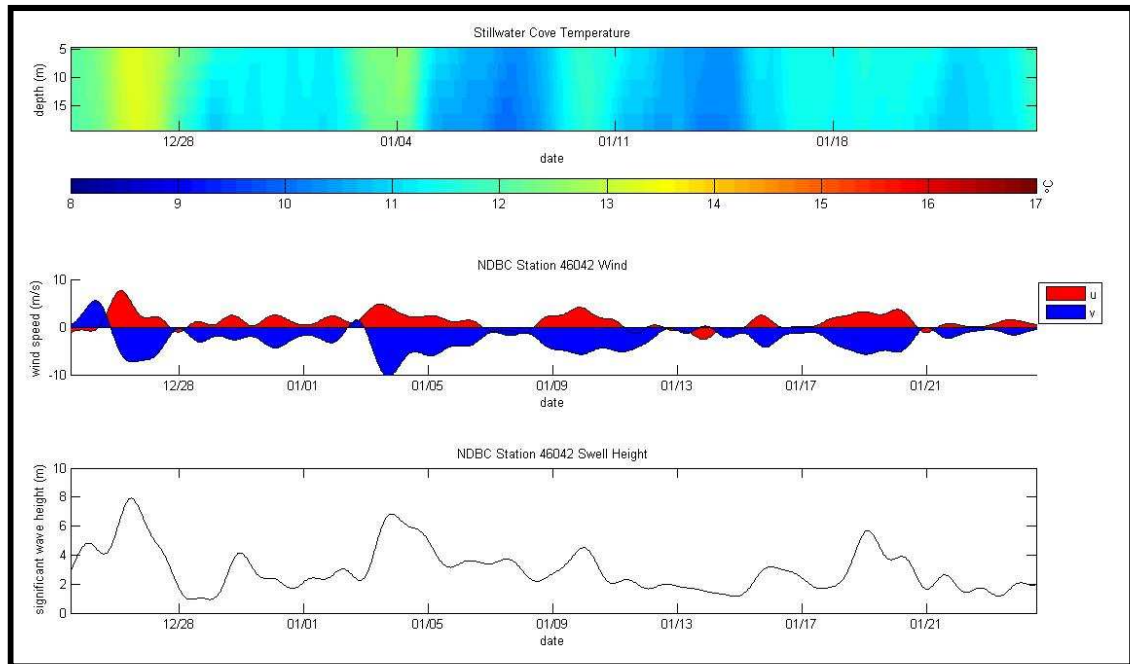


Figure 13: Winter conditions and storm events in the Stillwater Cove water column during December / January 2006.

The mean direction of the currents in the Stillwater Cove water column during summer conditions is shown in Figure 14. Throughout the entire water column, the v velocity is positive indicating consistent northward flow into Stillwater Cove. The average v velocity in the water column during summer conditions was 1.31 cm/s, while the average u velocity was 0.65 cm/s. The u velocity is positive from 9 – 12 m. At 12-m depth, the u velocity decreased and then started to approach negative values. This indicates that the currents consistently rotate from an onshore to offshore direction in the lower half of the water column. Below 17-m depth, the u velocity is negative while the v velocity is positive, indicating a northwest flow in the bottom boundary layer.

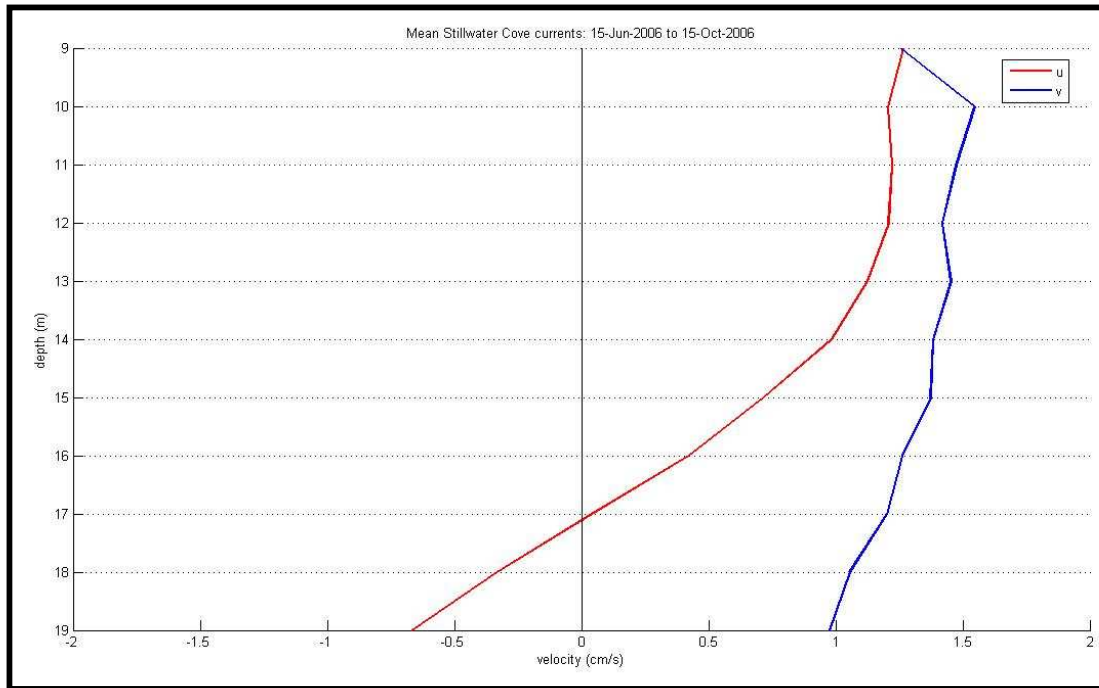


Figure 14: Average Stillwater Cove currents during summer [June 15th 2006 to October 15th 2006].

The mean direction of the currents in the lower half of the Stillwater Cove water column during winter was similar to summer conditions (Figure 15.) At ~ 11 – 13 m depth in the water column, currents flowed in a southwesterly direction. This feature was the only location in the water column where v velocities were negative. Winter v velocities ranged between 0 – 0.5 cm/s, far smaller than summer velocities. The average winter v velocity was 0.2 cm/s, while the average u velocity was -0.5 cm/s. The winter u velocities tended to be stronger than summer conditions, specifically in the bottom boundary layer.

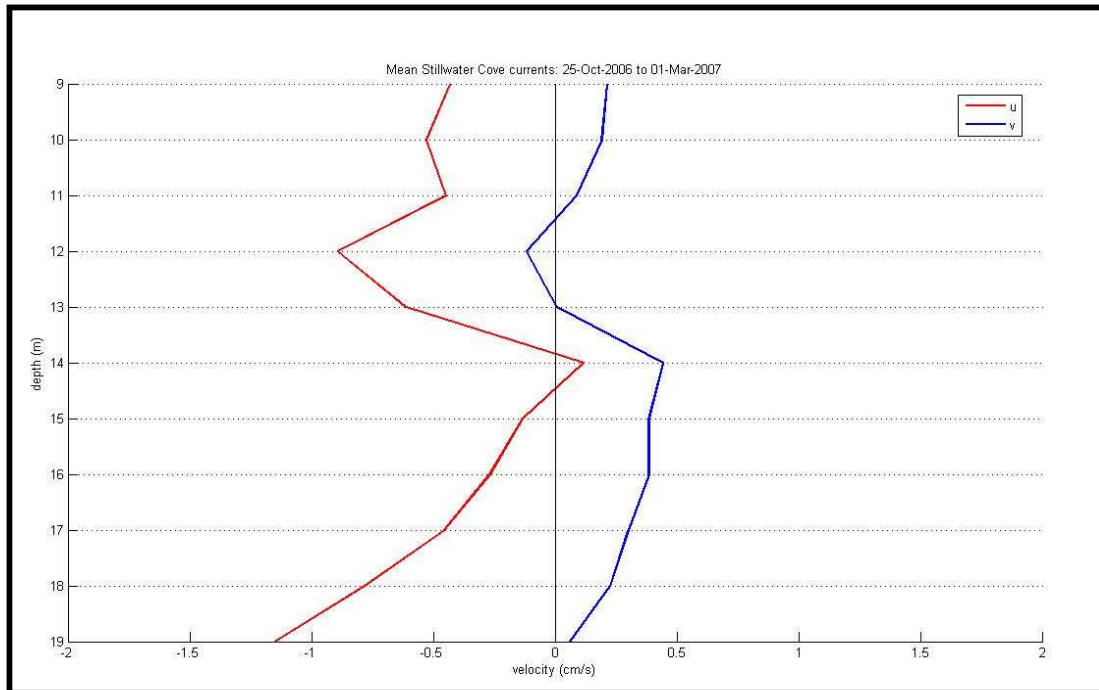


Figure 15: Average Stillwater Cove currents during winter [October 25th 2006 to March 1st 2007].

During spring, the 11 – 14-m depth feature became even more pronounced (Figure 16). In this region, the u velocity is negative while the v velocity is positive, indicating a northwest flow. The average spring v velocity was 0.887 cm/s, while the average u velocity was -0.005 cm/s. The average u velocity was smaller than both summer and winter average u velocities, while the average v velocity increased compared to winter.

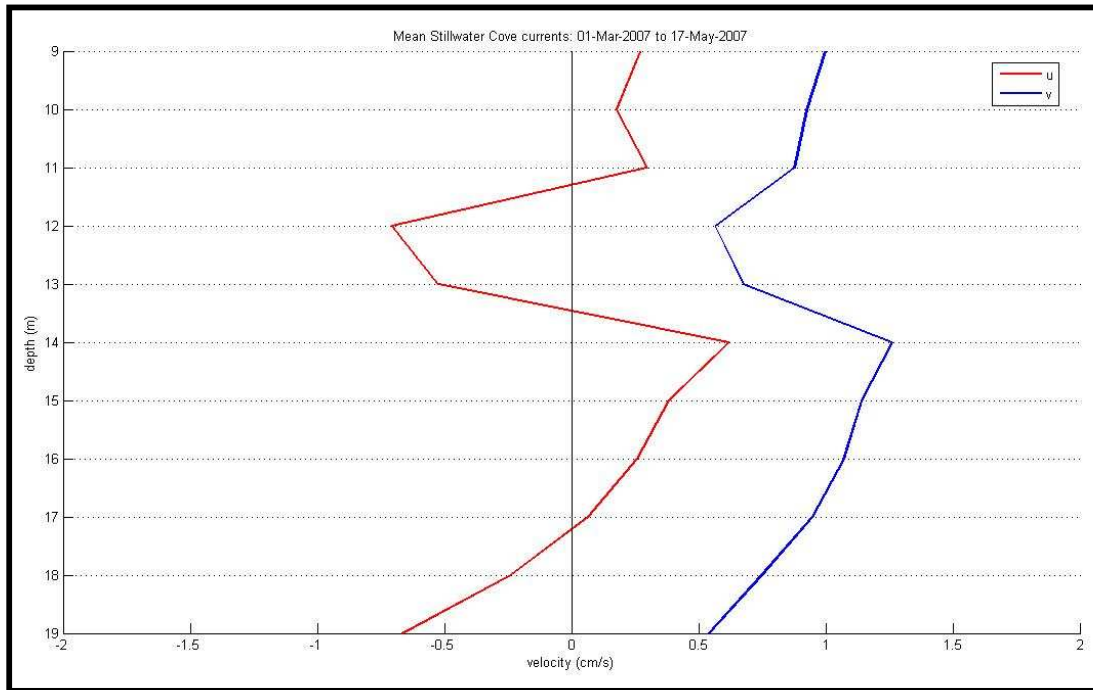


Figure 16: Average currents in Stillwater Cove during spring [March 1st 2007 – May 17th 2007].

A progressive vector diagram (pvd) of currents from 9 – 19m in the Stillwater Cove water column from June 15th 2006 to May 18th 2007 is shown in Figure 17. The ADCP data from the Stillwater Cove mooring is an Eulerian measurement; however, the Lagrangian method of following movement of water parcels is often more illuminating than looking at records of current speed and direction because it can be used to estimate the tidal excursion of a parcel of water. This gives a sense of the direction and magnitude of net transport. Using a pvd diagram is a way to simulate a Lagrangian display from Eulerian measurements. The vectors are seasonally color coded with blue being summer [June 15th – October 15th], red winter [October 15th – March 1st], and yellow spring [March 1st – May 18th]. From the bottom depth at 19 m, the currents progressively rotate from an offshore to onshore direction as you move upward in the water column during

the entire time period. During summer, the total along-path excursion distance at 19-m depth was ~ 141 km. Moving upwards in the water column, this distance progressively increases. The excursion distance at 9-m depth was ~ 173 km, indicating stronger current velocities in the upper half of the water column. During winter conditions, currents in the Stillwater Cove water column alternated periods of northwest and southwest direction. Compared to the summer months, the excursion distance during winter conditions was greatly reduced. The total winter excursion distance at 19-m depth was ~ 70 km, while the excursion distance at 9-m depth was ~ 80 km. The winter excursion distance was roughly half of the summer excursion distance, and the increase in distance as you move upwards in the water column was greatly reduced. During spring conditions, currents throughout the water column resumed their northwest directional flow. The total spring excursion distance over the course of less than three months at 19-m depth was ~ 50 km, while the excursion distance at 9-m depth was ~ 75 km.

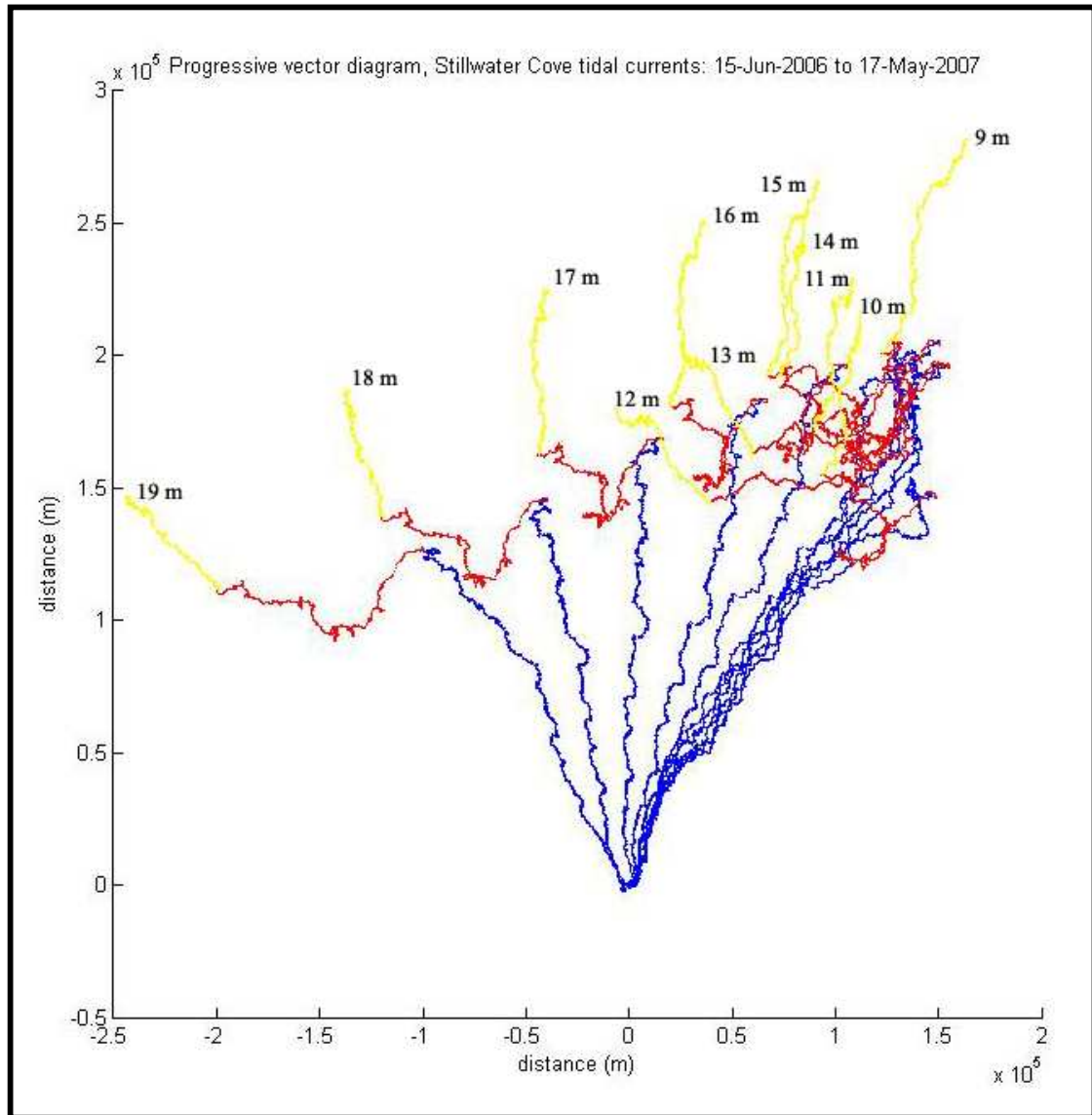


Figure 17: Progressive vector diagram of currents in Stillwater Cove [June 2006 – May 2007]. Each ADCP bin (m) is plotted with blue lines representing summer, red lines representing winter, and yellow lines representing spring.

3.2 Spectral Analysis

Spectral results from Stillwater Cove thermistor time series are displayed in Figure 18. The date range of this time series was from June 15th 2006 to October 10th 2006. This spectrum has strong distinct peaks in the diurnal and semi-diurnal frequencies, with multiple tidal harmonics present. The strength of the semi-diurnal signal dominates over the weaker diurnal signal. The strength of the bottom diurnal and semi-diurnal signals are significantly stronger than their surface counterparts.

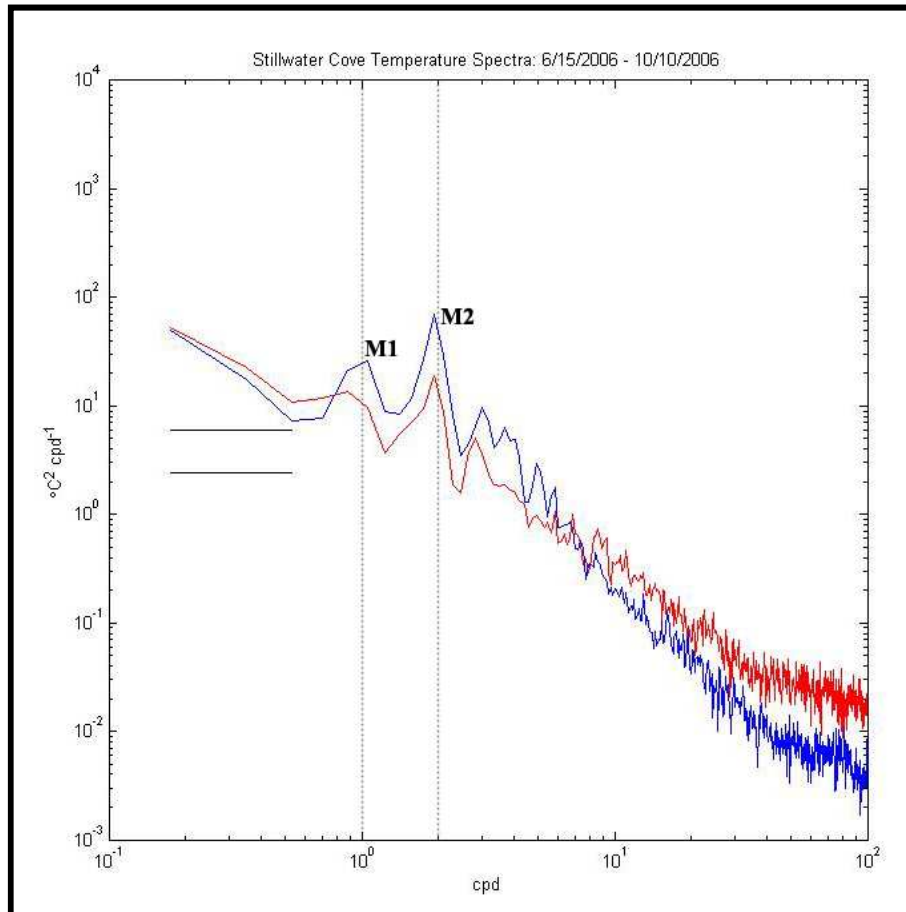


Figure 18: Spectral analysis of Stillwater Cove near-surface and bottom temperatures. [June 15th 2006 to May 18th 2007]. The red is near-surface depth and blue is bottom depth. Black horizontal lines represent error bars.

Coherence results between Stillwater Cove thermistor time series and Monterey Bay tidal height data is displayed in Figure 19. The date range of this time series was from June 15th 2006 – May 18th 2007. There are strong distinct peaks in the diurnal and semi-diurnal frequencies, with the strength of the semi-diurnal signal dominating over the diurnal signal. Both diurnal and semi-diurnal peaks are above the 95% confidence interval. The diurnal and semi-diurnal signals are both almost ~ 180 degrees out of phase with the tidal signal. This is an interesting result as it implies that internal waves in Stillwater Cove are persistently phase locked with both the diurnal and semi-diurnal tide.

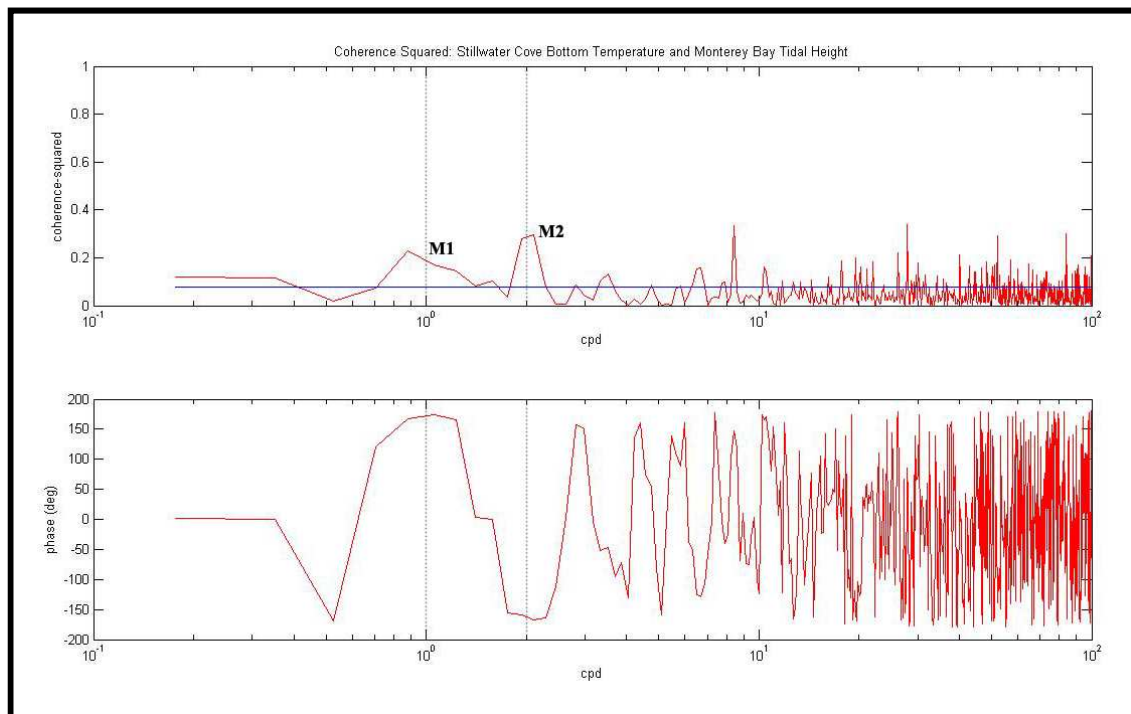


Figure 19: Coherence of Stillwater Cove bottom temperatures and Monterey Bay tidal height. [June 15th 2006 – May 18th 2007]. Blue line represents 95% confidence interval.

3.3 High Frequency Variability

Internal waves are a common occurrence in Stillwater Cove during stratified summer conditions. The arrival of these internal waves is strongly correlated and phase locked with the rising peak diurnal and semi-diurnal high tide (Figure 20). When combined with upwelling conditions and a shallow thermocline, these internal waves are an important mechanism for delivering nutrient-rich bottom water to the upper water column. These durations were measured at bottom depth where the internal wave front dropped the temperature a least two degrees to when temperatures returned to background levels. The time duration of the internal waves associated with the diurnal tide is ~ 4 hours, while the time duration of the internal waves associated with the semi-diurnal tide is ~ 2 hours. The cold bottom water that is vertically displaced is 2°C colder than the mean temperature in the water column. This cold water associated with diurnal internal waves reaches near-surface depths, while the semi-diurnal internal waves only reach the lower half of the water column (20 – 10 m). During October, internal waves were still consistently propagating into the Stillwater Cove water column (Figure 21). The duration and phase of these internal waves were similar to summer conditions; however, the cold bottom water vertically displaced by the internal waves was up to 2.5°C colder than background temperatures in the water column. While during summer, temperatures in the upper water column (6 m) were often affected by diurnal internal waves. During October, the cold water pulses from diurnal internal waves did not reach as high in the water column, and near-surface temperatures remained far more constant.

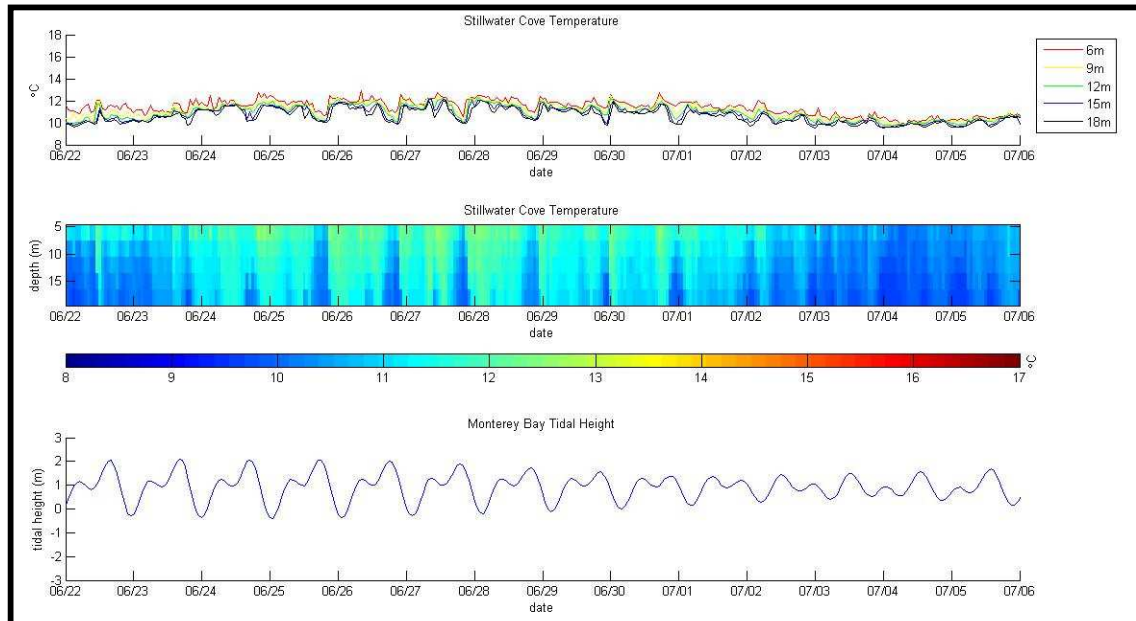


Figure 20: Internal waves in Stillwater Cove during two weeks of summer [June 22nd 2006 to July 6th 2006].

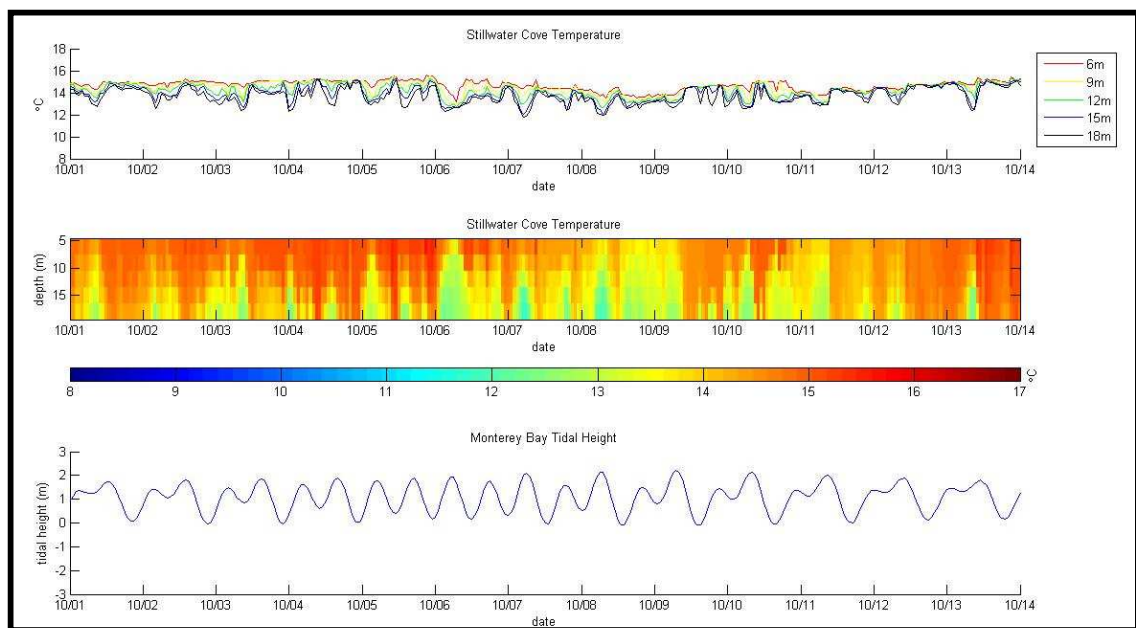


Figure 21: Internal waves in Stillwater Cove during two weeks of summer [October 1st 2006 to October 14th 2006].

3.3 Deep Response to Tides: Internal Waves between 0 and 100 m.

On October 31st 2007, repeated CTD profiles of the water column in Carmel Bay were made on the R/V Martin using a SeaBird SBE 25. The sampling location was located in the main branch of the Carmel Canyon at 36° 32' 35" N / 121° 58' 57" W. The depth was ~ 300 m. The objective of this cruise was to sample the effects of the internal tide on the water column. Sampling was conducted from 10:00 PDT to 16:00 PDT. This time range encapsulated the diurnal low tide rising to a semi-diurnal high. A total of 11 casts from 0 to 200-m depths were made over a period of 6 hours (Figure 22). CTD casts were made approximately every 30 minutes. During the sampling, the 9°C isotherm was upwardly vertically displaced by ~ 60 m. The 9°C isotherm reached its shallowest depth of ~ 120 m at 13:15 PDT, an hour and fifteen minutes after the peak semi-diurnal high tide. The effect of the internal tide on isotherm displacement was noticeable at shallower depths, but far less pronounced. Isotherms deeper than ~ 40 m experienced the same rate of shoaling, but the deeper isotherms shoaled for a longer time period. The 9.5°C isotherm at 140-m depth was vertically displaced 40 m, while the 10°C isotherm at 80-m depth was displaced 20 m.

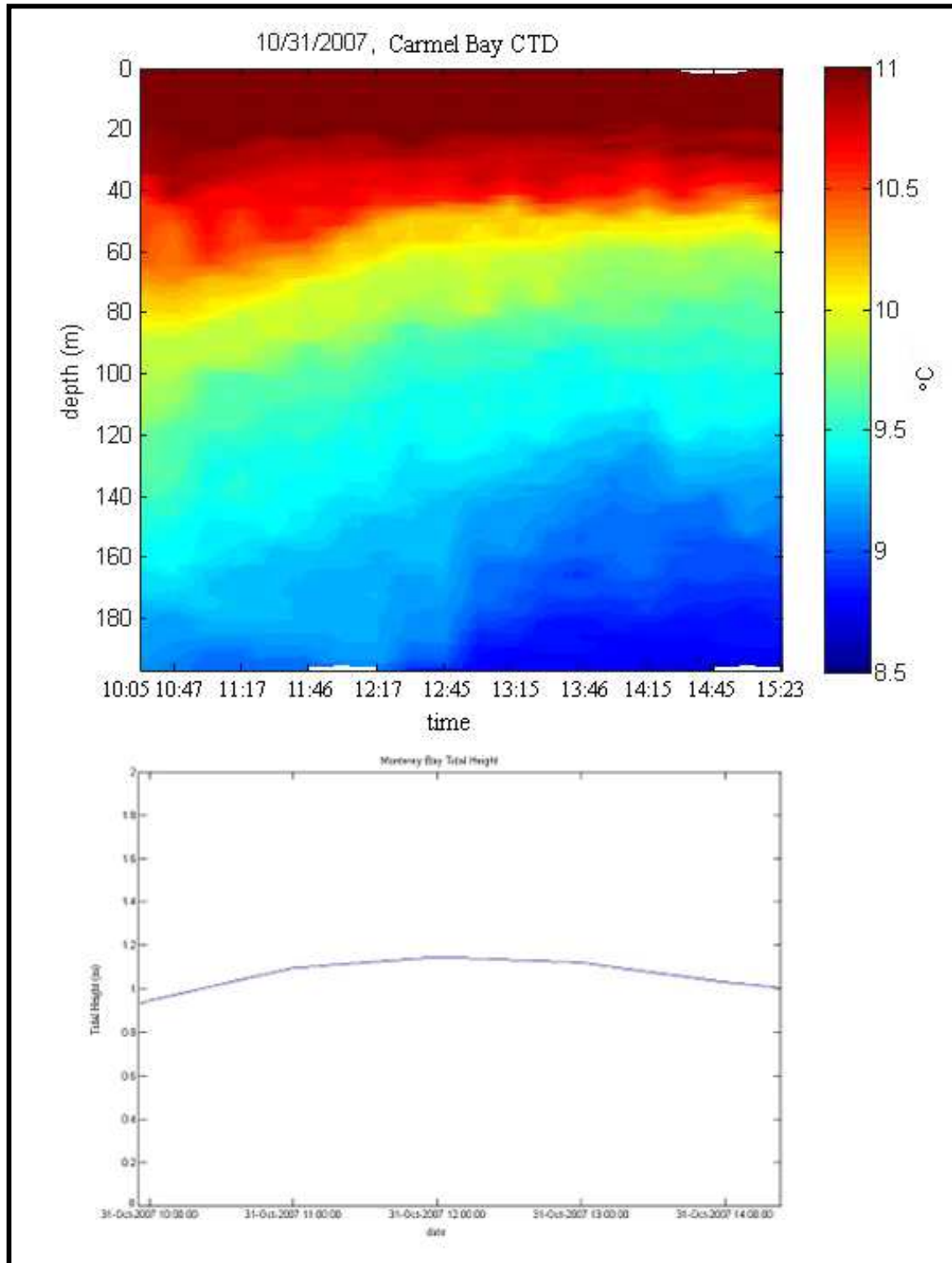


Figure 22: Repeated CTD casts in Carmel Bay on October 31st 2007.

Temperature profiles from Stillwater Cove during the October 31st cruise show the arrival of internal waves phase locked with the diurnal and semi-diurnal tide (Figure 23). The front of the semi-diurnal internal wave arrived at 4:00 PDT, approximately at the peak diurnal low tide. This front was visible only at bottom depth. Two hours after the arrival of the internal wave front, the temperature at 18-m depth had dropped by 0.2°C. Although this front cooled the bottom of the water column, temperatures in the rest of the water column did not decrease significantly until 8:00 PDT. At 8:00 PDT, a second cold water front in the upper portion of the water column caused temperatures at 15, 12, and 9-m depths to drop by 0.2°C. At 6-m depth, the temperature dropped 0.1°C. This front occurred during the rising semi-diurnal tide. The decrease in temperature due to the internal wave last lasted ~ 2 hours, consistent with the duration of summer and fall semi-diurnal internal waves.

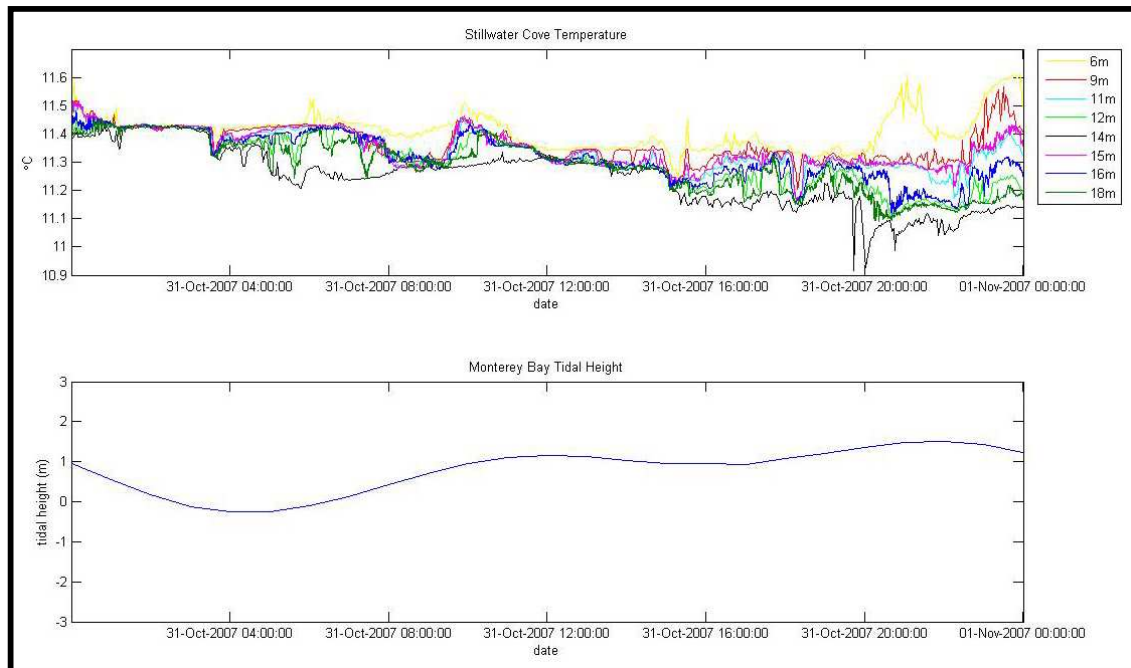


Figure 23: Internal Waves in Stillwater Cove on October 31st 2007.

Figures 24 and 25 show currents in the Stillwater Cove water column during a typical summer period when strong diurnal and semi-diurnal internal waves were present. The arrival of the internal waves is correlated with the rising diurnal and semi-diurnal tide. It took ~ 2 hours on average for the semi-diurnal front of cold water to reach its peak in middle of the water column and 1 hour for the temperature to return to the mean temperature of the water column. For the diurnal front of cold water, it took on average ~ 4 hours for the front to reach near surface depths. After the front had reached its peak, the return to background temperatures was very abrupt. This temperature increase on average lasted 1 – 2 hours. During the rising diurnal tide, cross isobath currents were directed offshore with the strongest currents at bottom depth. Immediately after the peak diurnal tide (< 1 hour), the cross isobath current direction rotated from onshore to offshore while the barotropic along-isobath currents were poleward. Both the offshore and onshore currents were strongest at depth. This change in cross-isobath current direction immediately follows the end of the internal wave front.

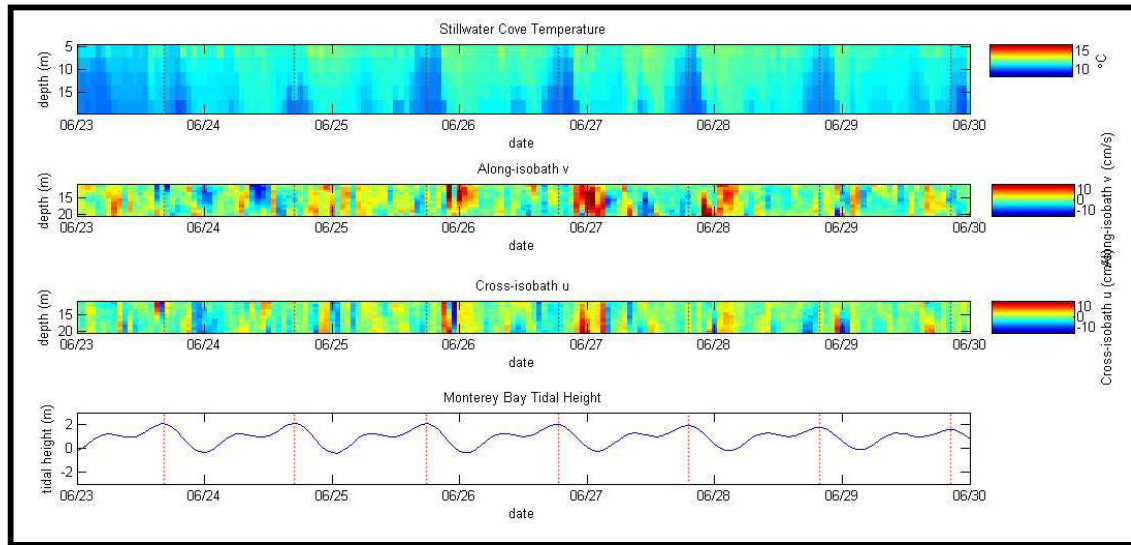


Figure 24: Pseudocolor plot of Currents in Stillwater Cove during June 2006. Currents are rotated into an along-isobath and cross-isobath coordinate system.

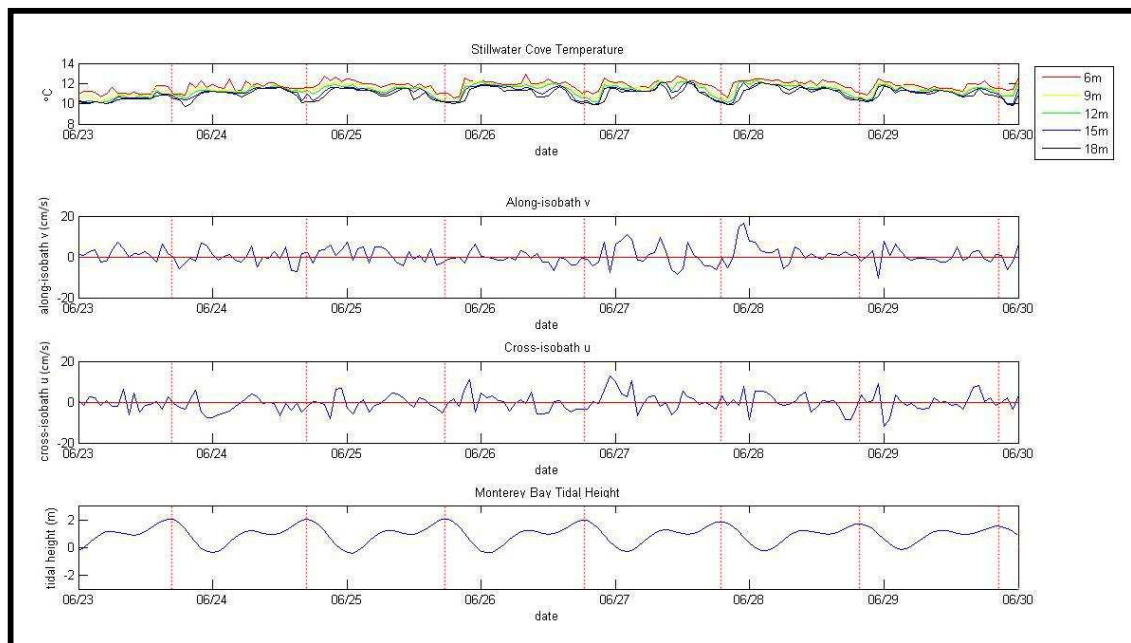
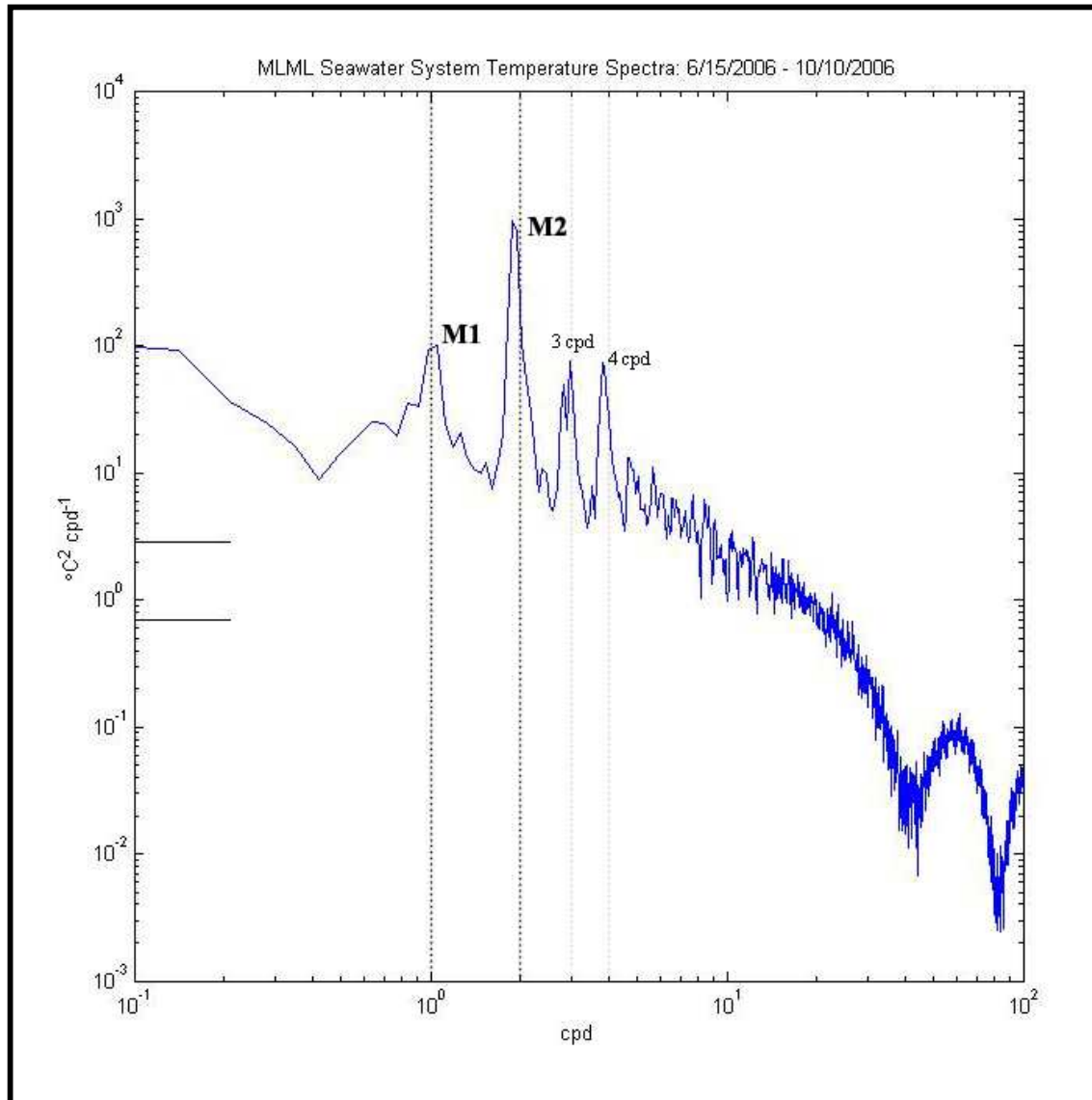


Figure 25: Currents in Stillwater Cove during June 2006. Currents are rotated into an along-isobath and cross-isobath coordinate system.

3.3 Monterey Bay Spectral Results – Along Coast Distribution

For this section of the paper, the spectral results from each mooring location will be described first, followed by the coherence results. For both the spectral and coherence results, locations will be described in order of closest proximity to a submarine canyon. Starting with the mooring location that has the closest proximity to a submarine canyon head, Figure 26 displays the spectral results from the MLML seawater intake system located at the head of the Monterey Canyon in shallow water (20m). This spectrum has extremely strong peaks at the diurnal and semi-diurnal tidal periods, with an array of distinctly shaped tidal harmonics. The peak at the semi-diurnal tidal period is the dominant signal in the spectra. Moving outside Monterey Bay to the three locations within close proximity to Carmel Canyon (Stillwater Cove, Weston Beach, and Sunset Point), strong peaks in the diurnal and semi-diurnal tidal signal are present in the spectra along with multiple tidal harmonics (Figure 27). These spectra bear a strong resemblance to the Monterey Canyon spectra, with the semi-diurnal tidal period having the strongest power. At all three locations within close proximity to Carmel Canyon, the semi-diurnal tidal signal intensifies with increased depth.



*Figure 26: Monterey Canyon head thermistor spectral results at near-bottom depth.
Black lines represent error bars.*

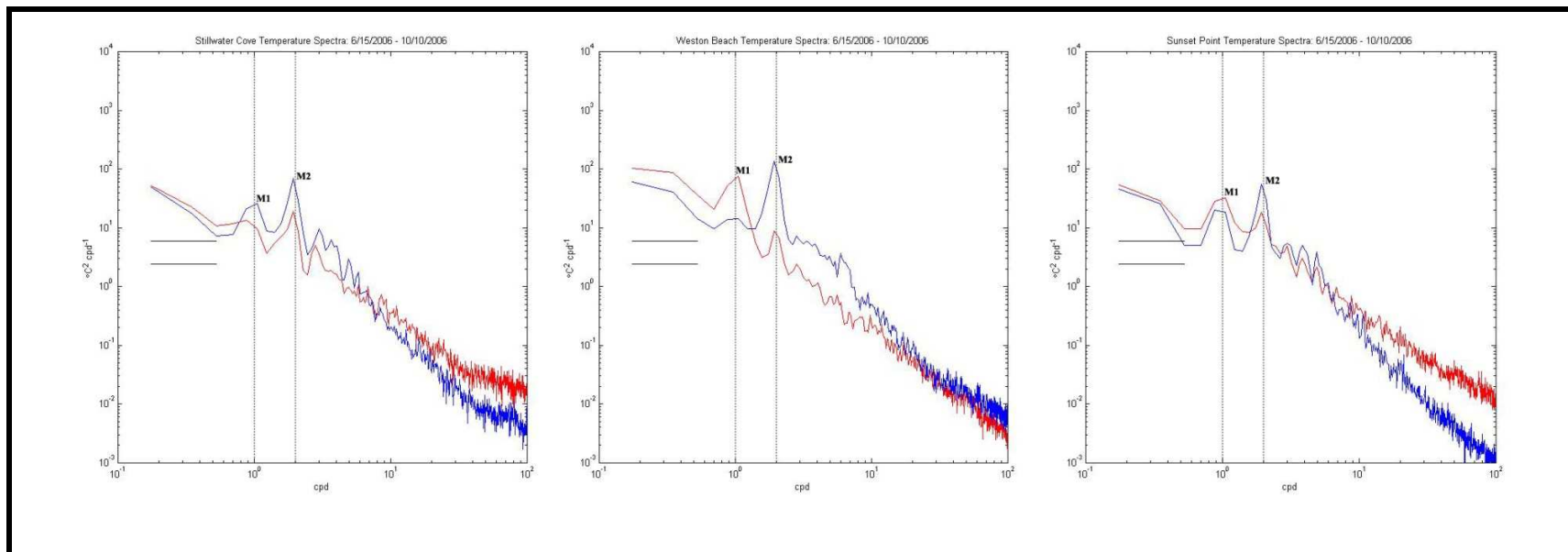


Figure 27: Carmel Bay thermistor spectral results at near-surface and near-bottom depths Black lines represent error bars.

Moving further away from close proximity to the Monterey and Carmel Submarine Canyons, the spectral results from the Inner Monterey Shelf are displayed in Figure 28. At these two locations (Point Joe and Lovers' Point), the diurnal tidal peak is stronger than the semi-diurnal tidal peak and there is no significant bottom intensification in either the diurnal or semi-diurnal tidal signal with increased depth. This is a very different system from the nearby mooring locations at Monterey and Carmel Submarine Canyons, where the semi-diurnal tidal peak dominates the spectra and increases significantly with depth. Multiple tidal harmonics are still visible in the spectra; however, their peaks are not as distinct as the harmonics observed at near canyon locations. Moving outward to the greater Monterey Shelf, the spectral results from Point Sur and Soquel Point are shown in figure 29. At both locations, the near-surface diurnal and semi-diurnal tidal signals are significantly stronger than the near-bottom signals. At both the near-surface and near bottom depths, the diurnal tidal signal dominates over the semi-diurnal tidal signal. At the Point Sur location, there is no visible diurnal tidal signal at the near-bottom depth and tidal harmonics are greatly diminished compared to near canyon locations. The spectral results from these locations are the reversal of the spectral results from the near canyon locations.

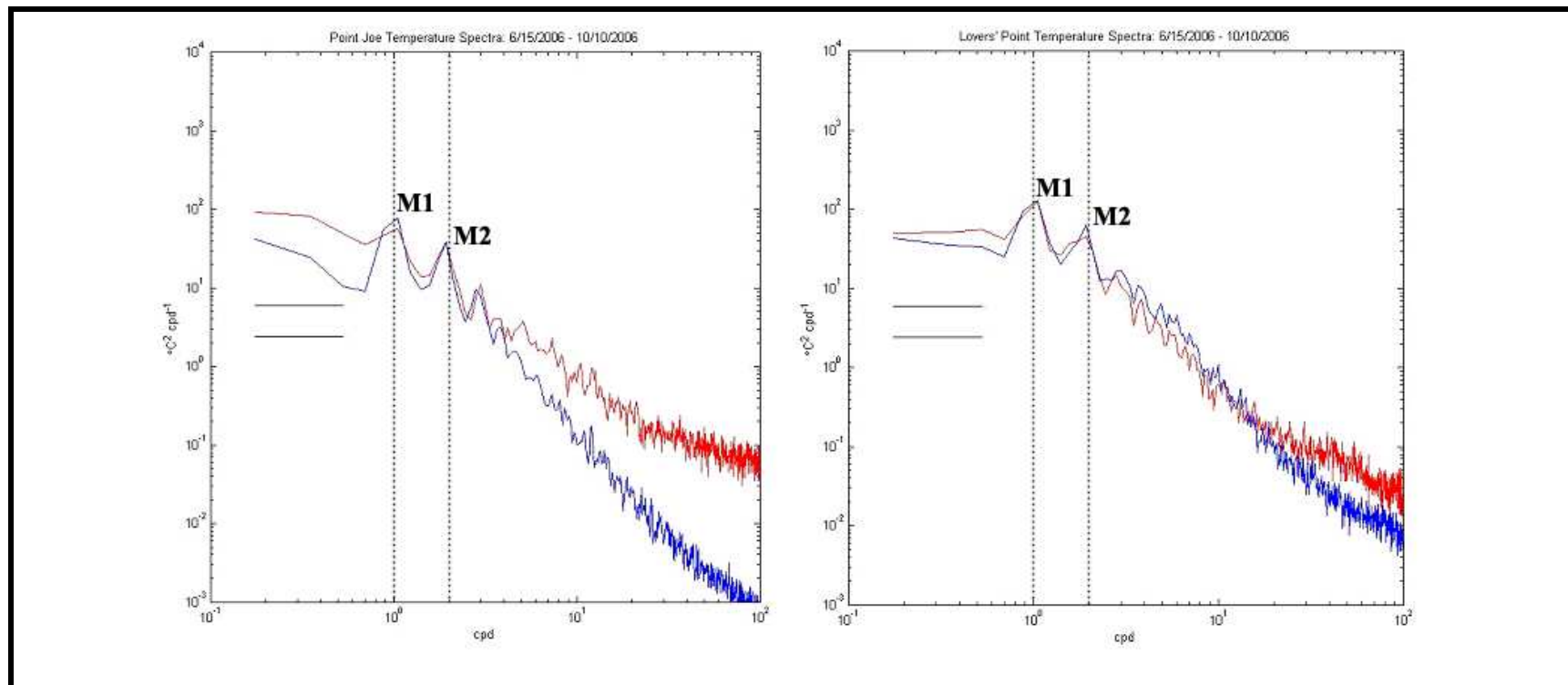


Figure 28: Inner Monterey Shelf thermistor spectra at near-surface and near-bottom depths. Black lines represent error bars.

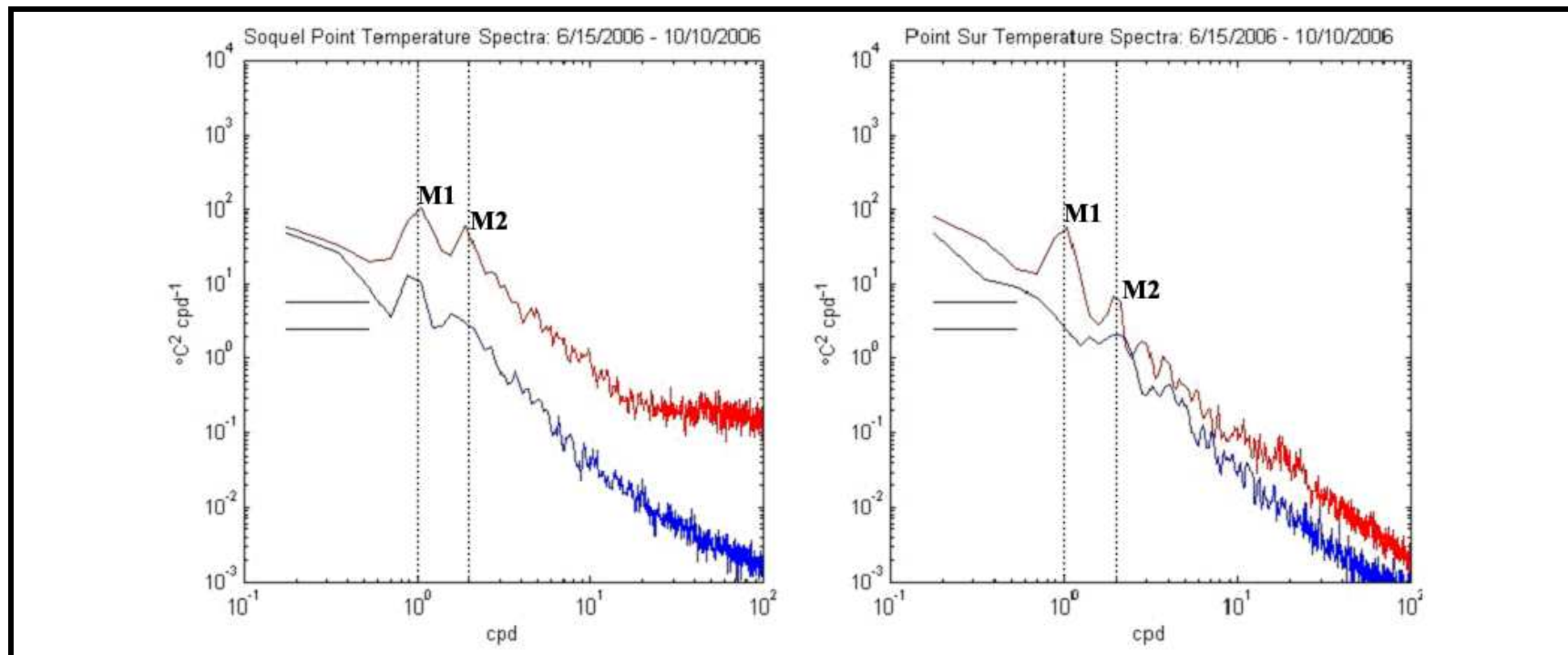


Figure 29: Greater Monterey Shelf thermistor spectral results at near-surface and near-bottom depths. Black lines represent error bars.

Figure 30 displays the coherence results of the MLML seawater intake system near-bottom thermistor and the Monterey Bay tidal height. There is a strong correlation between the near-bottom thermistor and tidal signal at the diurnal and semi-diurnal tidal period. The diurnal temperature signal is almost completely in phase with the diurnal tidal signal, while the semi-diurnal temperature signal is ~ 180 degrees out of phase with the semi-diurnal tidal signal. This result implies that the crest of the internal waves at the head of the Monterey Canyon is correlated with a rising semi-diurnal tide. Moving outward to the three locations within close proximity to Carmel Canyon (Figure 31), there is a correlation between the near-bottom thermistor and the tidal signal at the diurnal and semi-diurnal tidal period. At all three locations, the diurnal and semi-diurnal coherence is above the 95% coherence level and the semi-diurnal temperature signal is ~ 180 degrees out of phase with the tidal signal. This result is the same as Monterey Canyon, suggesting that the phase locking of internal waves with the rising semi-diurnal tide is a consistent feature in both submarine canyons. The Weston Beach and Sunset Point diurnal temperature signals are not in phase with the tidal signal, while the Stillwater Cove diurnal temperature signal is ~ 180 degrees out of phase with the tidal signal. This is an interesting result, as it implies internal waves in Stillwater Cove are phase locked with both the rising diurnal and semi-diurnal tide.

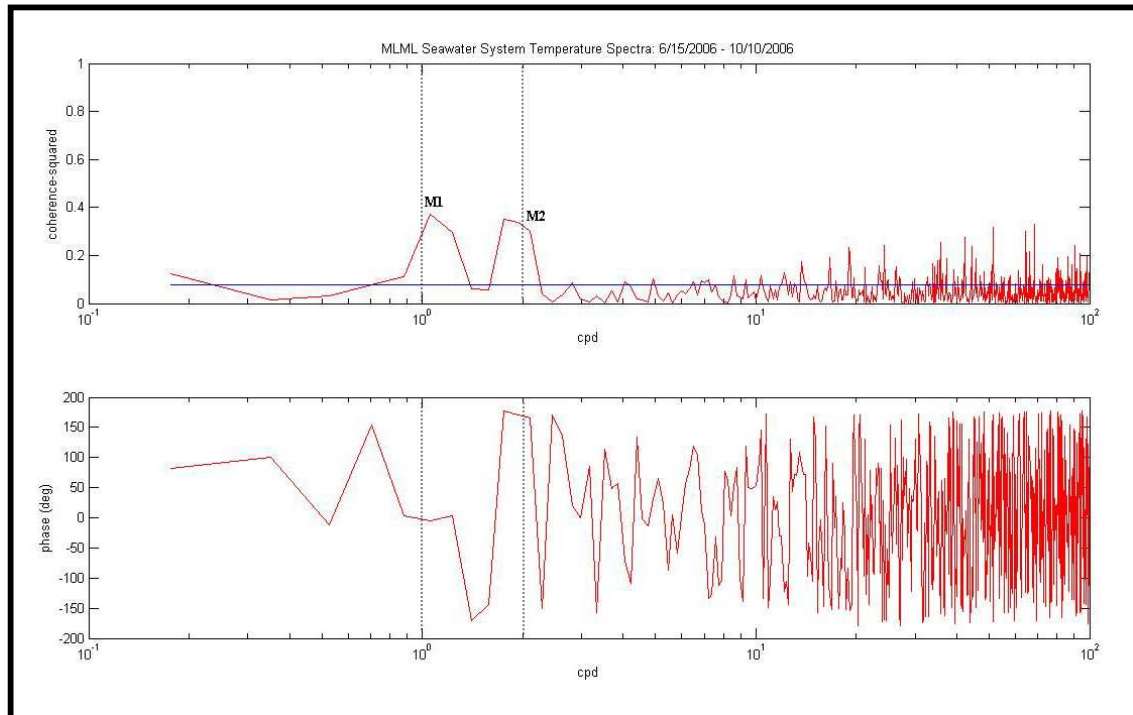


Figure 30: Monterey Canyon head near-bottom thermistor and Monterey Bay tide coherence results.

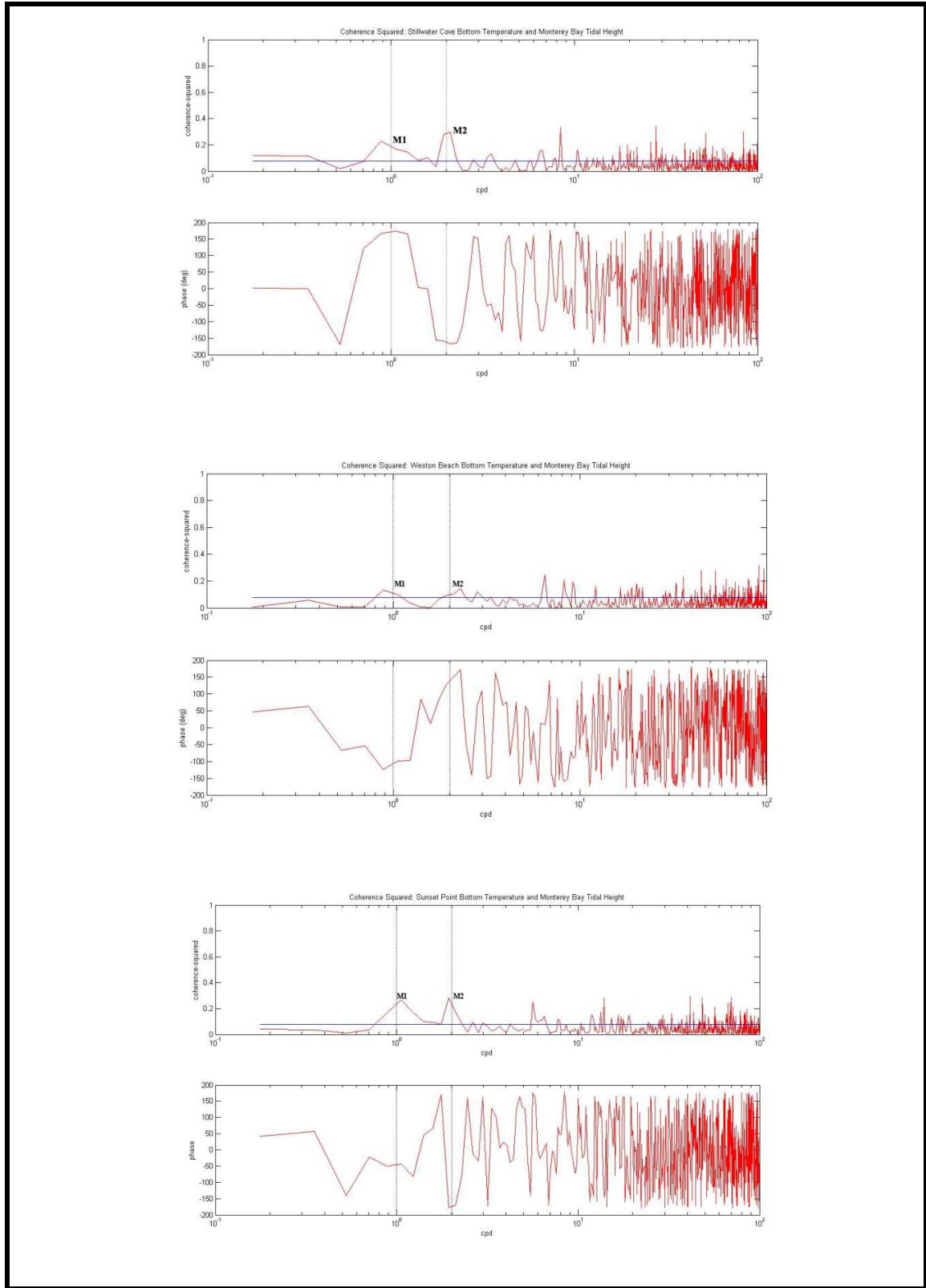


Figure 31: Carmel Bay near-bottom thermistor and Monterey Bay tide coherence results.

Moving further away from close proximity to Monterey and Carmel Submarine Canyons, the coherence results from the Inner Monterey Shelf are shown in Figure 32. There is coherence between the near-bottom thermistor and tidal signal at both the diurnal and semi-diurnal period tidal period. Unlike nearby Monterey and Carmel Submarine Canyons, the correlation at the diurnal period dominates the Inner Monterey Shelf. Point Joe's semi-diurnal near-bottom temperature signal is $\sim 25^\circ$ out of phase with the semi-diurnal tidal signal, while Lovers' Point near-bottom temperature signal is $\sim 100^\circ$ out of phase with the semi-diurnal tidal signal.

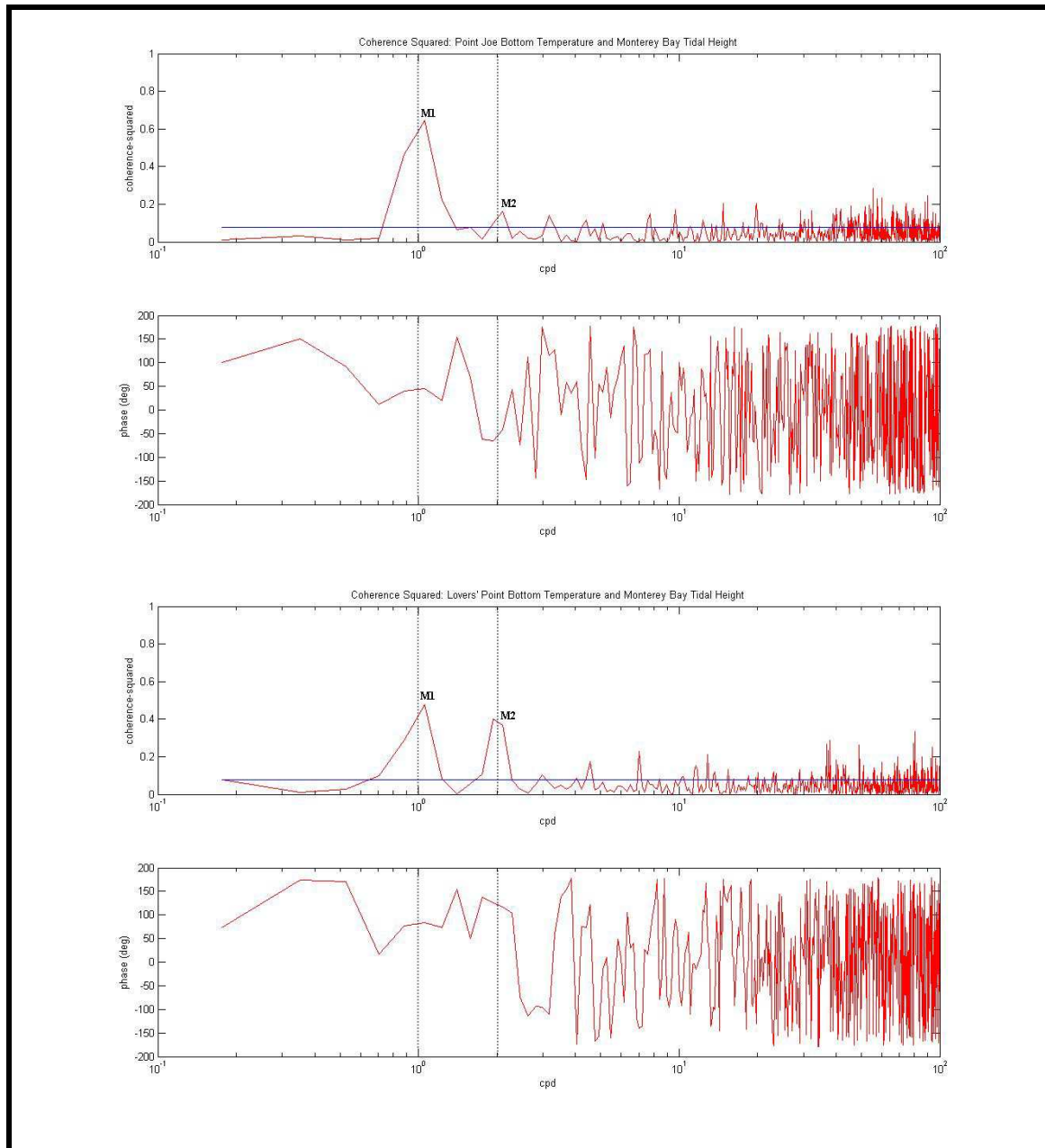


Figure 32: Inner Monterey Shelf near bottom-thermistor and Monterey Bay tide coherence results.

Moving outward to the greater Monterey Shelf, the coherence results from Point Sur and Soquel Point are displayed in Figure 33. At Soquel Point, there is significant diurnal coherence and weak semi-diurnal coherence that is below the 95% confidence level. This is dissimilar from locations near submarine canyons. At Point Sur, there is significant semi-diurnal coherence and weak diurnal coherence that is below the 95% confidence level. The near-bottom temperature diurnal signal is $\sim 50^\circ$ out of phase with the diurnal tide, and the near-bottom semi-diurnal temperature signal is $\sim 25^\circ$ out of phase with the semi-diurnal tide. Finally, the diurnal and semi-diurnal power spectral density values of the near-bottom and near-surface thermistors from all the mooring locations are displayed in Figures 34 and 35.

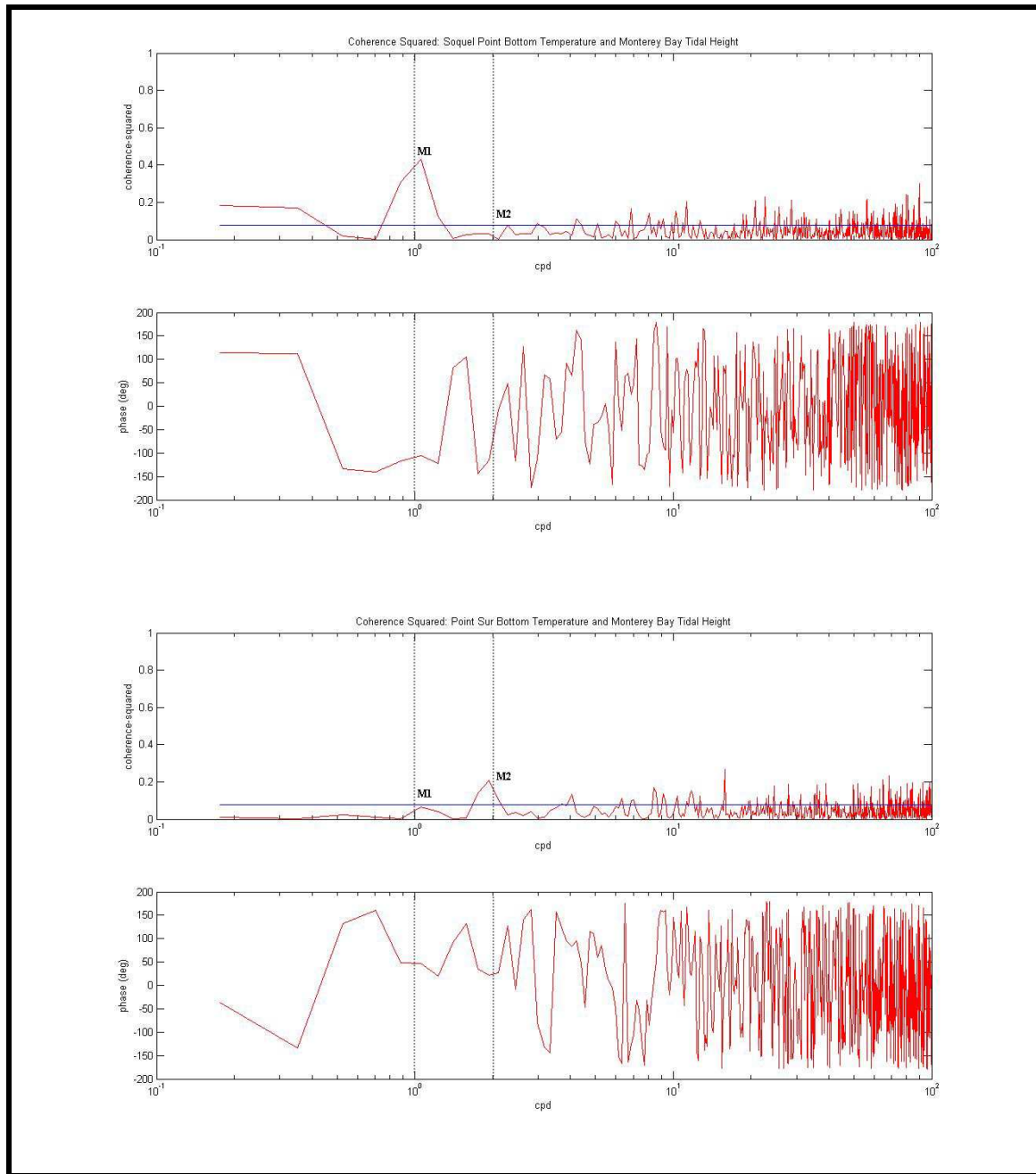


Figure 33: Greater Monterey Shelf near-bottom thermistor and Monterey Bay tide coherence results.

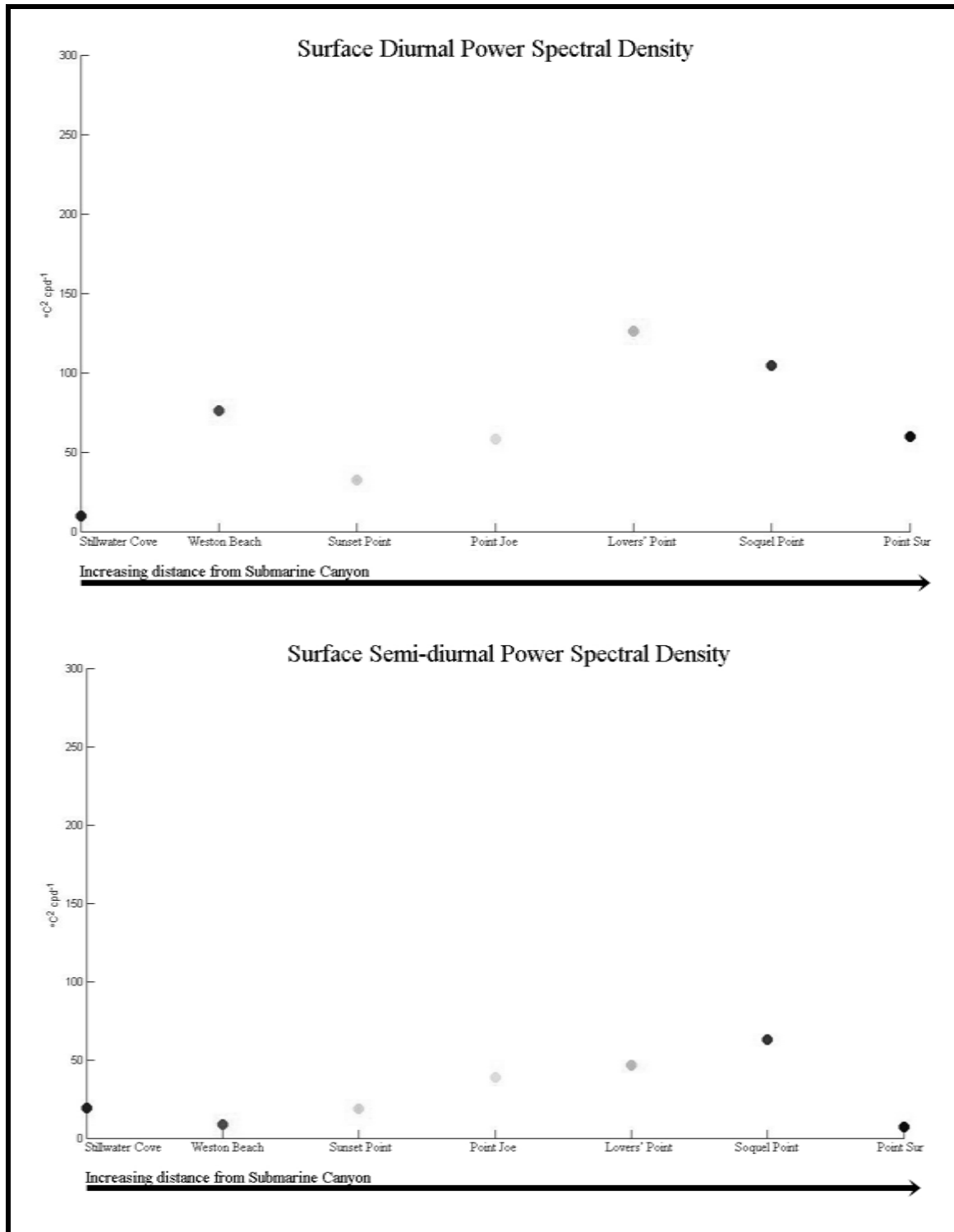


Figure 34: Diurnal near-surface and near-bottom power spectral density for all mooring locations.

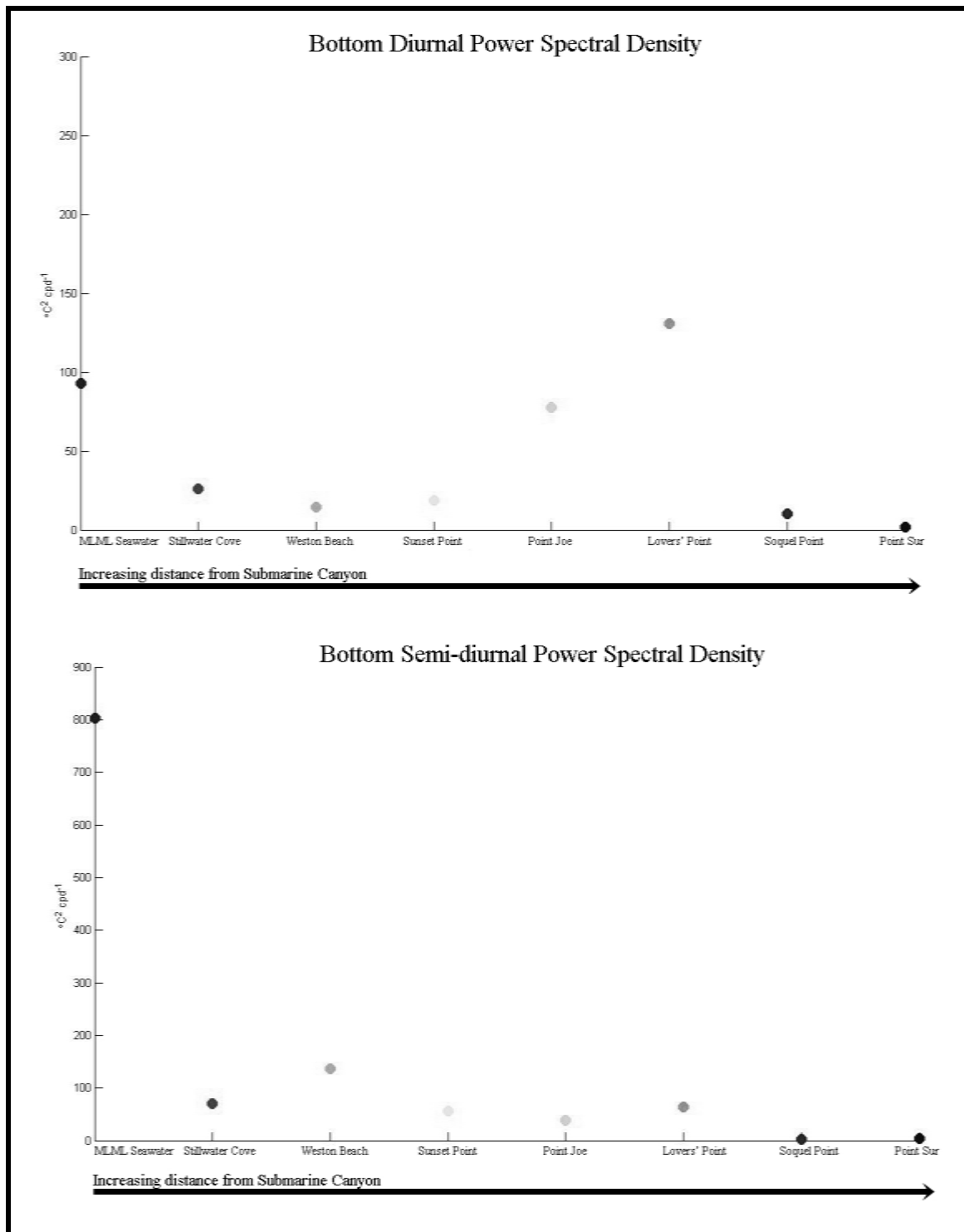


Figure 35: Semi-diurnal near-surface and near-bottom power spectral density for all mooring locations.

3.4 Stillwater Cove Nutrient Model

Flow rates and nutrient concentrations from the Stillwater Cove storm drain were manually measured during summer and winter (Table 1). A total of 5 separate winter storm events were sampled. Year round flow rates at Stillwater Creek were extremely low, and the resulting terrestrial input from the creek was considered insignificant for the purposes of this model. Storm drain flow rates were strongest during the winter storm events, ranging from 0.45 to 0.67 m/s. Summer flow rates were much lower, averaging 0.2 m/s. The highest nitrate concentrations were observed during summer, with a maximum of 563.2 μM and an average of 330 μM during dry summer conditions. Winter nitrate concentrations were greatly diluted, with a maximum of 56.7 μM and an average 30.14 μM of during wet conditions. The average rainfall during the sampled winter storm events was 0.35 inches per day. Rainfall in the Monterey Bay is highly seasonal, and the majority of annual rainfall occurs during a small number of intense winter storms. During the 2007 winter season, Monterey Bay experienced 13 storms with rainfall levels above this average (Figure 36). The strongest storms occurred during January and February, while May through September were completely dry months.

Table 1: Summary of terrestrial samples.

Date:	Location:	Nutrient:	□ μM:	Flow rate (m/s):	Stormdrain:	Area(m ²):	Rate (m ³ /s):	Liters per day:	Rainfall per day (in):
7/4/2007	SW Drain	NO3	563.2	0.2	1/6 full	0.076	0.015	1296000	0
7/13/2007	SW Drain	NO3	96.8	0.2	1/6 full	0.076	0.015	1296000	0
10/10/2007	SW Drain	NO3	32.52	0.5	1/6 full	0.076	0.038	3283200	0.48
10/12/2007	SW Drain	NO3	20.74	0.45	1/6 full	0.076	0.034	2937600	0.17
01/25/08	SW Drain	NO3	56.7	0.67	1/6 full	0.076	0.05	4320000	0.54
02/02/08	SW Creek	NO3	1.68	N/A	N/A	N/A	N/A	N/A	0.27
02/02/08	SW Drain	NO3	23.31	0.45	1/2 full	0.23	0.103	8899200	0.27
02/24/08	SW Drain	NO3	17.44	0.45	1/4 full	0.11	0.049	4233600	0.39
Summer Avg	SW Drain	NO3	330	0.2	1/6 full	0.076	0.015	1296000	0
Winter Avg	SW Drain	NO3	30.14	0.5	1/4 full	0.11	0.055	4752000	0.35

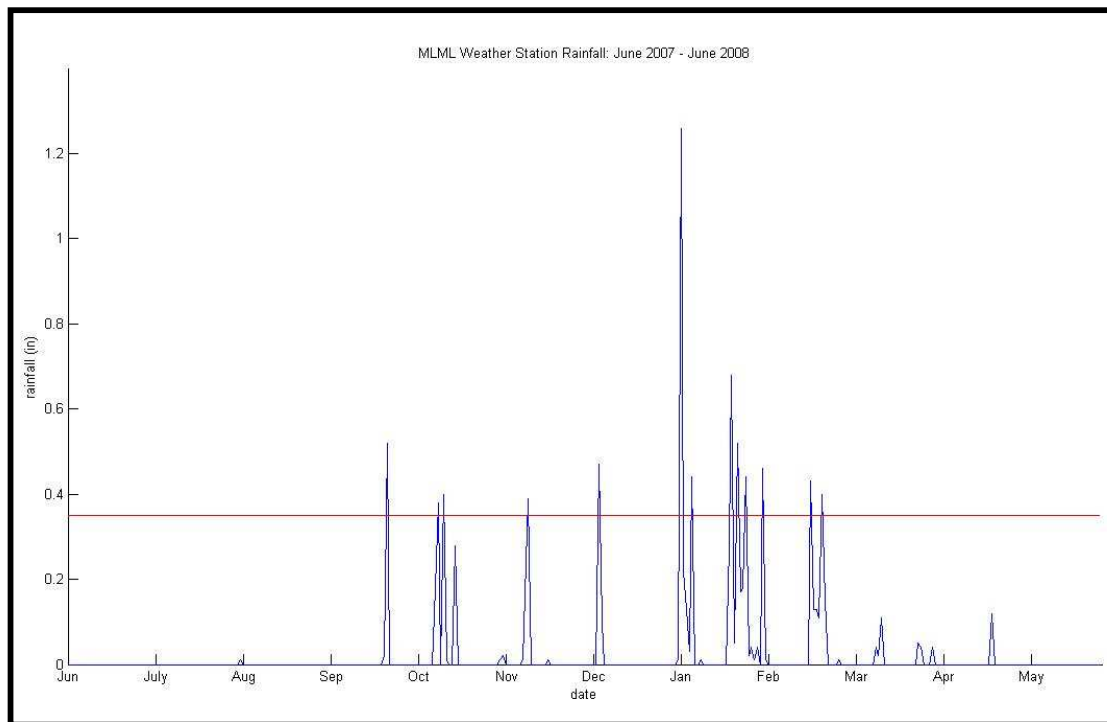


Figure 36: MLML Weather Station rainfall data. Red line indicates average rainfall during sampled winter storm events.

An estimate of nitrate concentrations in Stillwater Cove from both terrestrial and oceanographic sources is shown in Figures 37 and 38. Using the calculated temperature nitrate relationship from the MBARI M2 mooring, a continuous proxy nitrate time series was estimated using temperature data from Stillwater Cove. The temperature time series at near-bottom depth (18 m) was chosen because the signal was affected by both upwelling and internal waves. The estimated nitrate time series was then bandpass filtered and isolated around the wind and tidal frequencies so contributions from both from upwelling and internal waves could be calculated. The wind frequency band ranged from 2 days to 2 weeks [0.714 to 0.33 cpd], while the tidal frequency band encompassed both the diurnal and semi-diurnal frequencies [0.9 to 2.2 cpd]. These

bandpassed signals were then added to the daily averaged minimum of the proxy nitrate time series. This provided a conservative estimate of the positive nitrate perturbations from the wind and tidal bands. The terrestrial estimates of wet and dry nitrate contributions to the Stillwater Cove volume were then applied to the MLML weather station rainfall time series (Figure 36). For the 1.5×10^9 liter volume, the calculations resulted in supply rates of $0.048 \mu\text{M L}^{-1} \text{ day}^{-1}$ for dry conditions and $0.157 \mu\text{M L}^{-1} \text{ day}^{-1}$ for wet conditions. For the 5×10^9 liter volume, the calculations resulted in supply rates of $0.012 \mu\text{M L}^{-1} \text{ day}^{-1}$ for dry conditions and $0.047 \mu\text{M L}^{-1} \text{ day}^{-1}$ for wet conditions. For the 1×10^{10} liter volume, the calculations resulted in supply rates of $0.006 \mu\text{M L}^{-1} \text{ day}^{-1}$ for dry conditions and $0.023 \mu\text{M L}^{-1} \text{ day}^{-1}$ for wet conditions. For the 183,970,000 liter volume based on Fish and Game GIS bathymetry of Stillwater Cove, supply rates ranged from $0.347 \mu\text{M L}^{-1} \text{ day}^{-1}$ for dry conditions, and $1.256 \mu\text{M L}^{-1} \text{ day}^{-1}$ for wet conditions. Wet conditions were determined as days when the rainfall level reached the average rainfall during sampled terrestrial winter conditions.

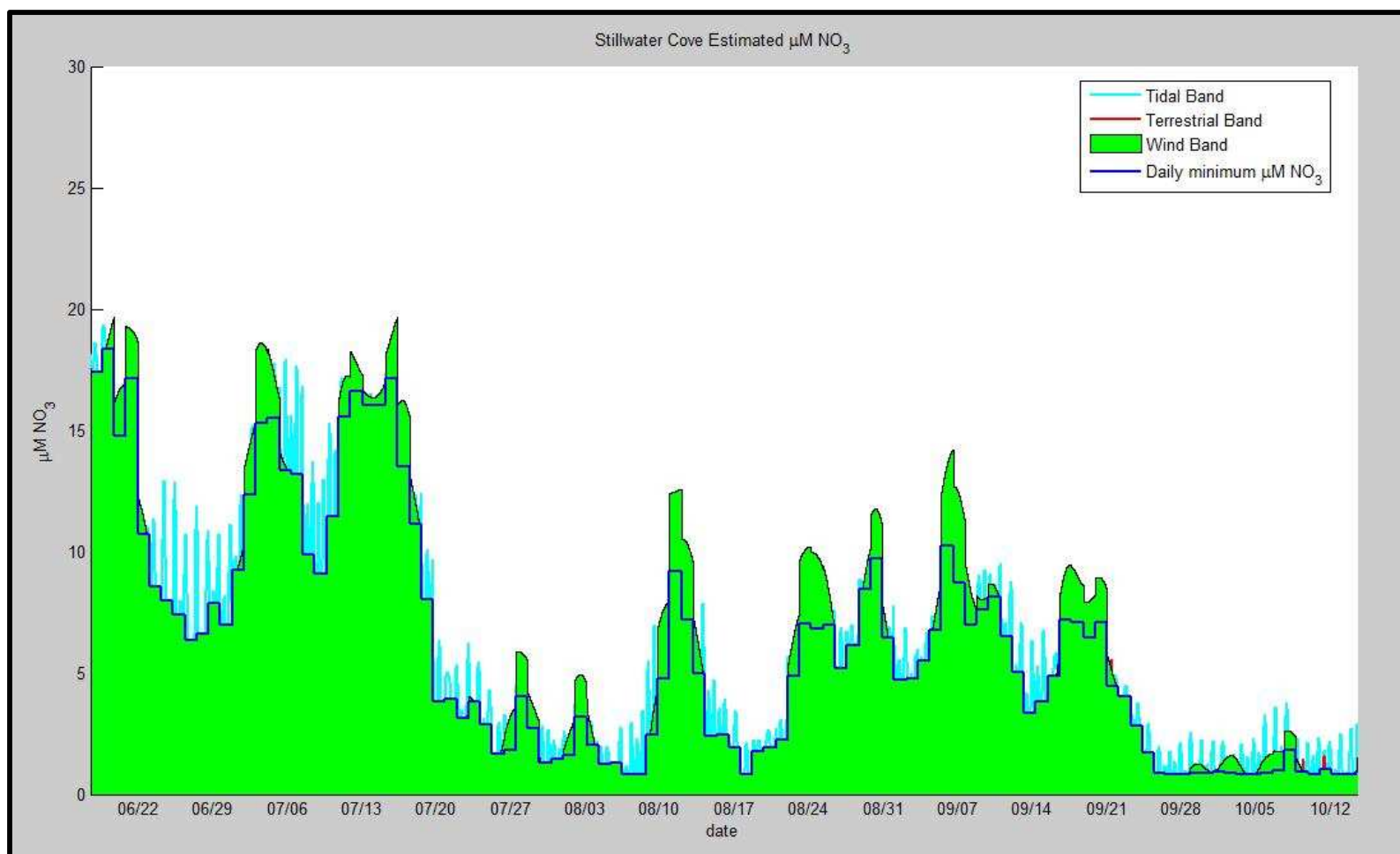


Figure 37: Stillwater Cove estimated NO_3 during summer conditions [6/15/2006 – 10/10/2006].

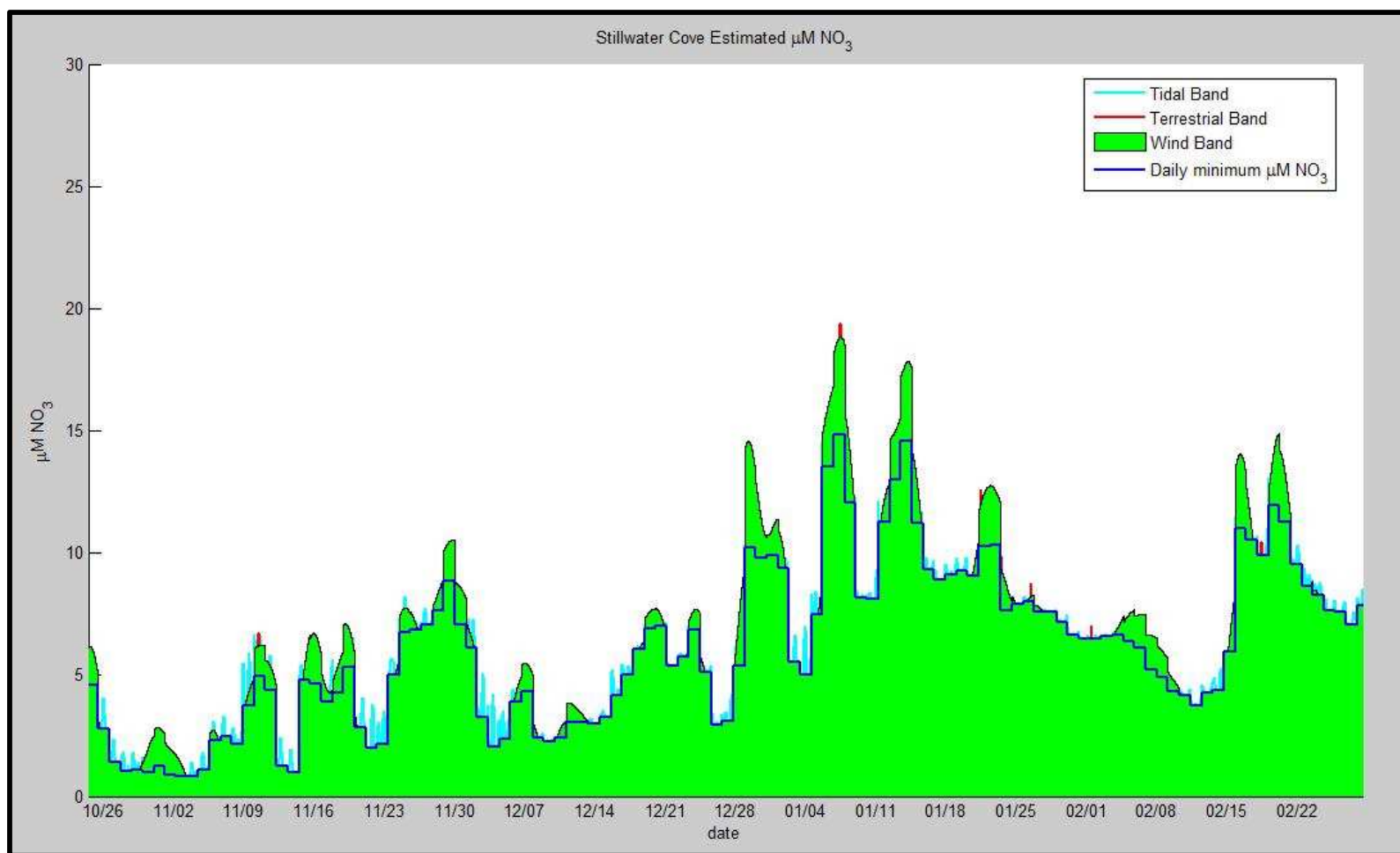


Figure 38: Stillwater Cove estimated NO_3 during winter conditions [10/25/2006 – 3/1/2007].

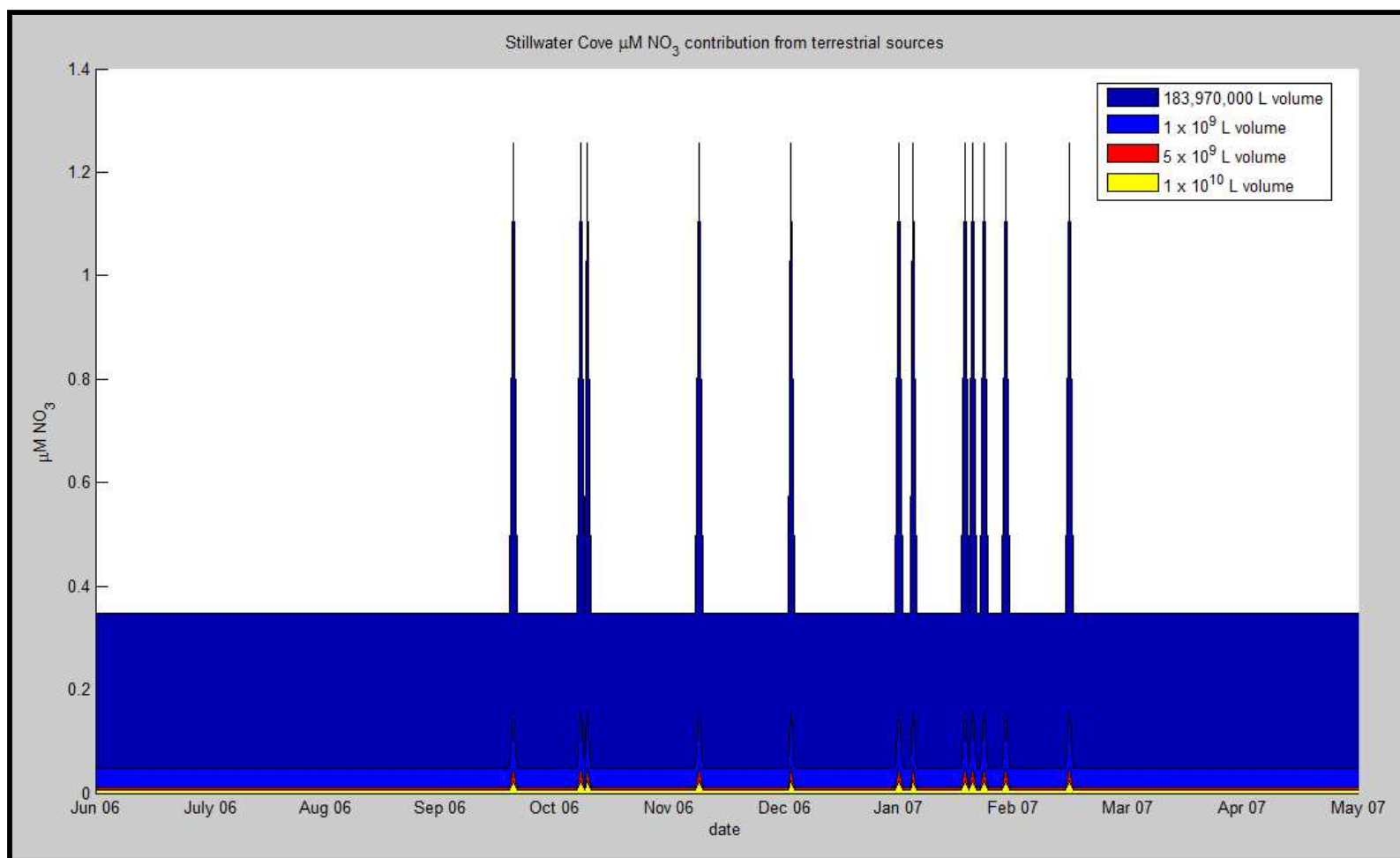


Figure 39: Stillwater Cove estimated NO_3 contributions from terrestrial runoff using four different mixing volumes.

3.4 Greater Monterey Bay Nutrient Model and Budget

An estimate of nitrate concentrations in the Greater Monterey Bay from oceanographic sources is shown in figures 40 through 46. The temperature time series at near-bottom depth (~ 20 m) was chosen for calculation of the nitrate proxy signal because the temperature signal at that depth was affected by both upwelling and internal waves.

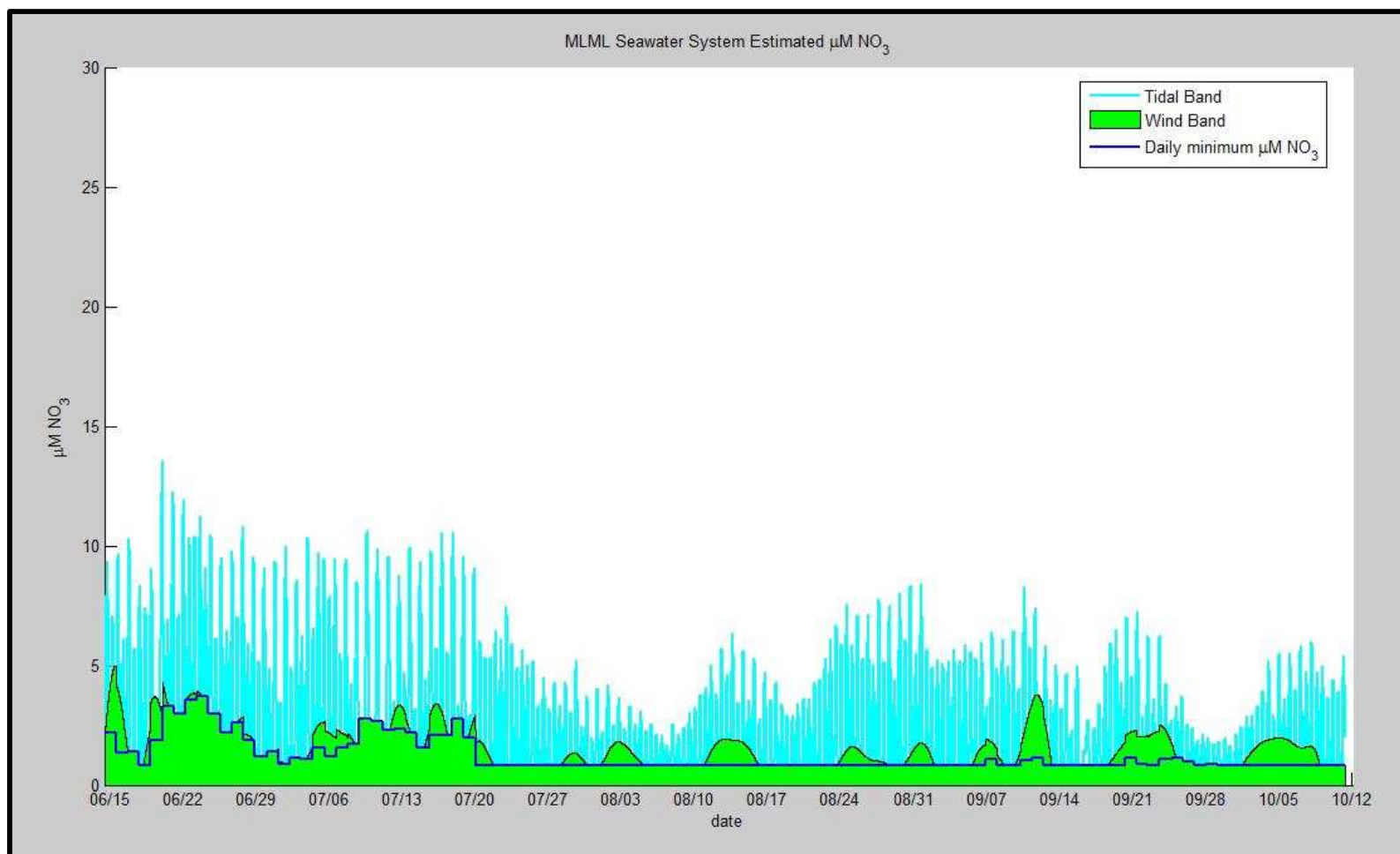


Figure 40: MLML Seawater System estimated NO_3 during summer conditions [6/15/2006 – 10/10/2006].

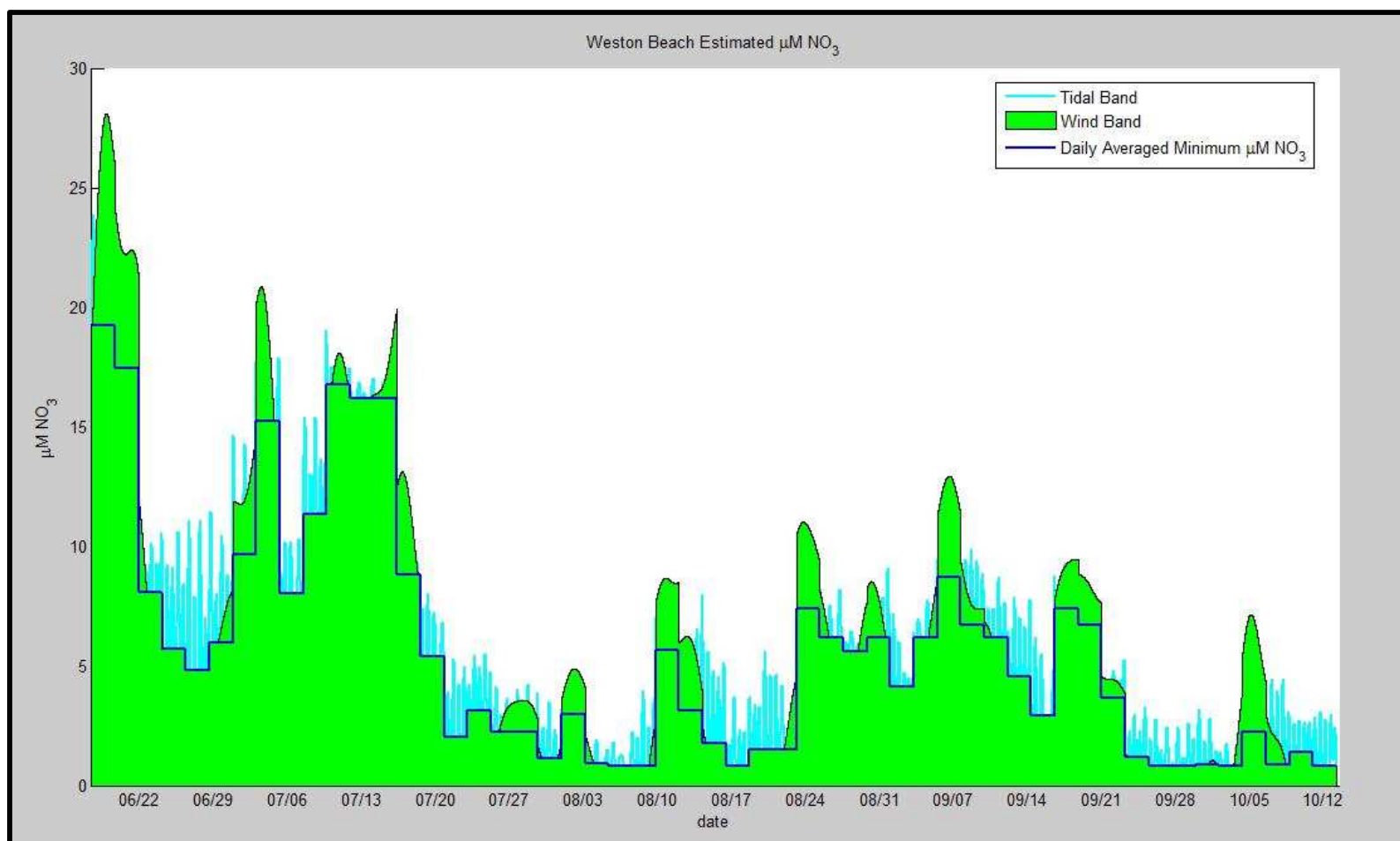


Figure 41: Weston Beach estimated NO_3 during summer conditions [6/15/2006 – 10/10/2006].

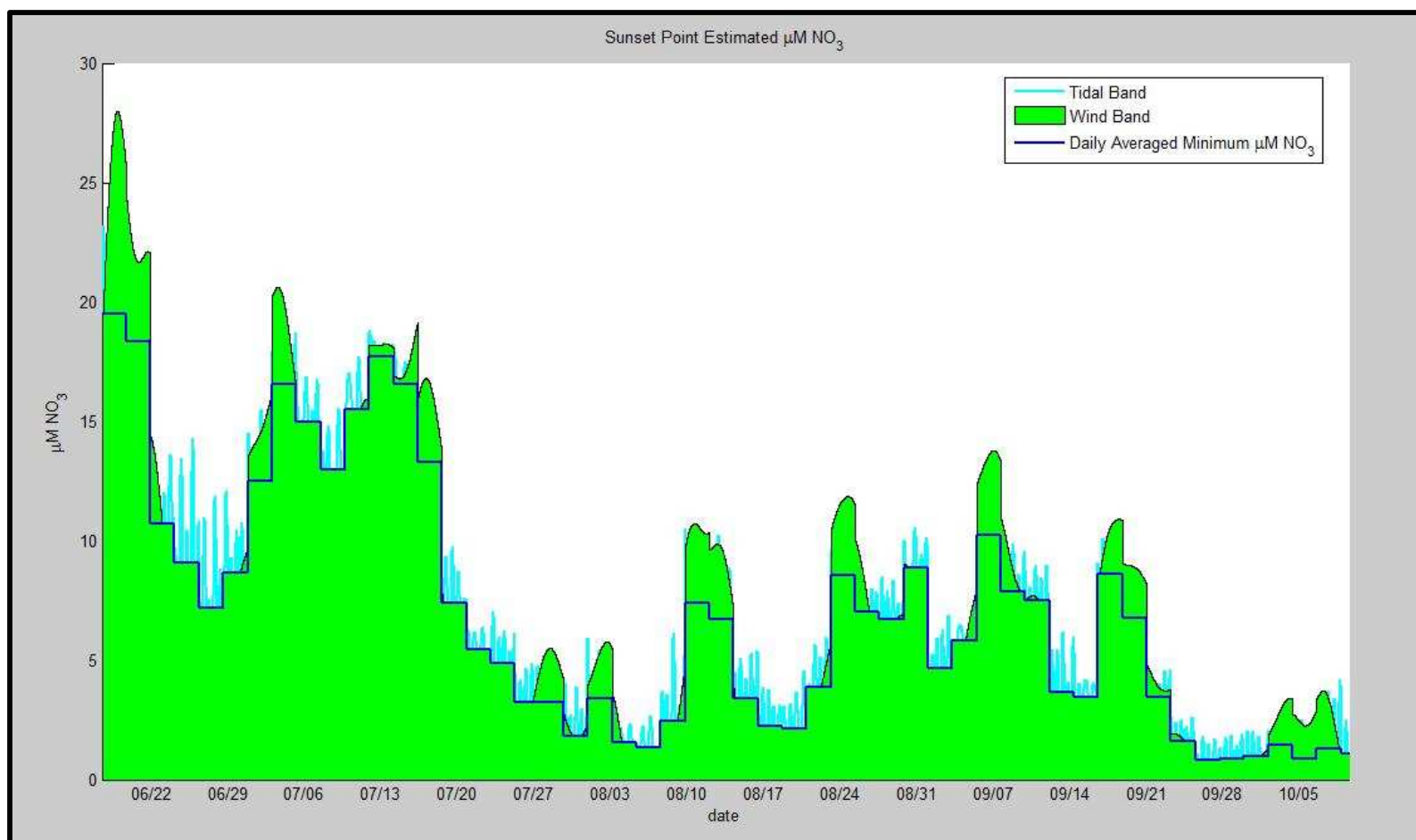


Figure 42: Sunset Point estimated NO_3 during summer conditions [6/15/2006 – 10/10/2006].

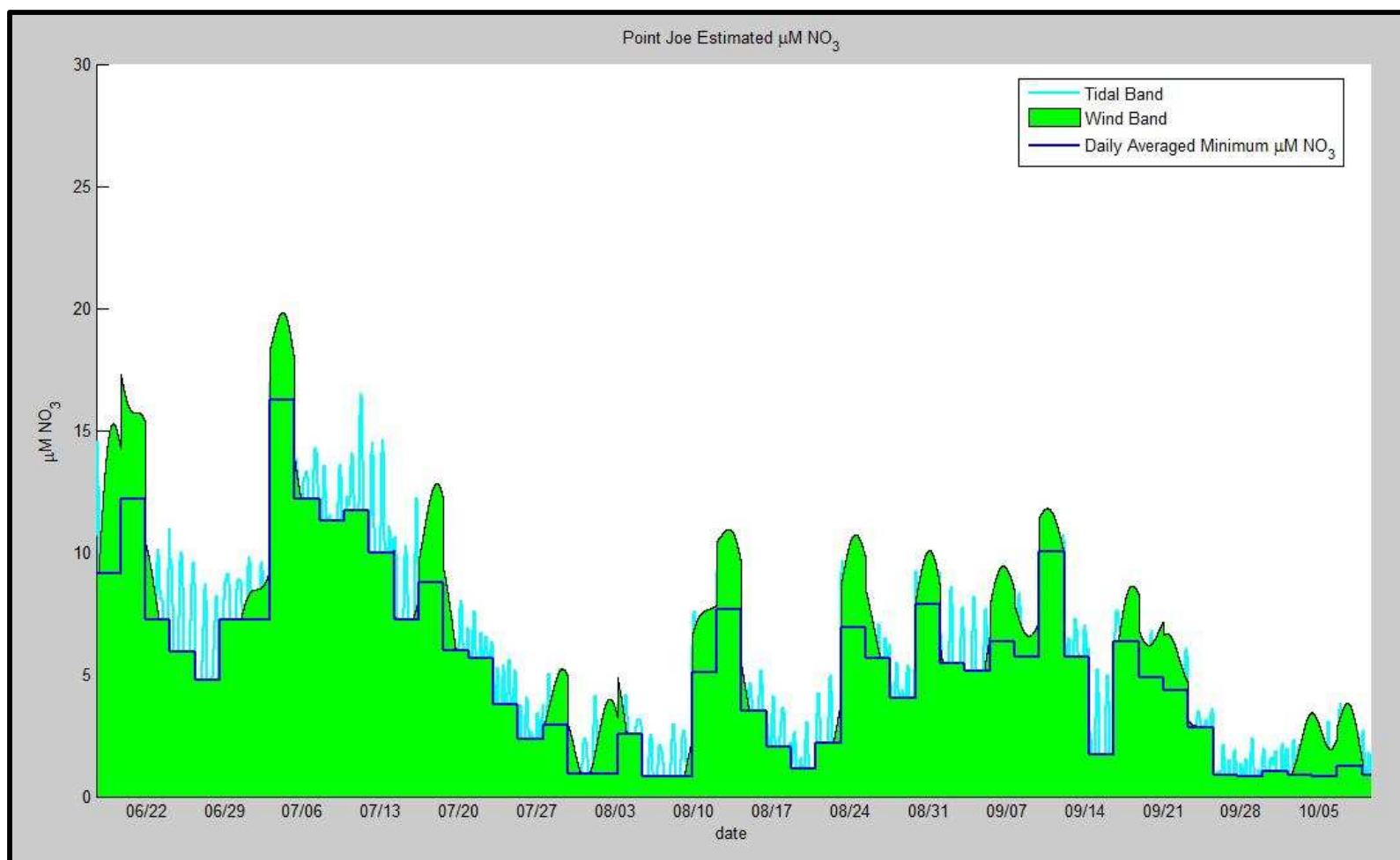


Figure 43: Point Joe estimated NO_3 during summer conditions [6/15/2006 – 10/10/2006].

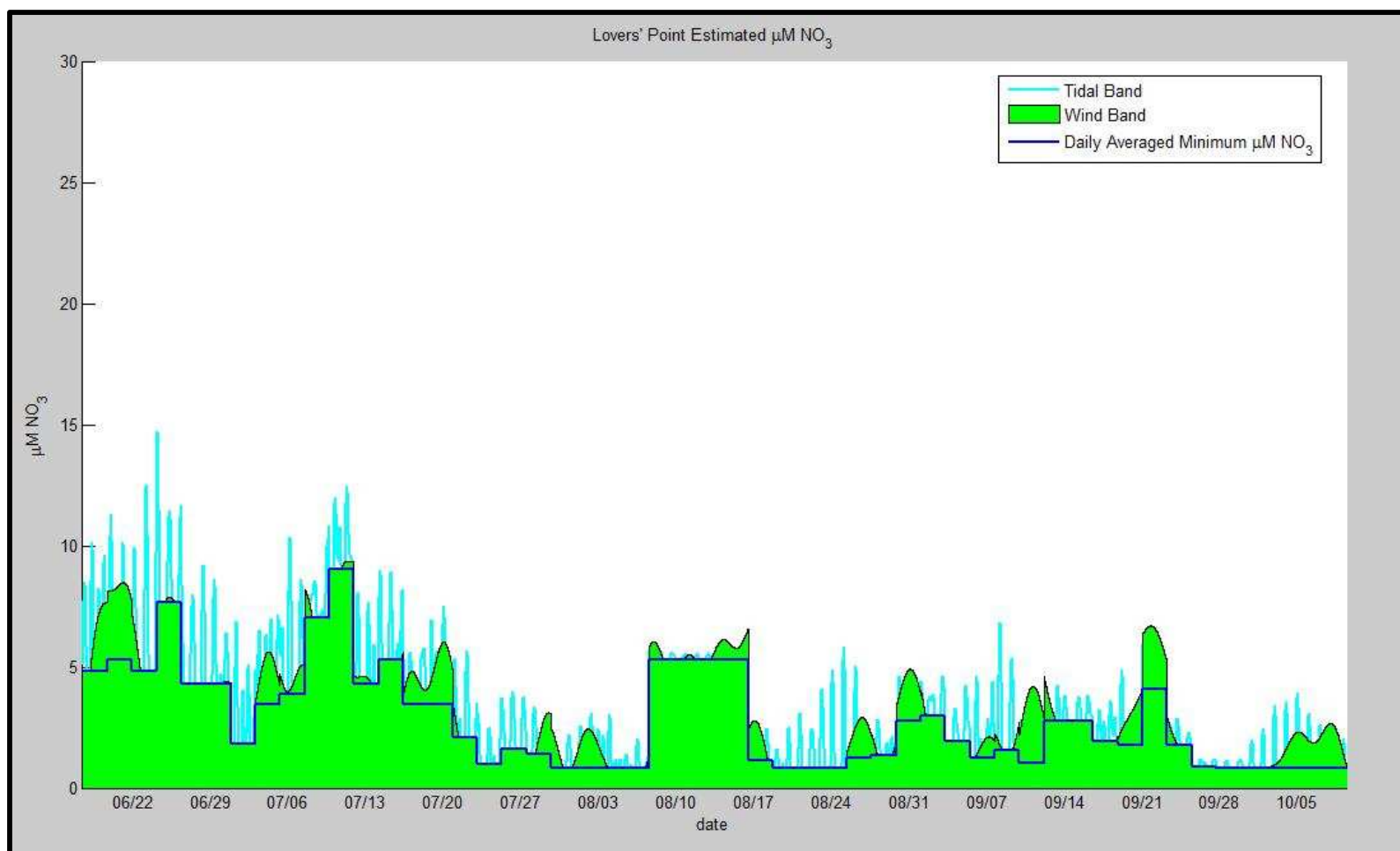


Figure 44: Lovers' Point estimated NO_3 during summer conditions [6/15/2006 – 10/10/2006].

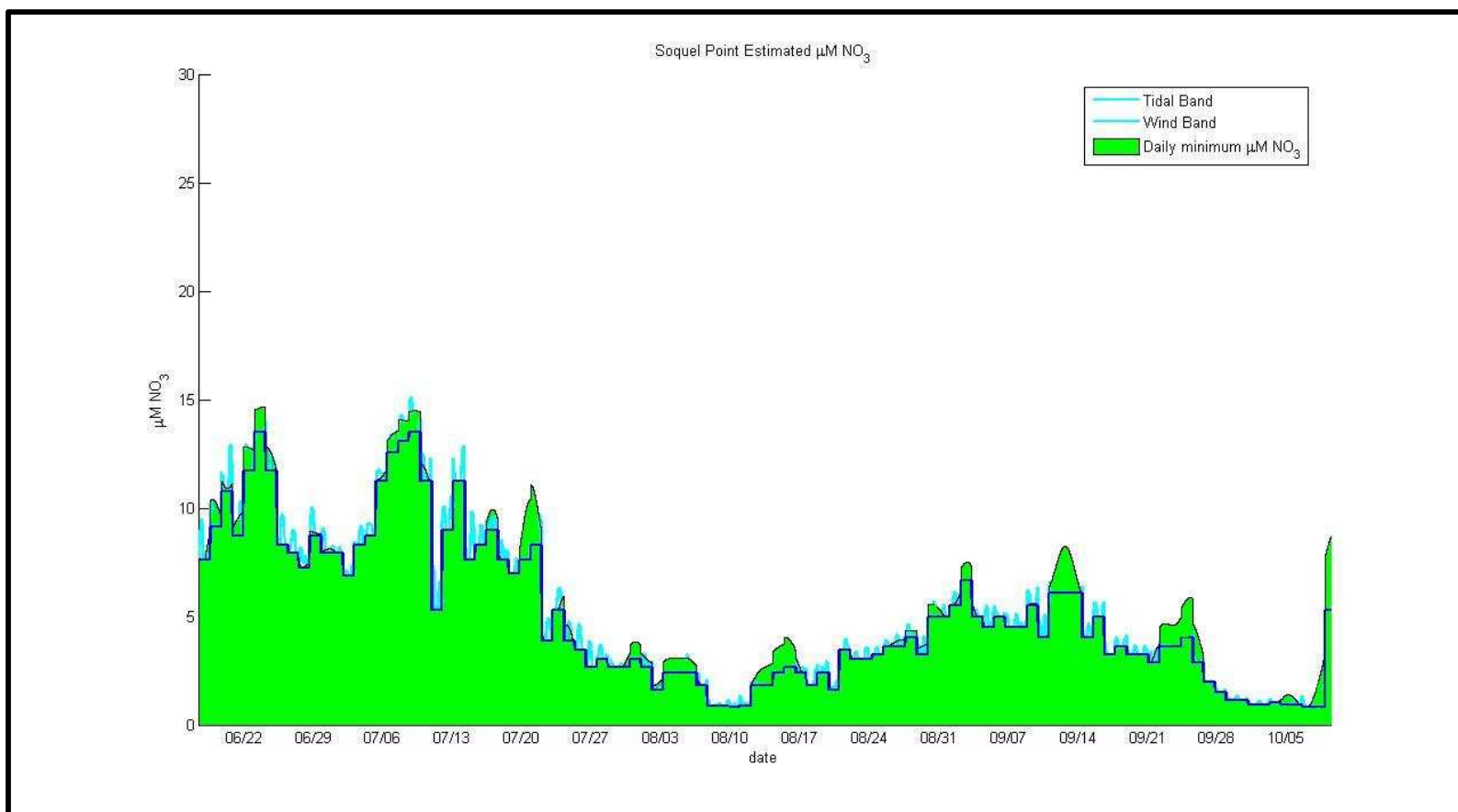


Figure 45: Soquel Point estimated NO_3 during summer conditions [6/15/2006 – 10/10/2006].

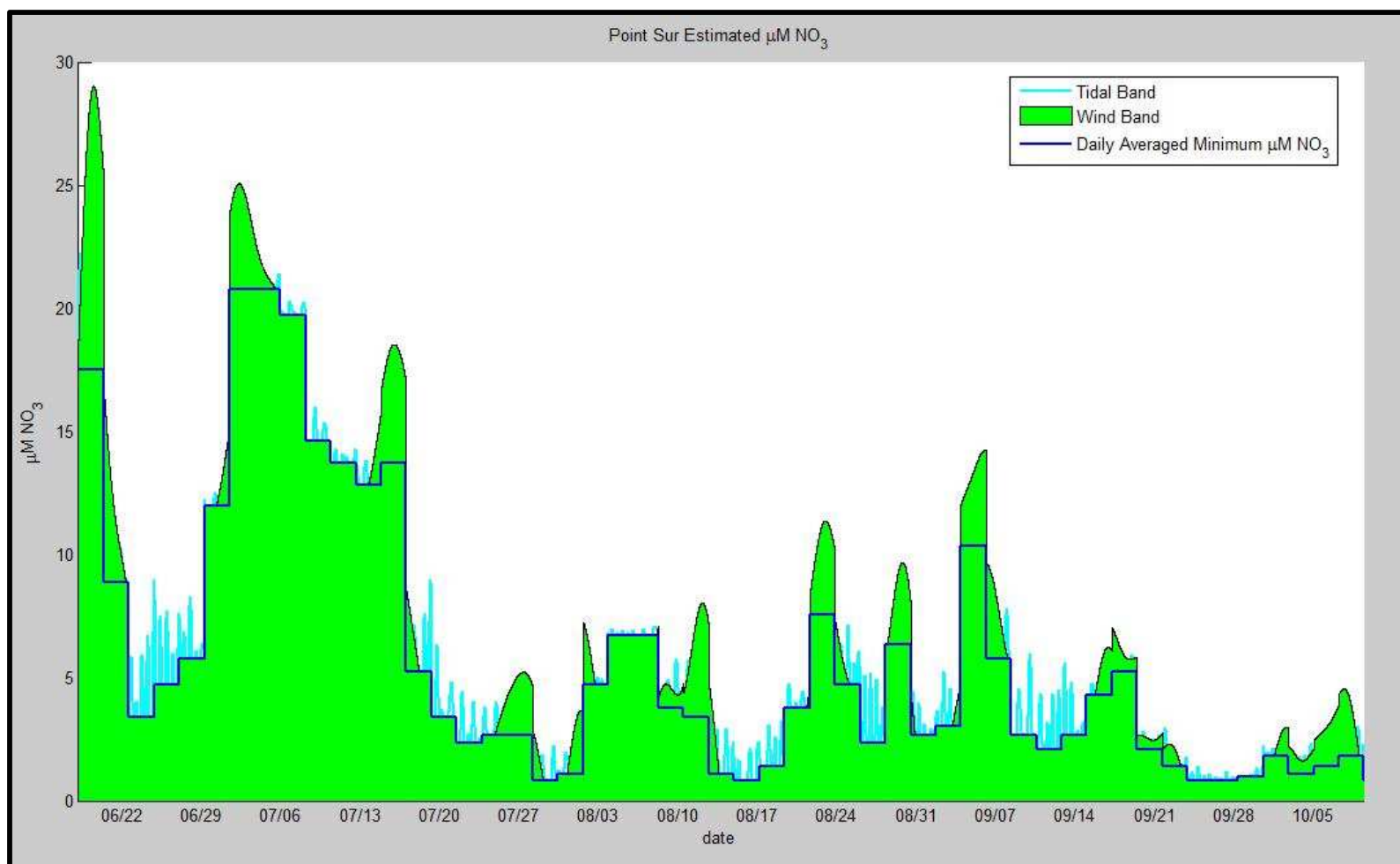


Figure 46: Point Sur estimated NO_3 during summer conditions [6/15/2006 – 10/10/2006].

The time series of wind and tidal band nitrate concentrations were integrated to provide seasonal nutrient contribution budgets. Total summer nitrate contribution from the wind band frequency is shown in Figure 47. Point Sur has the highest nitrate levels, followed by the three locations in Carmel Bay (Stillwater Cove, Weston Beach, and Sunset Point). Soquel Point had the lowest contribution of nitrate from the wind band, perhaps due to the upwelling shadow of the Monterey Bay.

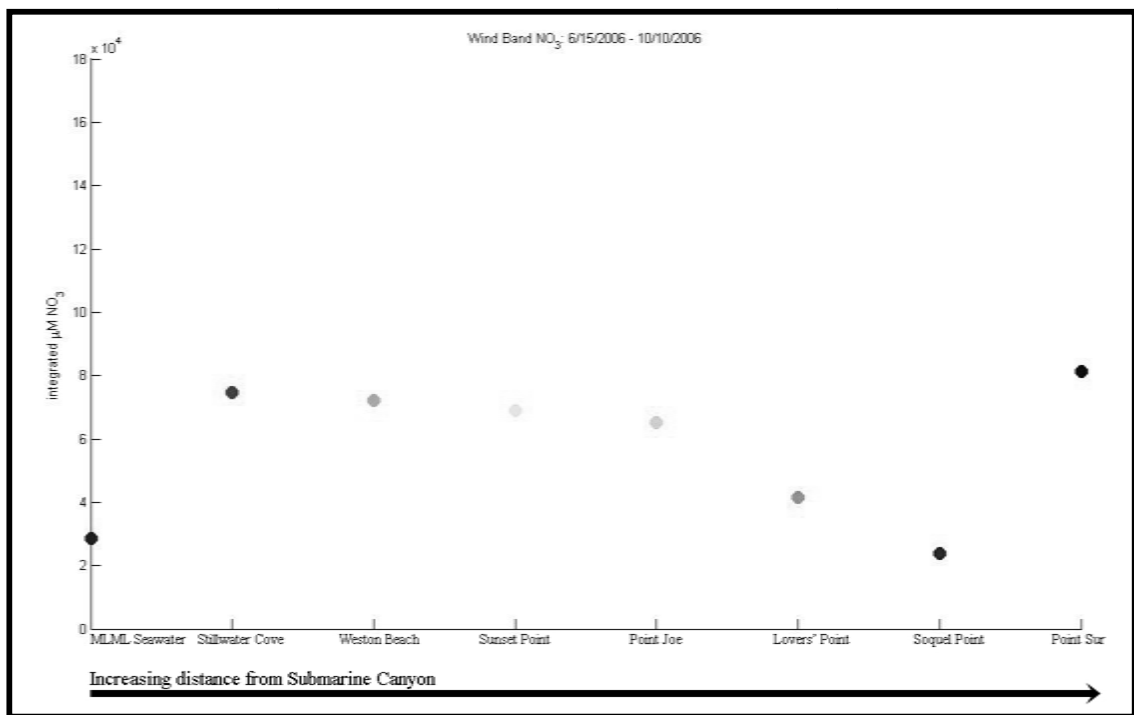


Figure 47: Wind band estimated NO_3 budget during summer conditions.

Lovers' Point had the highest summer nitrate contribution due to the diurnal tidal band, followed by the MLML Seawater System (Figure 48). Point Sur and Soquel Point had the smallest contributions. Figure 49 shows the semi-diurnal contributions, and total

nitrate budgets for both wind and tidal bands are shown in figure 50. The total nitrate values and contribution percentages are shown in tables 2 and 3.

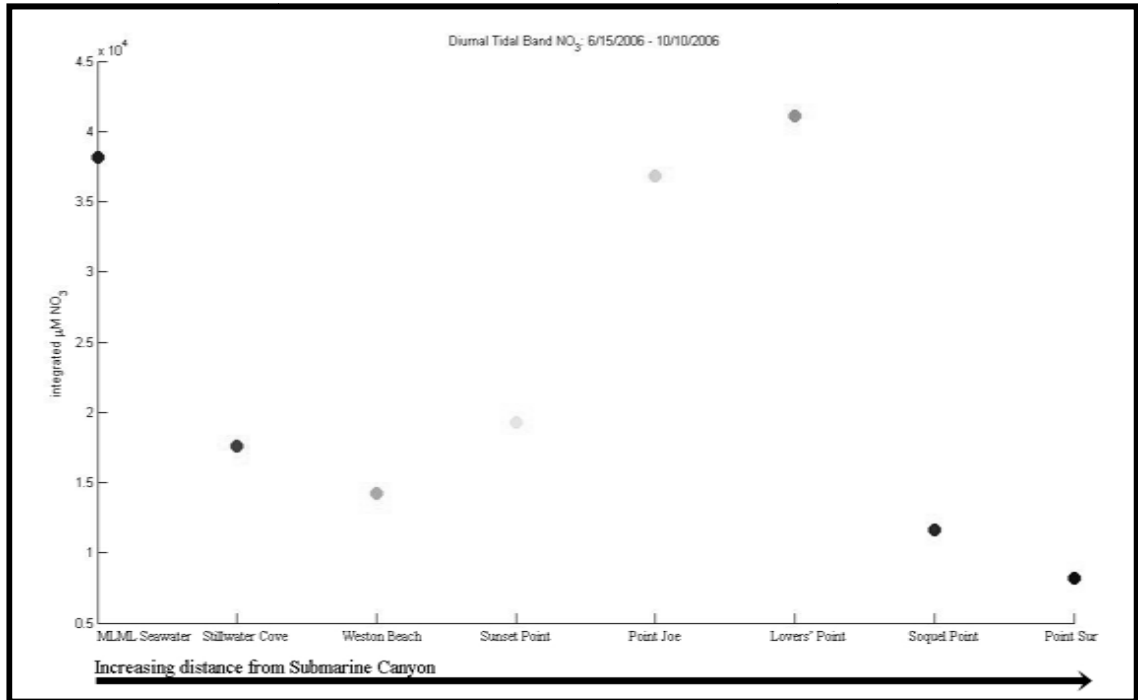


Figure 48: Diurnal Tidal band estimated NO_3^- budget during summer conditions.

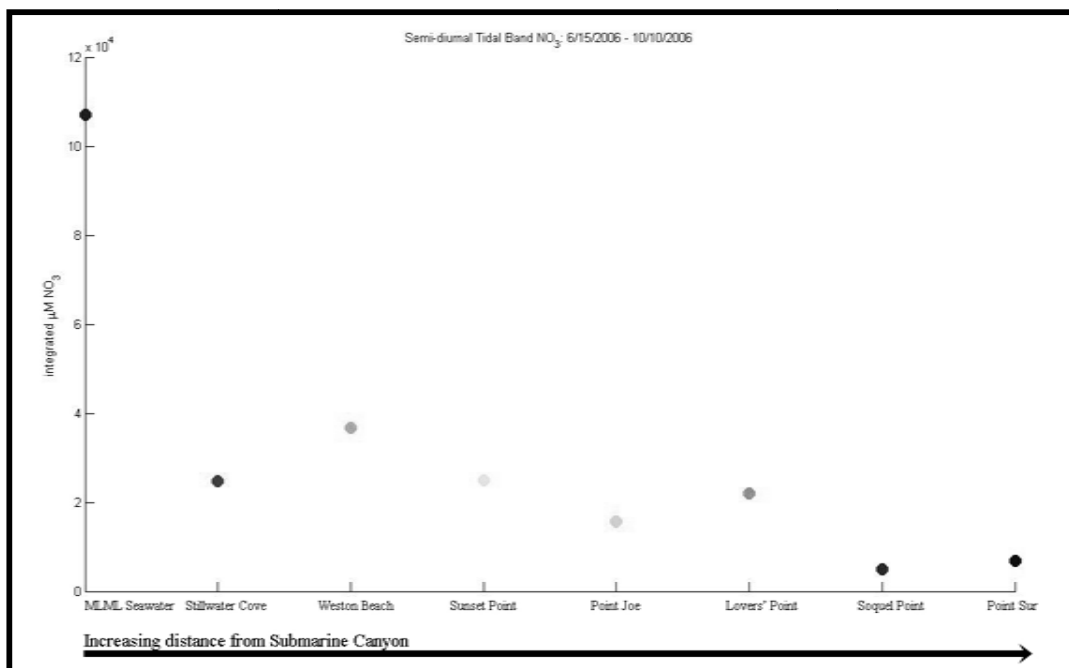


Figure 49: Semi-Diurnal Tidal band estimated NO_3 budget during summer conditions.

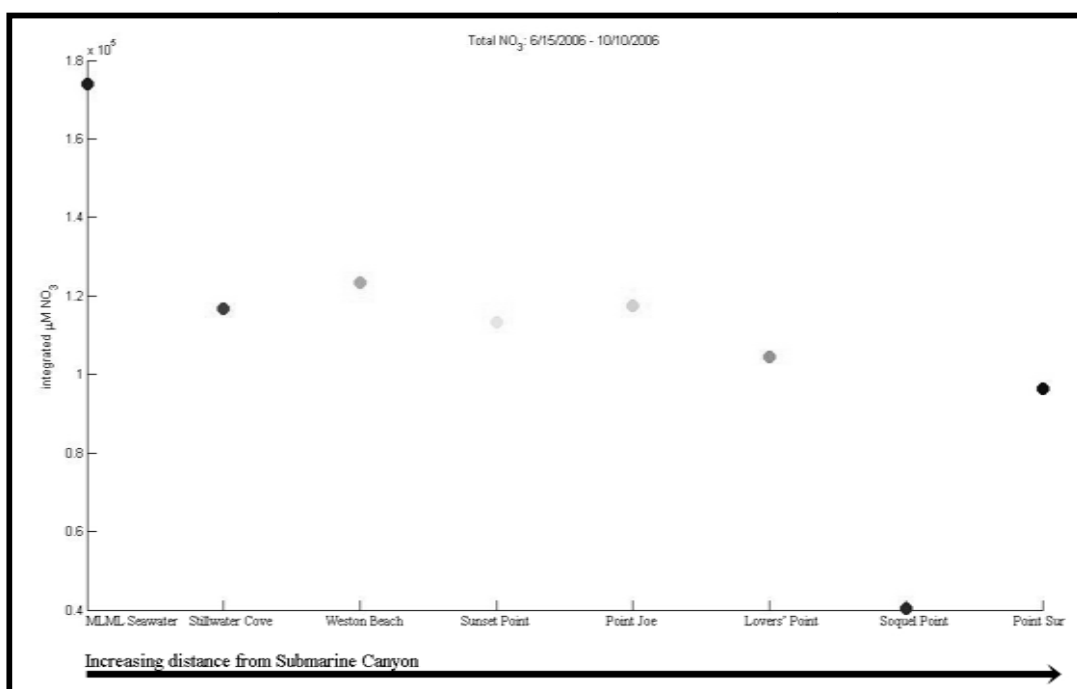


Figure 50: Total estimated NO_3 budget during summer conditions.

Table 2: Total estimated NO₃ during summer conditions.

Location:	Wind Band μM NO ₃ :	Diurnal Tidal Band μM NO ₃ :	Semi-diurnal Tidal Band μM NO ₃ :	Total μM NO ₃ :
Soquel Point	23693	11662	4918	40273
Seawater System	28731	38132	107090	173953
Lovers' Point	41414	41076	21914	104404
Point Joe	65116	36841	15644	117601
Sunset Point	69107	19282	24877	113266
Stillwater Cove	74586	17626	24652	116864
Weston Beach	72292	14244	36767	123303
Point Sur	81342	8220	6779	96341
Stillwater Mixing Volume:	1 x 10⁹	5 x 10⁹	1 x 10¹⁰	
Terrestrial μM NO ₃ :	13556	7110.7	1723.7	
Total Stillwater μM NO ₃ :	130420	123974.7	118587.7	

Table 3: Total estimated NO₃ % during summer conditions.

Location:	Wind Band %	Diurnal Tidal Band %	Semi-diurnal Tidal Band %	
Soquel Point	59	29	12	
Seawater System	16	22	62	
Lovers' Point	40	40	20	
Point Joe	56	31	13	
Sunset Point	61	17	22	
Stillwater Cove	64	15	21	
Weston Beach	58	12	30	
Point Sur	84.5	8.5	7	
Stillwater Mixing Volume:	1 x 10⁹	5 x 10⁹	1 x 10¹⁰	
Stillwater Terrestrial %	10.4	5.7	1.4	

4. DISCUSSION

4.1 Preamble

The primary goal of this project was to understand the dynamics of nutrient transport in Carmel Bay using an extensive mooring time series from the outer edge of Stillwater Cove on the northern end of the Bay. Carmel Bay is small embayment located at the northern end of the Big Sur coast, and it is distinguished by having a submarine canyon within extremely close proximity to the beach. Located inside of Carmel Bay, Stillwater Cove provides an enclosed habitat for a large *Macrocystis pyrifera* canopy, which exhibits unique temporal dynamics (Donnellan, 2004). This embayment is open to open ocean coastal California Current conditions; however, it also provides a sheltered environment from wind and swell. No previous studies have been conducted on the circulation features of Carmel Bay and Stillwater Cove. Despite its close proximity to the well studied Monterey Bay, it is much smaller in scale, and may experience very different dynamics from Monterey Bay. HF radar coverage does not extend into Carmel Bay, and consistent satellite coverage in the region is not available, so I embarked on research that is fundamentally exploratory in nature. Point source mooring time series measurements were used to explain in great detail the temporal variability of hydrographic conditions and nutrient delivery to Stillwater Cove and Carmel Bay. However, an overriding goal was to use as much additional data as possible to understand how unique Carmel Bay and Stillwater Cove are when compared to nearby regions. I tried to determine whether Carmel Bay exhibits dynamics that are similar to those of the Big Sur or Monterey Bay, or whether its dynamics differ enough from the larger coastal region to justify the idea

that Carmel Bay and Stillwater Cove might at times function as an enclosed embayment. This would imply that Carmel Bay's circulation features and dynamical forcing may be truly separated from the dynamics of the larger oceanographic system.

Nutrient Budget

Following the approach of McPhee-Shaw *et al*, (2007), of dividing oceanographic dynamics into distinct time scales of variability defined by Largier *et al*, (1993), we found that the diurnal and semi-diurnal tidal frequency band accounted for a significant contribution of nutrients at locations within close proximity to submarine canyons. Locations on the shelf received the majority of their annual nutrients due to upwelling, and the effects of internal waves at these regions were greatly diminished. When compared to the tidal and wind nutrient contributions, the effects of terrestrial runoff were minimal. In this section, I will compare both wind and tidal forced variability in Carmel Bay to that of locations both north and south along the coast.

Internal Waves

The nutrient budget results showed the importance of both diurnal and semi-diurnal baroclinic oscillations for delivering nutrients to Carmel Bay. Even in the absence of upwelling conditions, these internal oscillations could increase NO_3 concentrations in water column by up to $5 \mu\text{M}$. The internal waves were observed at both diurnal and semi-diurnal frequencies, and were likely forced by both wind and tides. An important remaining issue for clarifying our understanding of nutrient delivery by internal waves is

confirming whether the observed temperature variability is primarily due to shoreward transport of deep, sub-nutricline waters, or whether it might instead be due to along-coast advection of water masses of different temperature. Here we demonstrated the likelihood of vertical transport versus horizontal advection. Our data demonstrated interesting vertical structure of diurnal and semi-diurnal currents, and phasing with tides that suggested that shallow regions in Carmel Bay were intensely forced by “heaving” of the much deeper waters of the nearby Carmel Branch of the Monterey Submarine Canyon. This immediately begged the question, “how unique is such a signal?” Does the proximity to the canyon and the hypothesized effect on internal wave nutrient delivery make Carmel Bay a truly unique location on the coast for nutrient availability, and if so what are the implications for along-coast variability in ecosystem response? If, on the other hand, our comparisons to other sites suggest that internal-wave driven nutrient variability is not unique in Carmel Bay, what are the ecosystem implications?

Possible Stagnation in Stillwater Cove

This question has been brought to the forefront by indications that some ecosystems in Stillwater Cove behave differently from similar ecosystems in other Central Coast locations. For example, the Stillwater Cove *M. pyrifera* canopy has been found to have declined 2 to 3 months before kelp canopies at nearby Sunset Point and Carmel Point Donnellan (2004). Could the capture and retention of water within Stillwater Cove lead to the build up of terrestrial nutrients or pollutants, or could stagnation lead to the decrease of oxygen in Stillwater Cove waters? Answering these

questions is important for our overriding goal of assessing the “uniqueness” of the Carmel Bay system relative to more exposed coastal locations.

4.1.1 Stillwater Cove Annual Nutrient Budget

In this study, nutrient delivery to the near-shore environment in Stillwater Cove was modeled using the $\mu\text{M NO}_3$ contributions from three distinct frequency bands: wind, tidal, and synoptic terrestrial runoff events. The tidal frequency band consisted of contributions from both diurnal and semi-diurnal internal waves, while the wind frequency band accounted for spring / summer and winter upwelling conditions. Using this nutrient model, several questions were investigated. What frequency bands in Stillwater Cove are the most active during the year, and which band contributes the majority of the nutrients to the near-shore environment? Is terrestrial runoff from Pebble Beach a significant contributor of nutrients when compared to the wind and tidal bands? How does the nutrient model in Stillwater Cove compare to results from McPhee-Shaw *et al.* (2007) in the Santa Barbara Channel? The tidal band was the most active nutrient delivery mechanism in Stillwater Cove, with 170 active days during the year (Table 4). The wind band was active for 98 days, while terrestrial storm events accounted for 12 days. The tidal band was the most active nutrient delivery mechanism in Stillwater Cove; however, it did not supply the majority of nutrients. Diurnal internal waves were capable of increasing nitrate levels in the water column just as strongly as upwelling conditions. While diurnal and semi-diurnal internal waves occur more frequently in the cove than

upwelling conditions, they are short in duration (2 – 3 hours) when compared to the mean upwelling duration of 3 days. Internal waves accounted for 35% to 36% of annual nitrate contribution in Stillwater Cove. This was more than twice as much as internal wave contributions in Santa Barbara, and is due to the close proximity of the Carmel Submarine Canyon to Stillwater Cove and the associated internal tide dynamics.

The wind band contributed the majority of the nutrients during the year, 60 % to 63 % of the total annual nitrate contribution. Although the sampled terrestrial nitrate concentrations were extremely high when compared to measured oceanic sources, the dilution of the stormwater into the volume of Stillwater Cove reduced terrestrial runoff to a minor mechanism of nutrient delivery. Terrestrial storm input ranged from < 1% to 5 % of the annual nitrate contributions depending on the mixing volume used for the model. Compared to results from Santa Barbara Channel (McPhee-Shaw *et al.*, 2007), Stillwater Cove experienced far more days annually with upwelling conditions and internal waves. 52 days of winter and spring upwelling, 39 days of internal waves, and 6 days of terrestrial runoff were observed in the Santa Barbara Channel. Carmel Bay received annually almost twice as many active upwelling days, and over four times more internal wave days than Santa Barbara. In the Santa Barbara Channel, spring and winter upwelling accounted for 55% to 74 % of the annual nitrate contributions. Internal waves accounted for 10% to 14%, and terrestrial runoff accounted for 12% to 35%. In both Carmel Bay and the Santa Barbara Channel, upwelling was the dominant mechanism of nutrient delivery to the near-shore environment. Terrestrial runoff was a much smaller contribution in Stillwater Cove compared to Santa Barbara due to the low flow rates of

storm drains when compared to rivers. Flow rate was a greater deciding factor than discharge concentrations when terrestrial input is mixing in a large volume. Even though the Stillwater Cove storm drain nutrient concentrations were very high, the discharge flow rates were low compared to the Santa Barbara region.

The tidal band was the most active nutrient delivery mechanism during the year in Stillwater Cove; however, the wind band contributed the majority of nutrients to the near-shore environment. Although terrestrial nutrient concentrations were extremely high, the low discharge rates restricted terrestrial sources from being a significant nutrient contributor. Compared to the Santa Barbara Channel, Stillwater Cove experienced far more nutrients from the tidal band, possibly due to the close proximity of the Carmel Canyon, while the Santa Barbara Channel experienced a greater input of nutrients from terrestrial sources due to the larger watersheds in the region

Table 4: Stillwater Cove annual nutrient contributions.

Location:	Frequency Band:	Days active:	% Contribution to annual $\mu\text{M NO}_3$ budget:		
			1×10^{10} volume	5×10^9 volume	1×10^9 volume
Stillwater Cove	Wind	98	63	62	60
	Tidal	170	36	35	35
	Terrestrial storm input	12	< 1	3	5

4.4.2 Seasonal Currents

The use of a progressive vector diagram provided insight into the general direction of currents on a seasonal timescale; however, we were also interested in how the magnitude of surface and bottom currents varies seasonally in Stillwater Cove. Specifically, which season has the strongest currents, and how do tidal excursion distances vary seasonally? How do tidal and sub-tidal currents compare in terms of magnitude and direction on seasonal time scales, and are these currents directed into or away from Stillwater Cove? Seasonally, Stillwater Cove experienced positive along-isobath flows during spring and summer conditions at near-bottom depths (Figure 17). During these seasons, the mean direction of this bottom flow was oriented into the mouth of Stillwater Cove. At near-bottom depths, the cross-isobath velocity is neutral. Moving upwards in the water column, the cross-isobath velocity became positive and the flow begins to rotate towards an onshore direction. Bottom flow was oriented directly towards the mouth of Stillwater Cove, while flows at shallower depths in the water column are oriented towards the northern end of Carmel Beach. During winter conditions, bottom flow was positive along-isobath and negative cross-isobath. This resulted in net offshore flow towards the mouth of Carmel Bay. Flows at shallower depths in the water column were rotated towards an onshore direction, similar to summer and spring conditions.

Hourly current data from the Stillwater Cove mooring was filtered into tidal and sub-tidal components using a 33-hour low pass filter (Figure 51). The sub-tidal component was directed positive along-isobath, while the tidal component moved from negative to positive cross-isobath with a very small positive along-isobath component.

The seasonal and daily path length of mid-water column and bottom currents was then calculated (Figure 52). This measure of path length enabled us to estimate the maximum possible distance a particle in the water may travel during a season / tidal cycle. The path length was only influenced by the magnitude of a current and not the direction. By dividing the daily path length in half, we then constructed an estimate of diurnal excursion distance. The mid-water column depth was defined at 9 m, as this was the upward depth limit of reliable ADCP data. Figure 55 shows the seasonal tidal and sub-tidal path length in Stillwater Cove.

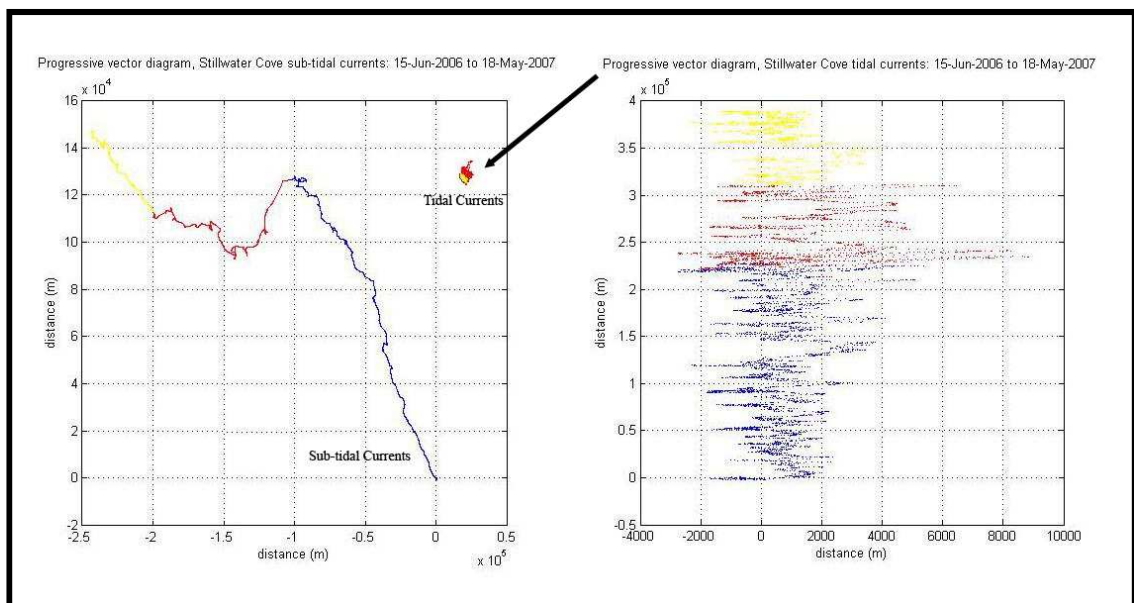


Figure 51: Bottom depth sub-tidal and tidal progressive vector diagram [June 15th 2006 – May 18th 2007]. Blue is summer, red winter, yellow spring.

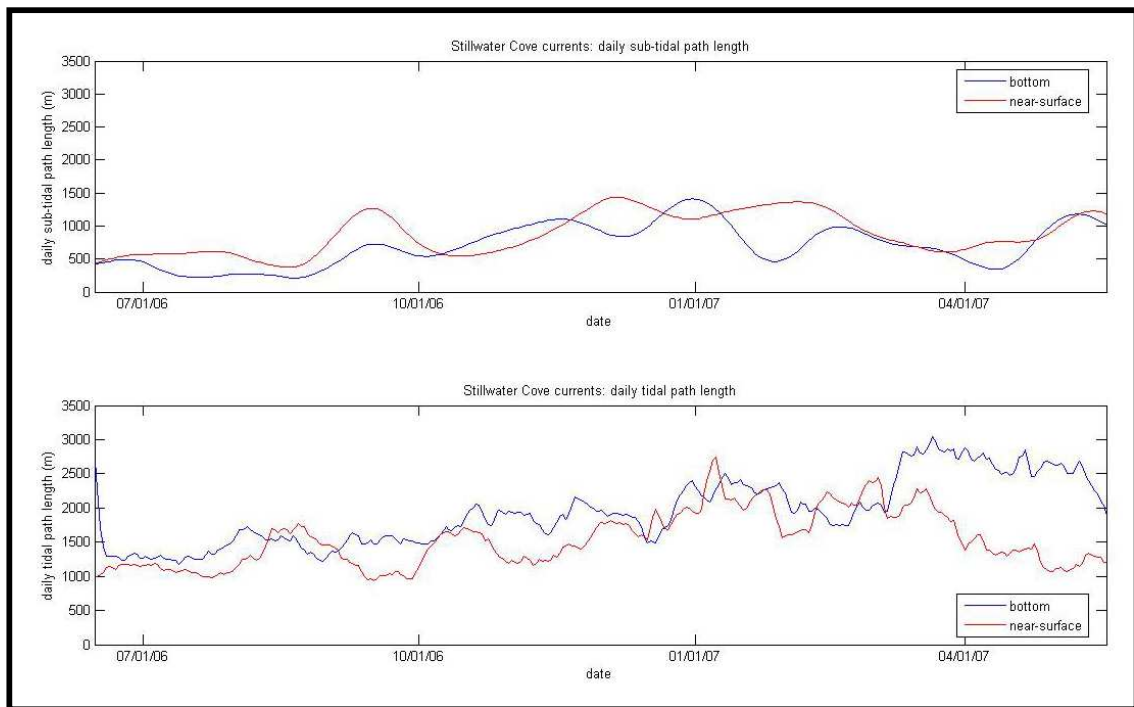


Figure 52: Seasonal tidal and sub-tidal daily path length. [June 15th 2006 – May 18th 2007].

The summer sub-tidal mean bottom path length was 1159 m, while the sub-tidal mean path length at 9-m depth was 1496 m. The winter sub-tidal mean bottom path length was 1875 m, while the sub-tidal mean path length at 9-m depth was 2456 m. The spring sub-tidal mean bottom path length was 1453 m, while sub-tidal mean path length at 9-m depth was 1643 m. Sub-tidal flows at 9-m depth are stronger year-round than bottom flows. The winter months had the longest daily path length and strongest mean sub-tidal current velocities, while currents during spring conditions were stronger than summer. The total annual sub-tidal path length was 1045 km, indicating weak net background currents.

Mean summer tidal bottom path length was 2945 m, while the tidal path length at 9-m depth was 2625 m. Mean winter tidal bottom path length was 3914 m, while tidal

path length at 9-m depth was 2456 m. The spring mean tidal bottom path length was 4935 m, while the tidal path length at 9-m depth was 3085 m. Tidal bottom flows were stronger year-round than mid-water column flows, suggesting a barotropic tidal component with intensified bottom flow. Tidal flows at 9-m depth were strongest during winter conditions; however at bottom depth the path length was longest during stratified spring conditions. This sharp increase in bottom depth path length was noticeable in the beginning of March, at the onset of upwelling conditions and the spring transition. This spring transition marked the beginning of stratification in Carmel Bay water column. This increase in bottom depth path length may have been due to the intensification of internal tidal pumping during stratified conditions. During this time the path length at 9-m depth length began to decrease.

On a seasonal scale, tidal currents dominated over sub-tidal currents in Stillwater Cove. Tidal currents were strongest at bottom depths, and have the longest excursion distances during stratified spring conditions. These increased excursion distances may be due to the up-slope horizontal advection associated with the internal tide in Carmel Canyon. Sub-tidal currents at 9-m depth were stronger year-round than sub-tidal bottom currents, and had the longest excursion distances during winter conditions. Tidal currents at bottom depth flowed directly into Stillwater Cove during stratified spring and summer conditions, while currents in the upper water column were oriented towards Carmel Beach.

4.1.3 Tidal Currents

We have described the general magnitude and direction of currents on a seasonal time scale, but how do currents behave on shorter timescales? In Stillwater Cove, currents that occur during the tidal frequency band are important as this is the timescale when internal waves and increased nutrient concentrations are observed. The strongest internal waves were observed during the rising diurnal tide, so we chose to investigate currents during the diurnal tidal cycle. Specifically, what is happening in the water column during the rising diurnal tide, when the strongest cold pulses are observed? Are near-shore currents oriented into or away from the Cove during the rising diurnal tide? Are bottom and mid-water column currents oriented in the same direction, and are currents in the water column barotropic or baroclinic? The daily diurnal peak high tides were first identified in a year-long tidal time series. The Stillwater Cove currents at 9-m depth and bottom depth were then averaged in 1-hour bins, ranging from 6 hours before peak high tide to 6 hour after. The diurnal tide was chosen as the feature of interest because the strongest observed cold pulses and highest nutrient concentrations arrive during the peak diurnal high tide. These hourly bins were then averaged over the entire time series to provide a seasonal mean current direction before and after the diurnal peak high tide.

During the rising diurnal high tide, currents at bottom depth were stronger on average than at 9-m depth (Figure 53). Both mid-water column and bottom currents are negative along-isobath, which was directed onshore towards the south end of Carmel beach (Figure 54). From 18-m to 8-m depth, the currents rotated towards the south,

flowing in a negative along-isobath direction. During the falling diurnal tide, surface currents were strongly positive along-isobath and slightly negative cross-isobath (Figure 55). The flow at 9-m was oriented towards the south end of Carmel Beach. Bottom currents were oriented positive along-isobath, flowing directly into Stillwater Cove (Figure 56). During the first three hours following peak high tide, currents at bottom depth were stronger than their mid-water column counterparts. From 4 to 6 hours after peak diurnal high tide, the currents at 9-m depth become stronger and the strength of the bottom currents diminished.

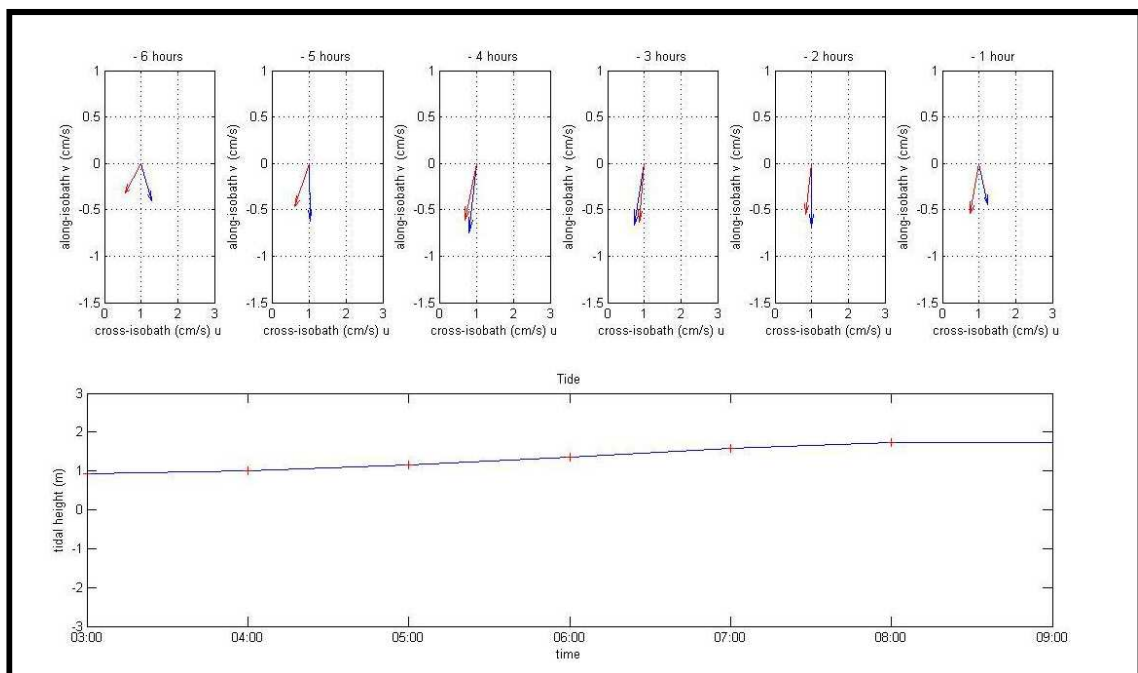


Figure 53: Bottom currents during the rising diurnal tide. Blue arrow is near-bottom; red is 9-m depth.

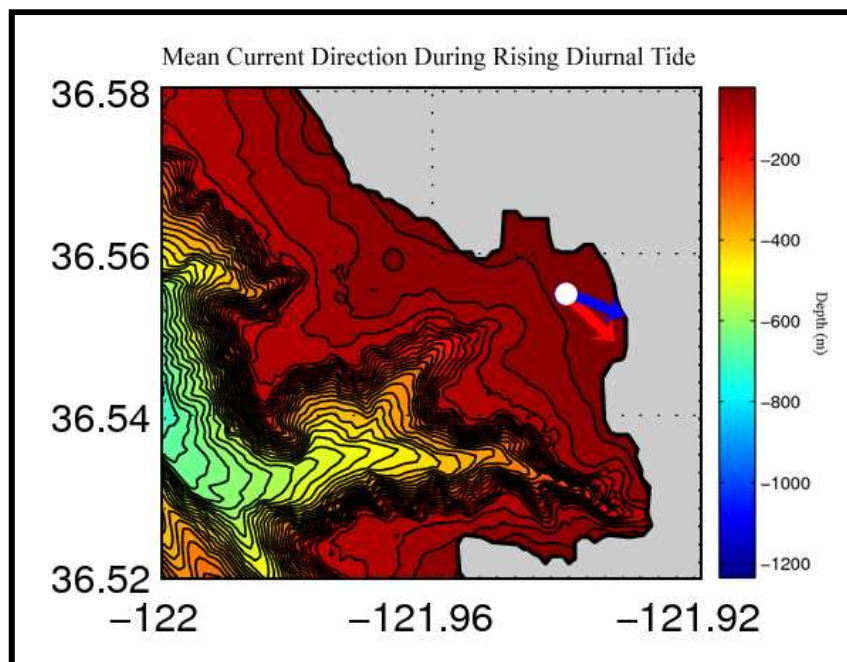


Figure 54: Current direction during rising diurnal tide. Blue arrow is near-bottom; red is 9-m depth.

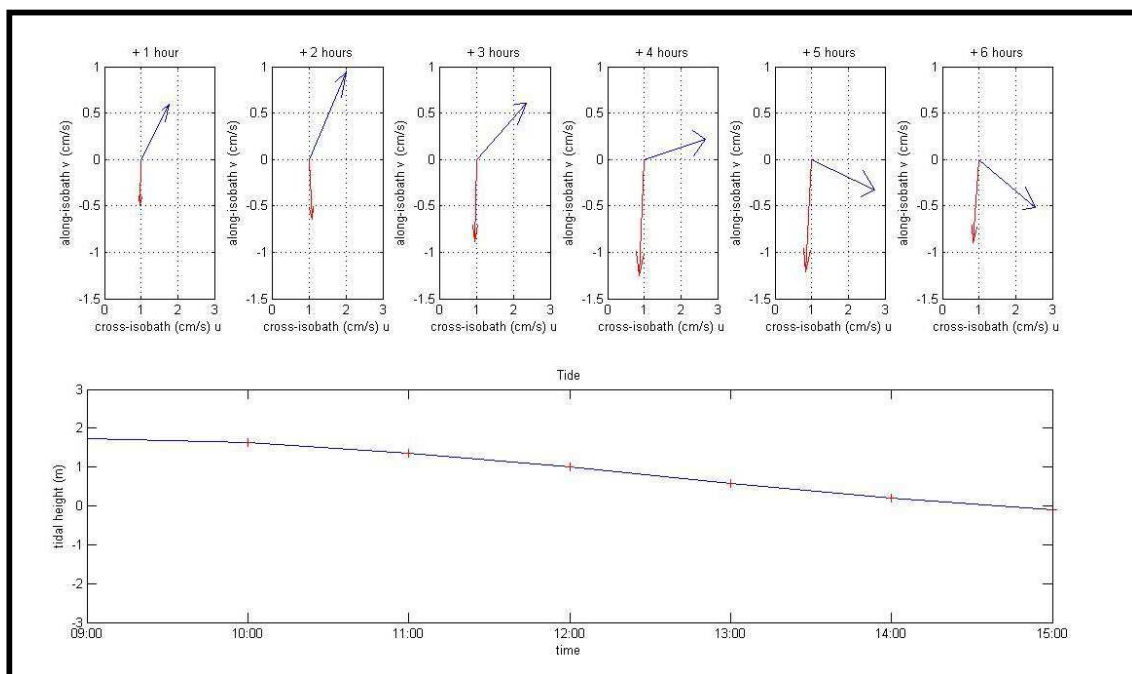


Figure 55: Bottom currents during the falling diurnal tide. Blue arrow is near-bottom; red is 9-m depth.

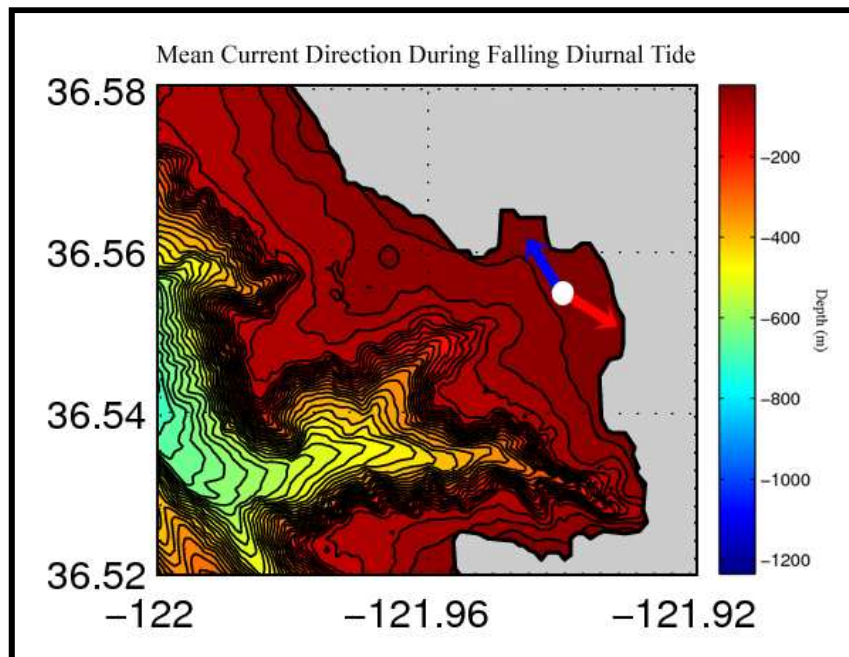


Figure 56: Current direction during falling diurnal tide. Blue arrow is bottom depth; red is 9-m depth.

Focusing on an even shorter timescale, how are currents throughout the water column behaving when the diurnal internal waves are observed? To investigate this question, the mean currents at each 1-m bin from the bottom to 9-m depth were examined. The currents were then averaged over a year-long time series, at 1-hour before and 1-hour after the peak diurnal high tide. Figure 57 displays a three dimensional view of currents in the water column from bottom depth to 9-m depth, one hour before peak diurnal high tide. There was significant rotation of currents in the water column, and the strongest currents were found at bottom depth. This showed the baroclinic nature of the Stillwater Cove water column during parts of the tidal cycle, emphasizing the dominance of the internal baroclinic tide over the barotropic tide. Figure 58 displays a three

dimensional view of currents in the water column one hour after peak diurnal high tide. The currents from bottom to 8-m depth were unidirectional and no significant rotation in the water column was visible. At this point in the tidal cycle, the barotropic tide is dominant. There is only a 1-hour time difference between the two figures; it shows how quickly the dynamics in the water column can change during the tidal cycle. During the rising diurnal tide, currents at both bottom and 9-m depths flowed negative along-isobath. This flow was oriented towards the south end of Carmel Beach, away from the mouth of Stillwater Cove. During the falling diurnal tide, bottom currents were oriented directly into Stillwater Cove while surface currents were oriented towards the south end of Carmel Beach. Over the course of the tidal cycle, both baroclinic and barotropic currents were observed in the water column. Due to the close proximity of the Carmel Canyon, the water column may be strongly affected by the baroclinic internal tide during the tidal cycle.

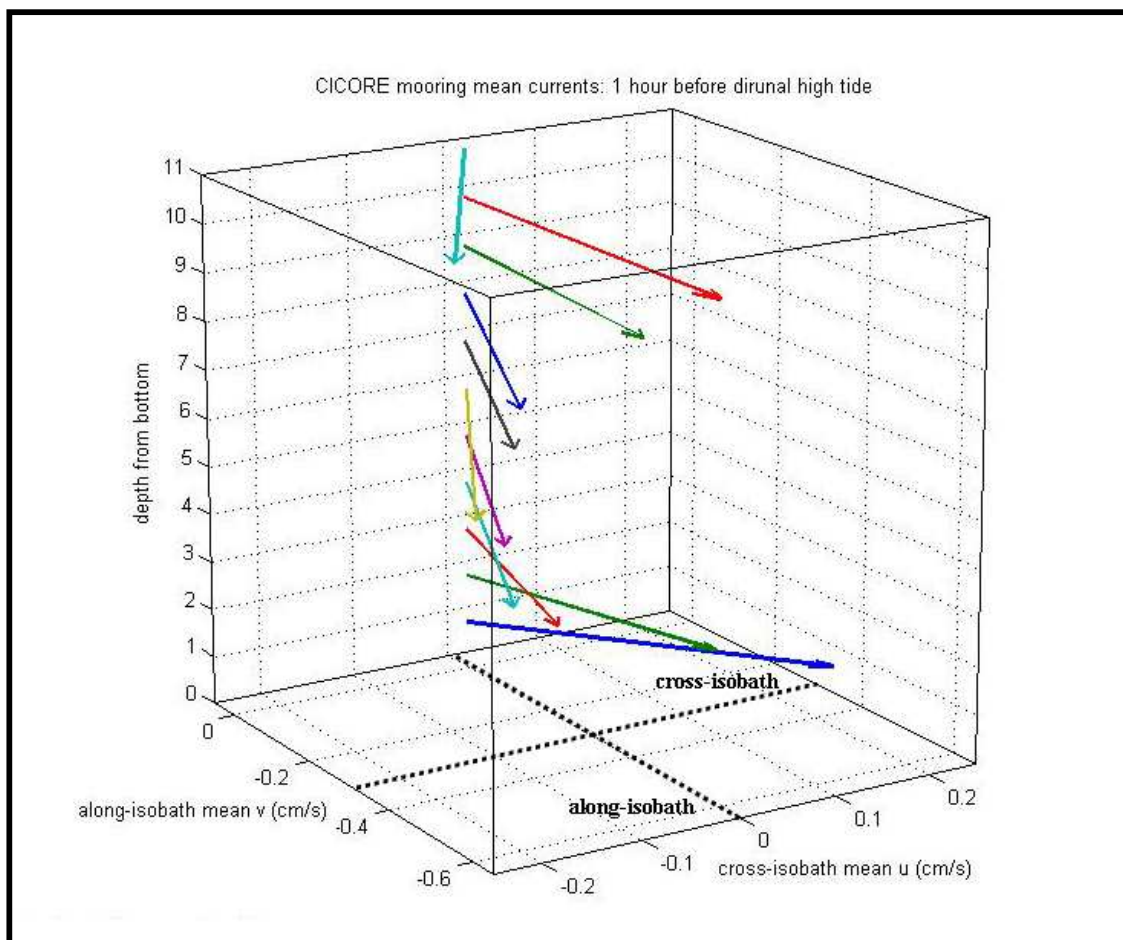


Figure 57: Mean currents 1 hour before peak diurnal high tide.

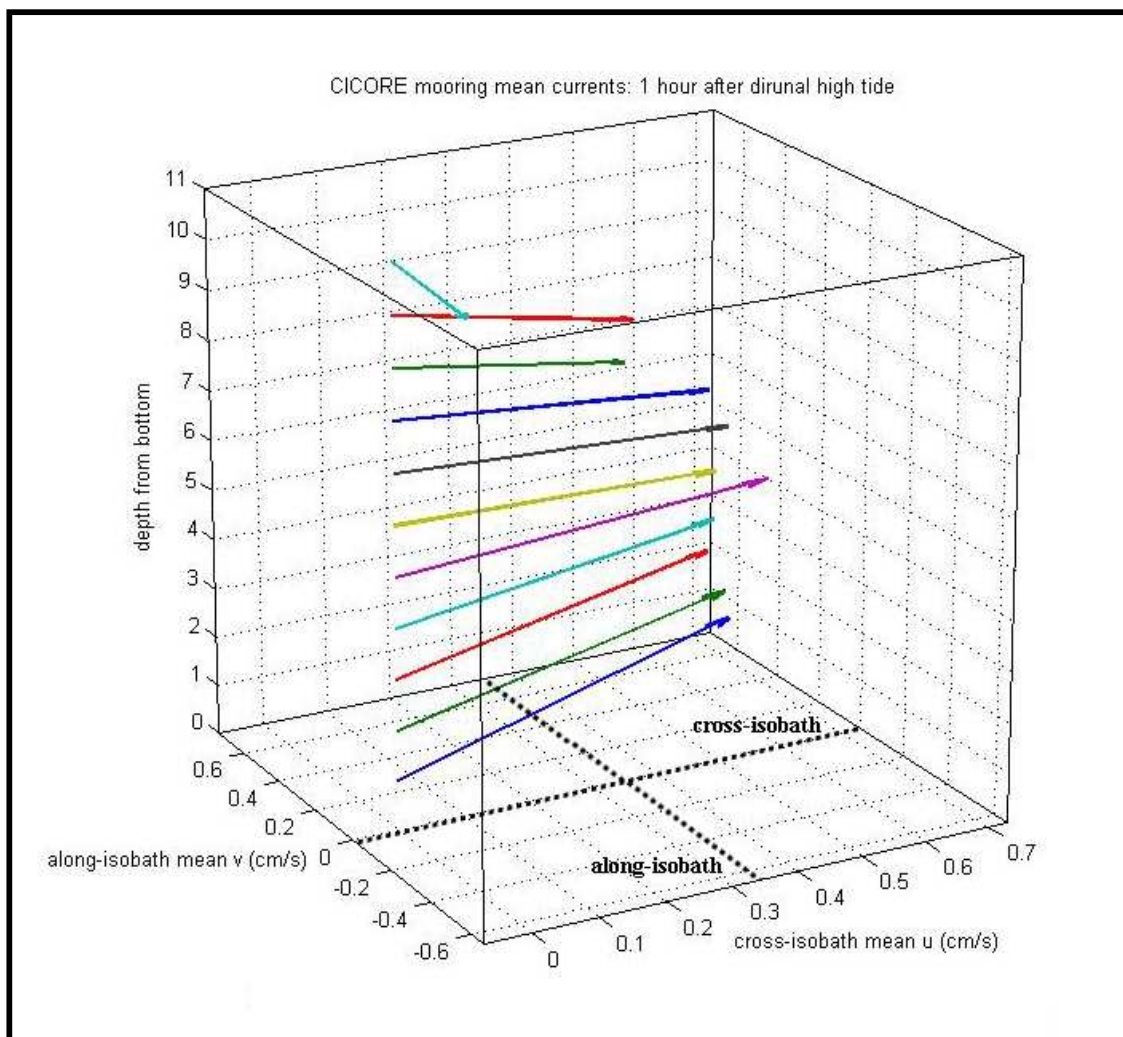


Figure 58: Mean currents 1 hour after peak diurnal high tide.

4.1.4 Synoptic Winter Mixing Events

During winter months, Stillwater Cove experienced periods of strong vertical mixing and synoptic warming of the entire water column. These periods of warming combined with intense vertical mixing lasted typically for 1 to 2 days. Temperatures at surface depths were the first to experience the warming in temperature. After this time period, the water column began to re-stratify with temperatures at bottom depths cooling first. What are the dynamics associated with these winter mixing events? Does wave action at nearby Pescadero Point cause vertical mixing of surface water, or does the warm water come from an offshore source? As shown in Figure 12, these mixing events first appear to be correlated with strong winter swell events. Pescadero Point at the western end of Stillwater Cove can generate some of the largest waves on the central California coast during strong winter storms. While these strong swell events may explain the vertical mixing shown in the time series, it does not explain the intense warming of the water column. During these mixing events, the entire water column temperature typically warmed by 2°C. If surface mixing by wave action is causing warm surface temperatures to become mixed evenly to bottom depth, we can calculate the necessary starting temperature of the surface water. If we assume that the source of the warm water being mixed downward extends from surface to 1-m depth, and that the depth of the entire water column is 20-m, a simple conservation of mass model can be constructed. Using the conservation of mass model shown below enables us to determine if surface mixing is a possible source for the observed warming events.

$$(surfaceT \times 1\ m) + (meanT \times 19\ m) = ((meanT + 2^\circ\ C) \times 20\ m) \quad (7)$$

$$surfaceT = \frac{((meanT + 2^\circ\ C) \times 20\ m) - (meanT \times 19\ m)}{1} \text{ m} \quad (8)$$

SurfaceT is the required temperature at the surface to heat the entire water column by 2°C and *meanT* is the average temperature of the water column. Using a typical winter mean temperature value of 12°C, solving this equation for *surfaceT* gives us a 1-m near-surface temperature of 52°C. This indicates that surface mixing is not a possible source for the warm water event. A wind reversal preceded the mixing event by approximately a day (Figures 59 and 60). During this period of upwelling wind reversal, the winds switched from a northwesterly to a southerly direction. This period of downwelling favorable winds lasted for 1 to 1.5 days, and the average wind speed during these periods was 10 m/s. Approximately 24 hours after the onset of the wind reversal, Stillwater Cove experienced strong positive cross-isobath flows in the entire water column. These currents were directed onshore towards Carmel Beach. The positive cross-isobath flows had velocities of 5 – 8 cm/s and lasted for the duration of one day. Approximately one day after the water column experienced these strong positive cross-isobath flows, the currents reversed to negative cross-isobath, and were directed offshore. These negative cross-isobath currents also persisted for the period of a day, and were accompanied by a warming of the entire water column. Using latitude of ~ 36° 33' 36" for the Stillwater Cove mooring location, the Coriolis frequency f is $0.866 \times 10^{-4}\ s^{-1}$ ($f = 2\ \omega\ \sin(\phi)$, where $\omega = 2\pi/(24\ \text{hours})$). The inertial period, $T = 2\ \frac{\pi}{f}$ for the Carmel Bay region is 20.146

hours. The time duration between the onset of the wind reversal and warming periods observed in Stillwater Cove was longer than inertial period. This suggested that the source of winter warming events may be downwelling caused by upwelling wind reversals. These downwelling events were often correlated with strong winter swells and storms. This is due to the accompanying low pressure systems that move down the coast, causing strong south winds. Due to the frequent periods of winter upwelling during these months, cold water temperatures often were found near the coast whereas warmer water masses are located slightly farther offshore. When downwelling conditions occurred, there was a time lag between the wind reversal and the arrival of warmer water temperatures from offshore water masses. As shown in Figures 59 and 60, this lag was approximately a 24 hours in Stillwater Cove. Figure 61 shows Monterey Bay SST from November 9th, 12th, 13th, and 15th of 2007. On November 9th, the 13°C isotherm was the dominant SST temperature in Carmel Bay region due to upwelling conditions from the previous week. The period of wind reversal and strong southerly winds began on November 12th. A day later, the 15°C isotherm moved significantly onshore, approaching the mouth of Carmel Bay. This 15°C water mass entered Carmel Bay and was observed in the entire Stillwater Cove water column on November 13th. These full-depth warming events observed during the winter months in Stillwater Cove were caused by downwelling conditions, and not wave activity. By using a conservation of mass model, we showed that vertical mixing by local wave activity at Pescadero Point was not a possible source for the warm water mass. Strong winter swells often coincided with downwelling favorable conditions; however, this is because low-pressure winter storms

systems were accompanied with downwelling favorable winds.

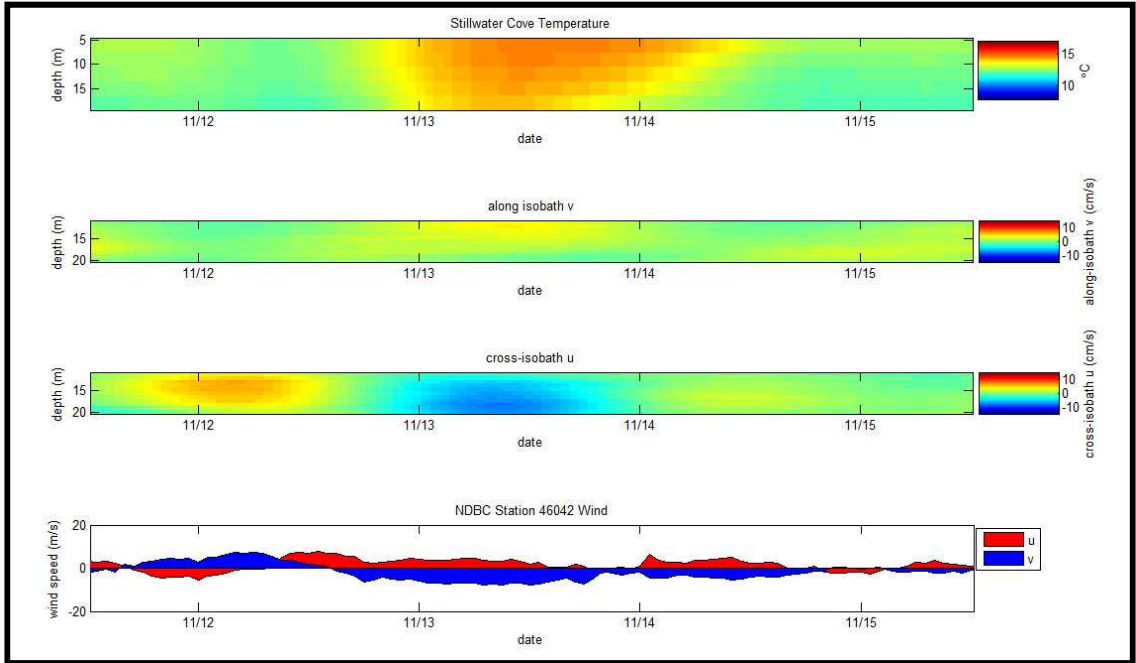


Figure 59: Winter mixing and warming events. U is eastward, v is northward

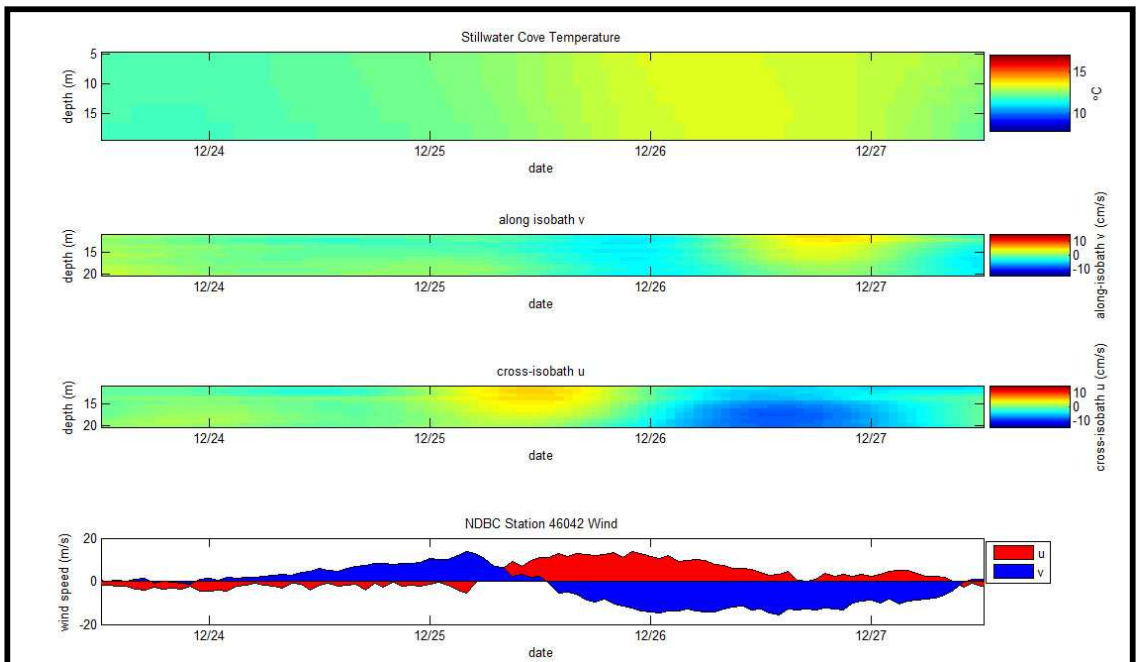


Figure 60: Winter mixing and warming events. U is eastward, v is northward.

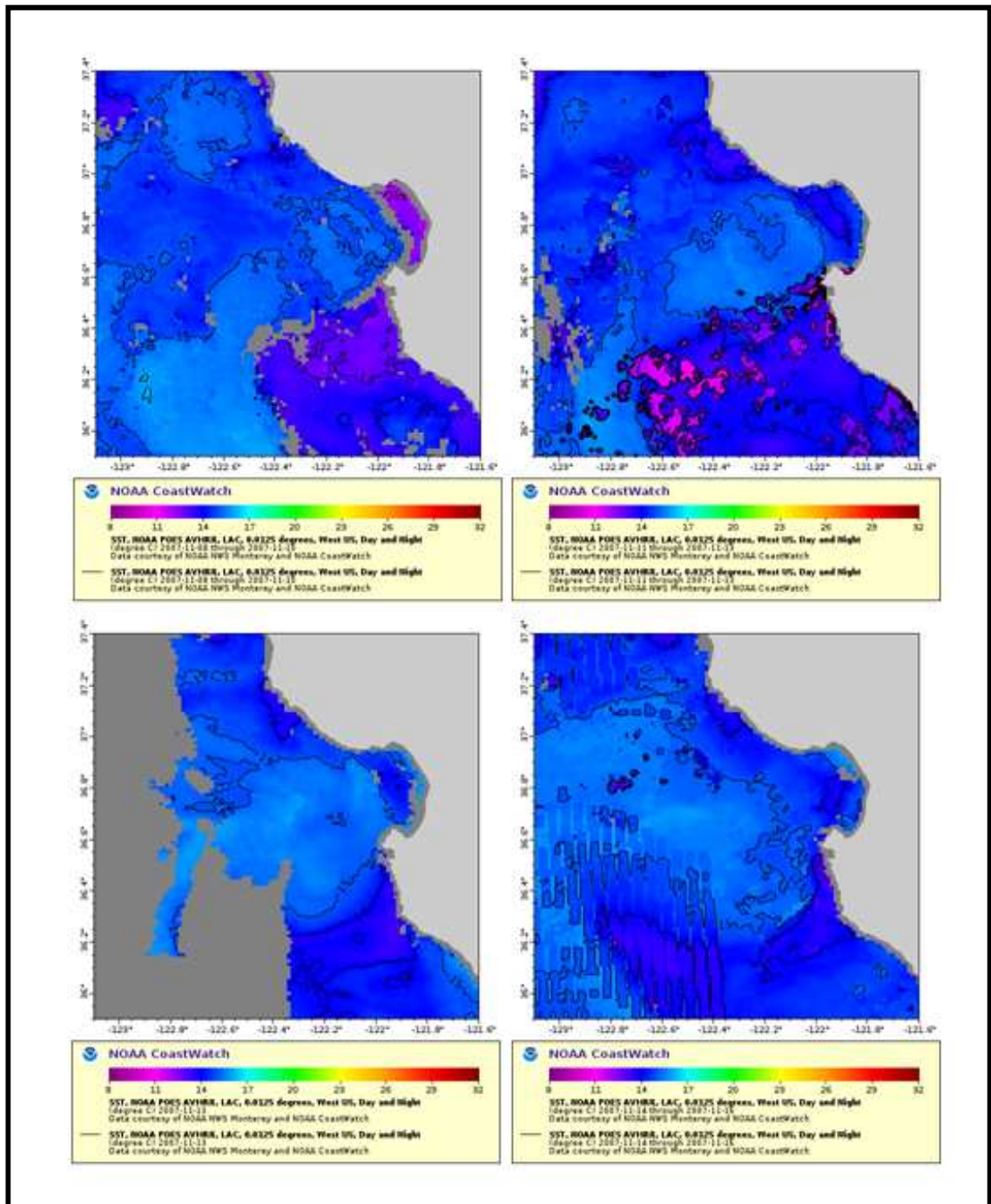


Figure 61: Monterey Bay SST during November 9th, 12th, 13th, and 15th 2007. Contour lines are 1°C temperature intervals.

4.1.5 Carmel Bay Upwelling

Carmel Bay has colder year-round temperatures than the nearby Monterey Bay and significantly colder temperatures during upwelling conditions (Figure 8). Why does Carmel Bay experience colder year-round temperatures than Monterey Bay? Upwelling conditions were frequently observed in Carmel Bay during spring and summer, and Stillwater Cove receives a larger annual nitrate contribution from the wind frequency band than all other mooring locations, except for Point Sur. Two primary areas of coastal upwelling are present in the greater Monterey Bay. One upwelling center is located at Point Año Nuevo (Rosenfeld *et al.*, 1994), north of Santa Cruz. A stronger upwelling center is located to the south of Point Sur (Traganza *et al.* 1981). Since the upwelling center at Point Año Nuevo has been shown to be a source of cold upwelled water in Monterey Bay, does Carmel Bay experience the same upwelling source? Or does the cold upwelled water observed in the Stillwater Cove time series come from a different source such as Point Sur? Rosenfeld *et al.*, (1994) suggested that upwelled surface waters enter the Monterey Bay principally from the north. Figure 62 shows temperature and wind time series from Carmel and Monterey Bay during upwelling and upwelling relaxation conditions during July 2006. Surface temperatures in Carmel Bay were 2°C colder on average than surface temperatures at the MBARI M1 mooring, and 3°C colder on average than the MBARI M2 mooring. Investigating SST during this upwelling period, we can see the clear distinction between the Point Año Nuevo and the Point Sur upwelling centers (Figure 63). A large water mass of 15°C upwelled water surrounds the region near Point Año Nuevo and extends offshore. Point Sur is surrounded by a smaller but

colder water mass of 14°C water. The 15°C isotherms do not connect at any point in the Monterey Bay, and a warmer water mass separates the upwelled water masses from the two upwelling centers.

Carmel Bay was clearly experiencing an influx of cold water upwelled water from the Point Sur upwelling source. Although this was a frequent occurrence during spring and summer conditions, there were time periods when upwelling conditions were so strong that the Point Año Nuevo and Point Sur upwelling sources connect into a single mass of cold water. Geographically, Carmel Bay is connected to and located on a side branch of the Monterey Canyon. We would expect some similarity in oceanographic conditions between Monterey and Carmel Bay due to this feature; however, Carmel Bay faces a different direction than the main orientation of Monterey Canyon. Carmel Bay is also separated from the Monterey Bay by Point Pinos, and is located in a protected environment. Although Monterey and Carmel Bay are located with close proximity to each other, they may experience completely different oceanographic dynamics and events. During summer conditions, both Monterey and Carmel Bay experience the same large scale upwelling and relaxation events. These upwelling events were correlated between the two locations, and the major difference was the colder temperatures experienced in Carmel Bay. There appears to be significant along-coast correlation of upwelling events between Point Año Nuevo and Point Sur; however, the temperature difference may be an issue of proximity to the upwelling source. Carmel Bay is located with ~ 28 km of the Point Sur upwelling center, while the M2 mooring is located ~ 45 km from Point Año Nuevo. Recently upwelled water moving northward from Point Sur

would have less time to heat by the time it reached Carmel Bay, and may be consistently colder than water upwelled from Point Año Nuevo.

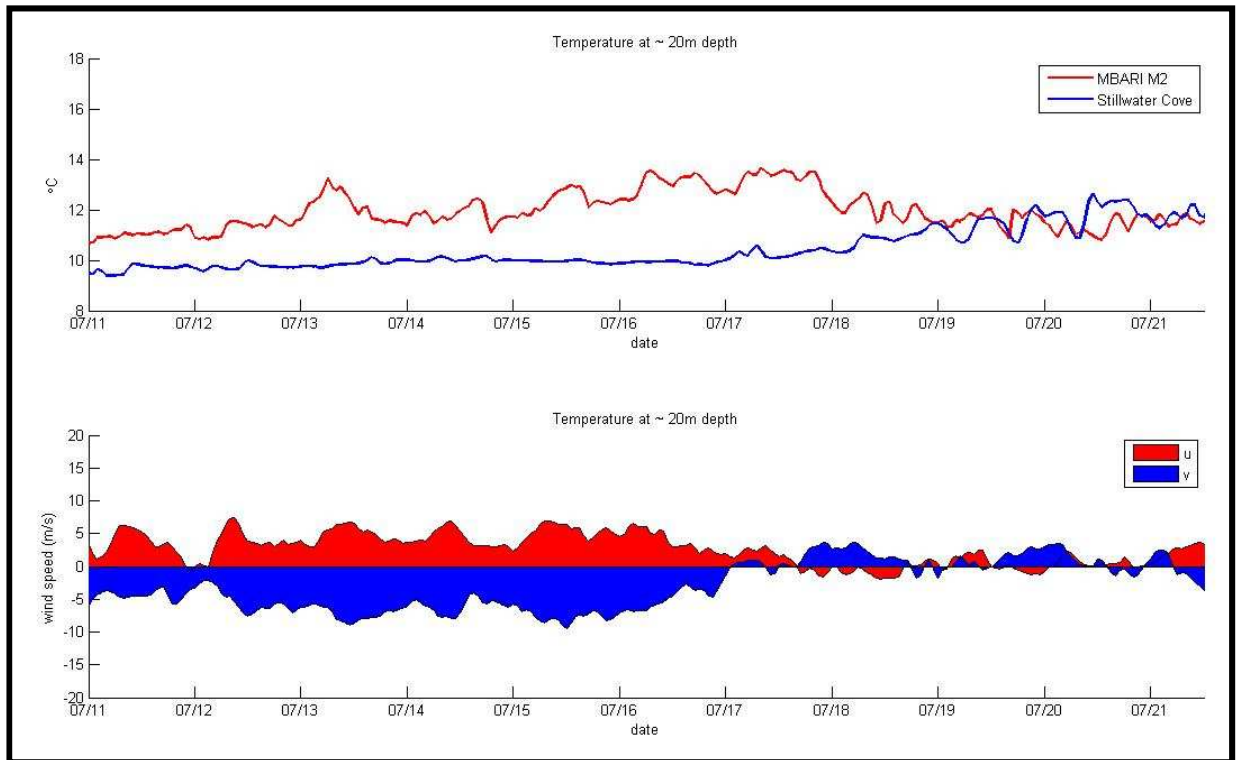


Figure 62: Carmel and Monterey Bay surface temperatures during upwelling and upwelling relaxation conditions during July 2006.

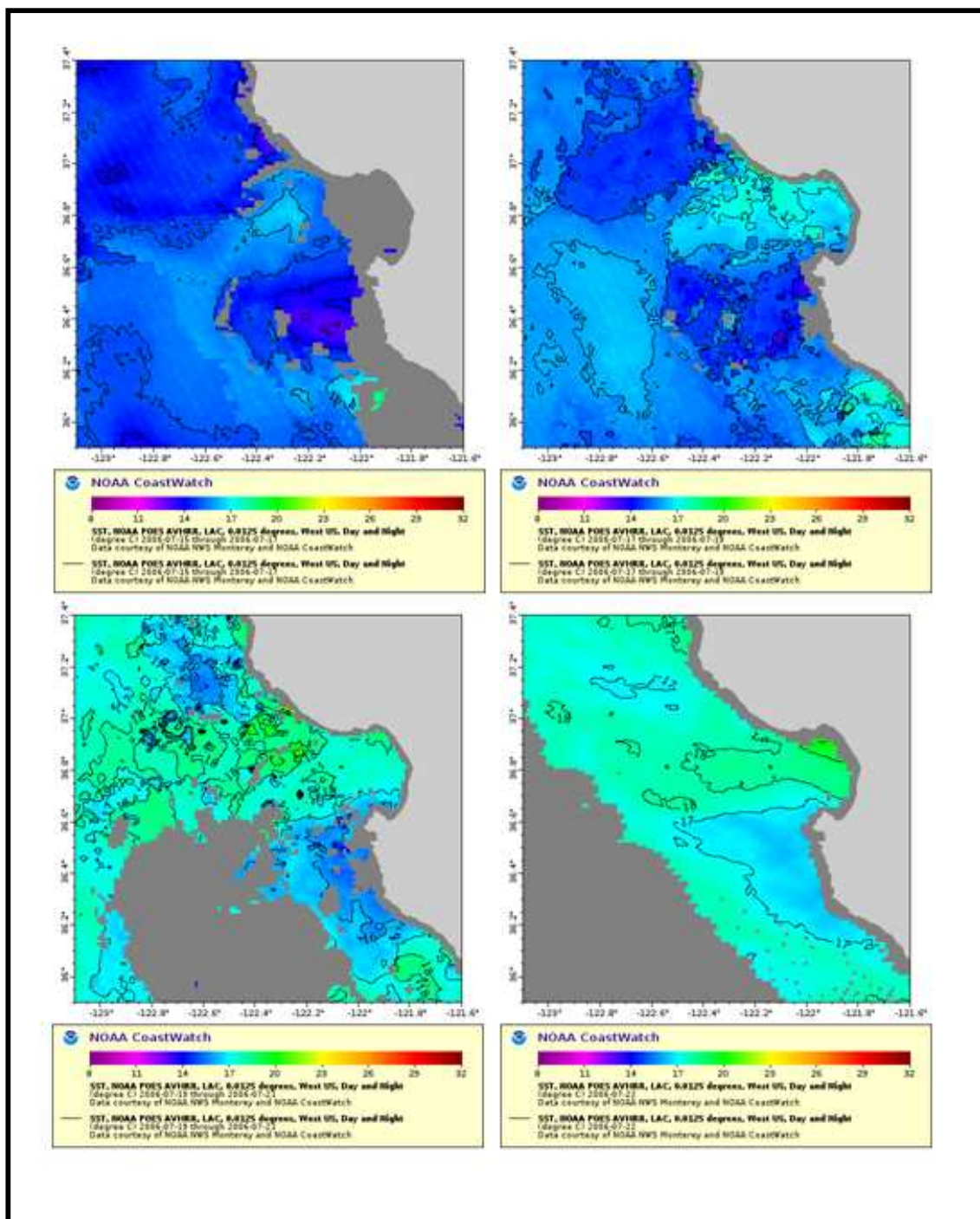


Figure 63: Monterey Bay SST during July 16th, 18th, 20th, and 22nd 2006. Contour lines are 1°C temperature intervals.

4.2 Internal Tide in Carmel Bay

Diurnal and semi-diurnal internal motions consistently flood the lower half of water column with cold nutrient-rich water at the 20-m deep mooring near the outer part of Stillwater Cove. While visible year-round in the Stillwater Cove time series, these baroclinic internal oscillations were coldest and reach the shallowest depths in the water column during stratified spring and summer conditions. During extremely stratified conditions, these internal motions increased the NO_3 concentration in the lower half of the near-shore water column by up to $5 \mu\text{M}$. These pulses of cold water were on average 2.5°C colder than the mean temperature of the water column, and 2 to 4 hours in duration. The deepest thermistor was located at 18-m depth and the bottom depth at the mooring is 20 m. It was unlikely that a 2.5°C temperature difference existed within the 2-m spatial scale between the 18-m thermistor and bottom depth, pointing to a non-local source for the cold water pulses. The question remains: what is the source of the cold water observed in the diurnal and semi-diurnal internal motions? Are the observed pulses of cold water due to horizontal advection of a water mass from nearby Carmel Bay or further offshore? Are they due to vertical advection of cold bottom water driven by internal tidal pumping from the Carmel Submarine Canyon?

4.2.1 Horizontal Advection

The three-dimensional advection the equation for a constituent C:

$$\mathbf{v} \cdot \nabla C = u \frac{\partial C}{\partial x} + v \frac{\partial C}{\partial y} + w \frac{\partial C}{\partial z} \quad (1)$$

To assess the likelihood of horizontal versus vertical advection addressed above, let us consider the two-dimensional case of horizontal advection of a cold water mass moving past the Stillwater Cove mooring due to tidal flow. We will assume there is no vertical motion in the water column, and that vertical velocities are zero.

Constricting motion to a horizontal plane with no vertical velocity, the advection equation becomes:

$$\mathbf{v} \cdot \nabla C = \mathbf{u} \frac{\partial C}{\partial x} + \mathbf{v} \frac{\partial C}{\partial y} + 0 \quad (2)$$

In the envisioned scenario, cold water from another region was being horizontally advected past the Stillwater Cove mooring during the rising diurnal and semi-diurnal tide. As the tide begins to fall, the cold water mass retreats back towards the source and observed temperatures at the mooring begin to increase. The assumed horizontal advection of the cold water mass from an outside source into Stillwater Cove would have to occur over a 12-hour and a 6-hour temporal scale, half of the duration of the diurnal and semi-diurnal tidal cycle. Using data from the Stillwater Cove ADCP, the mean diurnal tidal excursion distance during summer conditions was estimated to be ~ 1000 m. Wang *et al.* 2006 modeled the barotropic tide in Monterey Bay using the Regional Ocean Modeling System (ROMS). Using the mean major axis tidal velocities generated from their model, the estimated mean diurnal excursion distance for the Monterey Bay is 1308 m. This gives us confidence that our estimated diurnal tidal excursion distance for

Stillwater Cove is representative of conditions further offshore. If horizontal advection were the only physical process responsible for the observed pulses of cold water, we would expect a water mass at least 2.5°C colder to be located within the 100-m spatial scale of the daily tidal excursion from the mooring. Figure 64 shows surface temperatures in Carmel Bay from 08:00 PDT to 15:00 PDT during August 8th 2008. These surface temperatures were recorded with the portable UDAS system on the R/V Sheila B. This was the only available SST data from Carmel Bay, so we will assume this temperature field represents average summer conditions in the bay. We lacked sea surface temperature data for this region during summer conditions, as Carmel Bay experienced heavy summertime cloud cover. Satellite imagery of the region lacked substantial coverage during summer months. The maximum temperature difference from the northern to the southern end of Carmel Bay was only 1.8°C. Using the mean daily tidal excursion distance from Stillwater Cove, surface temperatures varied less than 1°C within a 1000-m spatial scale. Figure 65 displays an eight day composite of sea surface temperatures in Monterey Bay from the week of August 1st 2008. Contour lines are drawn at 1°C temperature intervals. An eight day composite of SST was used because it represented the mean temperature field in the Monterey Bay over the duration of at least one week. An eight day composite also averages the temperature field over ~ 16 tidal cycles. Looking at the region surrounding Carmel Bay, temperature differences on the order of one degree occurred on scales that are much larger than twice the entire length of Carmel Bay. The smallest spatial scale over which a one degree SST difference occurred was ~ 9 km. Since these internal cold pulses are observed at the semi-diurnal and diurnal

frequencies, the cold water mass would have to horizontally travel a distance greater than 9 km in 12 hours. This would require a horizontal velocity of ~ 21 cm/s for the entire 6 hour period, far above the mean velocities observed in Stillwater Cove currents. If a 2.5°C surface temperature difference was not present within the spatial scale of a diurnal excursion, we can assume that horizontal advection was not the primary physical process delivering cold water pulses to the near-shore ecosystem in Stillwater Cove.

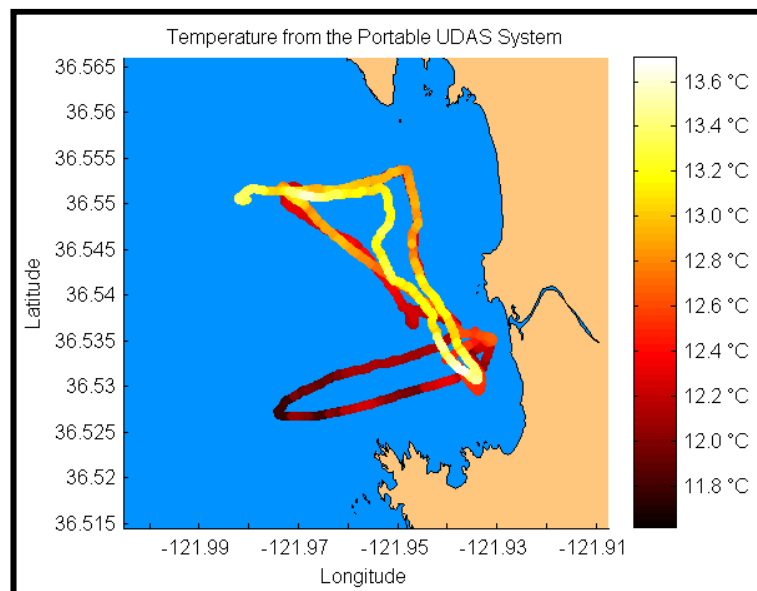


Figure 64: Carmel Bay SST from August 8th 2008.

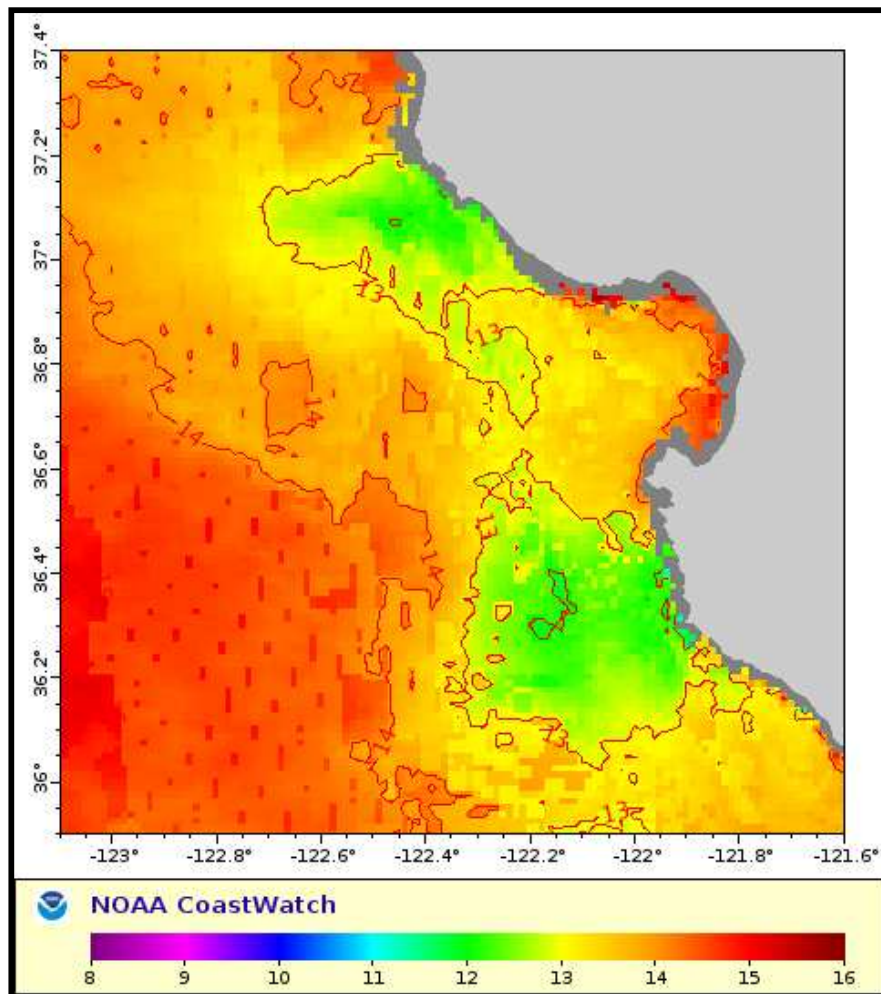


Figure 65: Eight day composite SST for the week of August 1st 2008.

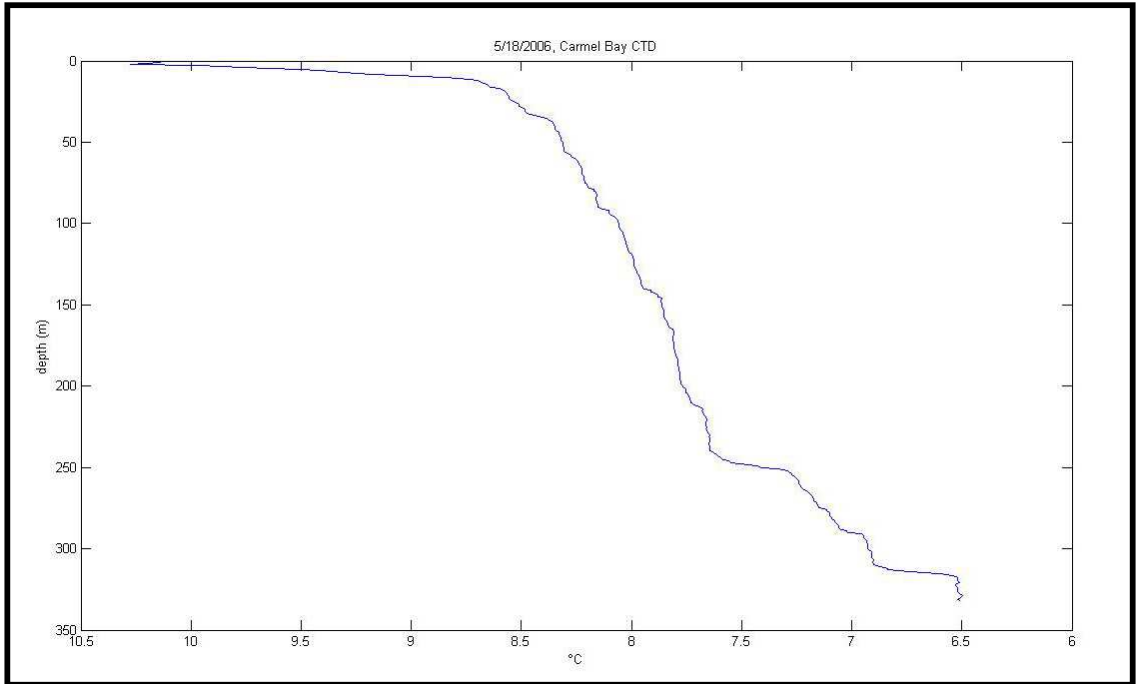


Figure 66: Carmel Canyon CTD, May 18th 2006.

4.2.2 Vertical Advection

Let us now examine the second suggestion; vertical advection of cold water from a deep source within a tidal cycle.

The advection equation restricted to the vertical component:

$$\mathbf{v} \cdot \nabla C = w \frac{\partial C}{\partial v} \quad (3)$$

The closest source of significantly colder water is the nearby Carmel Submarine Canyon.

During stratified conditions, temperature in Carmel Canyon decreases rapidly with depth.

A CTD cast conducted in Carmel Canyon during May 18th 2007 is shown in figure 66. From surface to 325-m depth, the maximum temperature difference was 3.75°C. A 2.5°C difference was present within a vertical scale of 175 m. As shown in Figure 21, the 9°C isotherm in Carmel Bay water column experienced a 60-m vertical excursion during four hours of the rising semi-diurnal tide. Since the strongest cold water pulses were observed during the peak diurnal high tide, we would expect even larger vertical excursions during the rising diurnal tide. We can calculate the vertical velocity component of the water column during the 4-hour measured vertical excursion shown in figure 21 as:

$$w = \frac{dz}{dt} \quad (4)$$

Where w is the vertical velocity component, dz is the vertical excursion distance, and dt is the time elapsed during the excursion. Therefore using the 60-m excursion distance of the 9°C isotherm over the course of 4 hours, $w = 15$ m/hr. Using this estimate of vertical velocity, could vertical advection cause a temperature difference on the order of 2.5 °C over the time scale of a diurnal tidal excursion?

Calculating the possible ΔT for the estimated value of w :

$$\frac{dT}{dt} = w \frac{dT}{dz} \quad (5)$$

$$dT = 15 \frac{m}{hr} \times \frac{2.5^\circ C}{175_m} \times 12 hrs = 2.7^\circ C \quad (6)$$

Over the time scale of a diurnal tidal excursion, vertical advection in Carmel Canyon would bring water that was 2.57°C colder to near-surface depths. This value was greater than the observed 2.5°C decrease in temperatures observed during the diurnal and semi-diurnal internal motions.

This showed that vertical advection forced by the internal tide in Carmel Canyon was a likely source for the cold water pulses observed in Stillwater Cove; however, we also need to consider whether the horizontal velocity component of this vertical excursion was strong enough to transport the cold bottom water from the offshore canyon into the near-shore environment. Using the estimated value for the vertical velocity component during the rising semi-diurnal tide, we can estimate the horizontal velocity component of the cold water lens that is moving up-canyon and into the near-shore environment in Carmel Bay. Two grid points were chosen to estimate an average bathymetric slope in Carmel Bay. These points were 36° 33' 3.6" N, -121° 57' 35.9" W and 36° 32' 9.6" N, -121° 58' 48" W. The first point is located near the CICORE mooring in Stillwater Cove and the second point is located in Carmel Canyon near the mouth of Carmel Bay. The difference in depth between these two points was 242 m, and the grid distance between them was 1733 m. These values give us a bathymetric slope of 0.14 radians, or 8°. The horizontal velocity component of the vertical excursion can be calculated as $h = w / \sin(0.14)$. This gives us a horizontal velocity component of $h = 108$ m/hr, which is 0.03 m/s. Figure 67 displays a schematic of the physical process. Compared to the very small

seasonal mean current velocities in Figures 13 – 15, the horizontal velocity component of $h = 3$ cm/s was only slightly greater than range of horizontal currents velocities observed at the Stillwater Cove mooring during the year. Over the time scale of a diurnal tidal excursion, this horizontal velocity component could transport cold water from 1296-m offshore and from 180-m depth into Stillwater Cove. In Carmel Bay, a temperature decrease of 2.5°C from the recorded surface temperature was reached at ~ 175-m depth (Fig 66). Bathymetry at this depth in Carmel Bay was located within 1500 m of the Stillwater Cove mooring, a slightly greater distance than our estimated diurnal horizontal up-canyon excursion. As a result, we have shown that the most reasonable source of cold water pulses observed in Stillwater Cove was located at depth in the nearby Carmel Canyon.

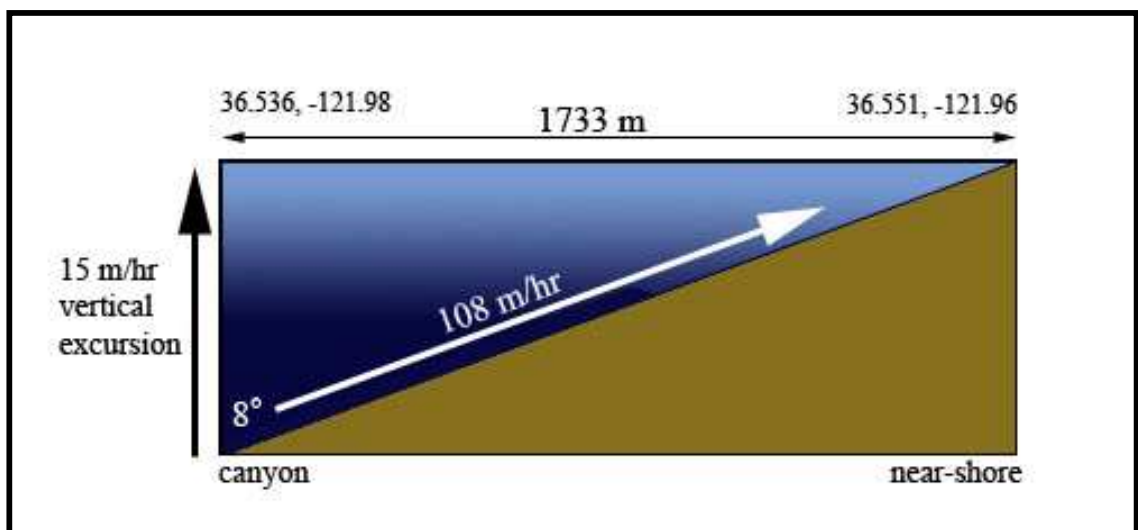


Figure 67: Horizontal velocity component during the rising semi-diurnal tide.

4.2.3 Spatial Variability of the Internal Tide in Monterey Bay

Carmel Canyon experienced internal tides that generated strong vertical excursions (15 m/hr) during the rising semi-diurnal tide. This dynamic appears to be the best candidate for delivering nutrient-rich bottom water from the Carmel Canyon to the near-shore ecosystem in Stillwater Cove. During stratified conditions, Stillwater Cove experienced internal waves during both the diurnal and semi-diurnal tidal cycle. The internal waves observed during the rising diurnal tide were much stronger and longer in duration than their semi-diurnal counterparts, and the diurnal internal tide in Carmel Canyon may generate vertical excursions that have even higher velocities than the estimated semi-diurnal vertical velocity of 15 m/hr. Do other locations in Monterey Bay / Central Coast experience this same dynamic, or is Carmel Bay unique? The head of the Monterey Canyon has been shown to have strong internal tides (Rosenfeld, 1999), but little is known about the strength of the internal tide at other locations in the bay. How does the diurnal and semi-diurnal internal tide at other locations in Monterey Bay compare to Carmel Bay in terms of strength and phase with the tide? Are there similarities between locations that are within close proximity to submarine canyons and locations far away on the shelf? I hypothesized that in the case of canyon overspill due to the internal tide, locations closest to deeper submarine canyon isobaths would experience the effects of stronger vertical excursions. Is the strength of the internal tide at locations within close proximity to submarine canyons simply a function of distance from deeper isobaths?

One of the primary goals of this project was to quantify the spatial variability of

the semi-diurnal internal tide across the along-coast Monterey Bay region, examining locations within close proximity to submarine canyons and on the outer shelf. This is important because locations that experience stronger internal tides will have an additional source of nutrients via internal waves during stratified conditions. Little variation in the surface semi-diurnal power was found across the spatial scale of the Monterey Bay; however, there was a high variation in the near bottom semi-diurnal power and a significant decrease in variance as you move away from proximity to a submarine canyon. Both Point Sur and Soquel Point have extremely low semi-diurnal bottom power. I interpreted this to be because the internal tidal strongly affects the near-shore temperatures at locations that are within close proximity to submarine canyons, while at locations on the shelf this mechanism was greatly reduced or completely absent. The MLML seawater system had the strongest semi-diurnal power bottom depth of all the mooring locations as it was located directly in the head of the Monterey Canyon. The MLML seawater system had eight times more semi-diurnal power at bottom depth than Stillwater Cove. Both canyon locations experienced year-round internal waves; however, the amplitude of these internal pulses was much higher at the head Monterey Canyon. In Carmel Bay, Weston Beach had the most semi-diurnal bottom power, while Stillwater Cove and Sunset Point had similar values.

There was an increase in surface diurnal power as you move towards the shelf, possibly due to the regions being more exposed the diurnal seabreeze. Interestingly, Point Sur was subject to strong diurnal sea breezes, yet weaker diurnal surface power was present there than Lovers' Point and Soquel Point. These two locations had the highest

surface diurnal power, while Stillwater Cove had the lowest surface diurnal power of all the moorings. This may be due to the wind sheltered environment of the Stillwater Cove, which protects the cove from the effects of the diurnal northwest seabreeze. Bottom diurnal power was strongest at Lovers' Point, with Stillwater Cove and Point Joe having significant power as well. Carmel Canyon was an unique location compared to the Monterey Canyon, as both the diurnal and semi-diurnal cold water pulses observed in Stillwater Cove were approximately 180° out of phase with the tide (Figure 68). The two other mooring locations in Carmel Bay do not follow this same pattern. Weston Beach was $\sim 100^\circ$ out of phase with the diurnal tide, and Sunset Point was $\sim 50^\circ$ out of phase with the diurnal tide (Figure 68). Stillwater Cove experienced cold water pulses on both the rising semi-diurnal and diurnal tide, whereas the MLML seawater system at the head of the Monterey Canyon experienced cold water pulses on the rising semi-diurnal tide and the falling diurnal tide. All locations within close proximity to a submarine canyons experience internal waves that were $\sim 180^\circ$ out of phase with the semi-diurnal tide. The time lag for all mooring locations is shown in Figures 71 and 72. Variability in the bottom semi-diurnal power was also present on smaller spatial scales at locations within close proximity to a submarine canyon. In Carmel Bay, Weston Beach had higher bottom semi-diurnal power than both Stillwater Cove and Sunset Point. Figure 73 displays the distance from the moorings to the 500-m isobath. In Carmel Bay, Sunset Point was the closest mooring to the 500-m isobath, while Stillwater Cove and Weston Beach were almost equidistant. The distance from the seawater system to the 500-m isobath was further than all Carmel Bay moorings.

Semi-diurnal power appeared to be strongest at locations within close proximity to submarine canyons. This indicates the presence of a strong semi-diurnal internal tide in the Monterey and Carmel Canyons, which may be a mechanism for near-shore nutrient delivery via introduction of cold bottom water. The head of the Monterey Canyon had the highest power of all the mooring locations, with eight times as much power as Stillwater Cove. At all canyon locations, the observed internal waves were phase locked at $\pm 180^\circ$ out of phase with the semi-diurnal tidal signal. At locations on the shelf, semi-diurnal power was extremely small and the surface diurnal signal dominated. The internal tide at these locations was very weak, and internal waves were minimal or completely absent. The distance to 500-m isobath does not appear to be correlated with bottom semi-diurnal power. The Monterey Canyon head had eight times as much power as Stillwater Cove; however, the distance from the seawater system to the 500-m isobath was 2 km further than Stillwater Cove.

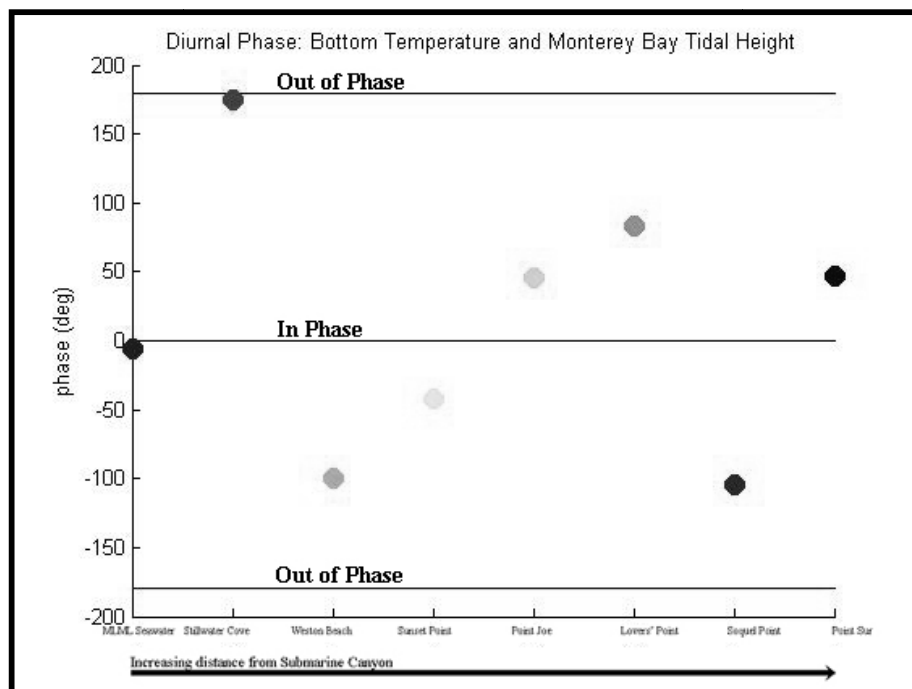


Figure 68: Diurnal phase between bottom temperature and Monterey Bay tide.

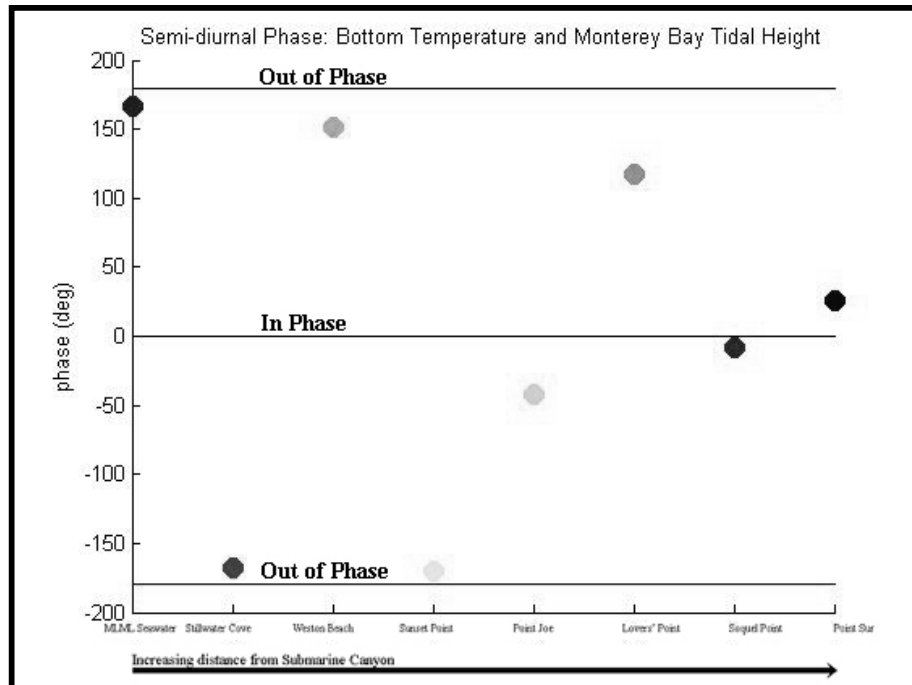


Figure 69: Semi-diurnal phase between bottom temperature and Monterey Bay tide.

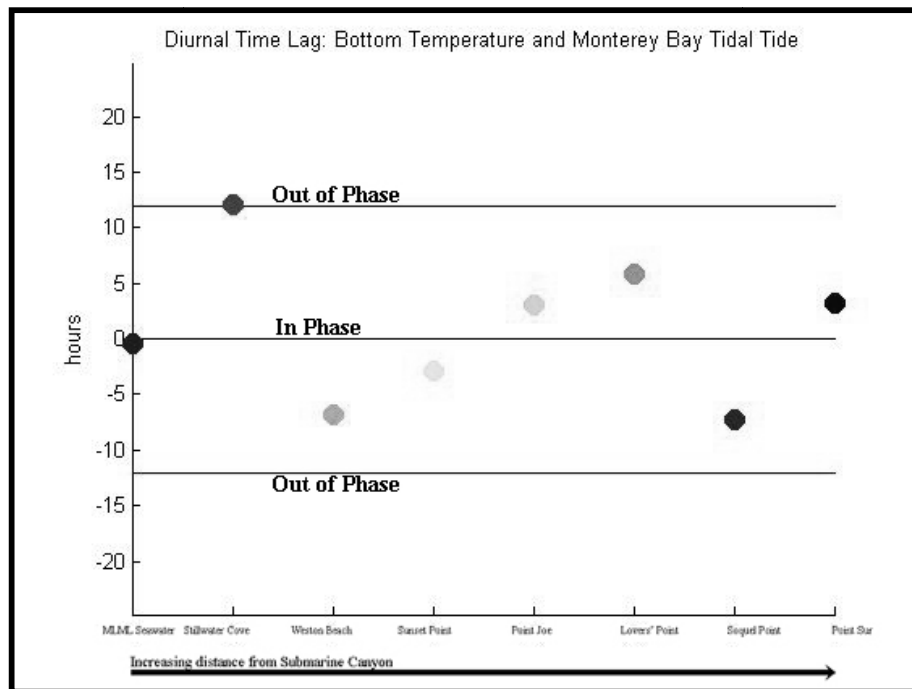


Figure 70: Diurnal time lag between bottom temperature and Monterey Bay tidal height.

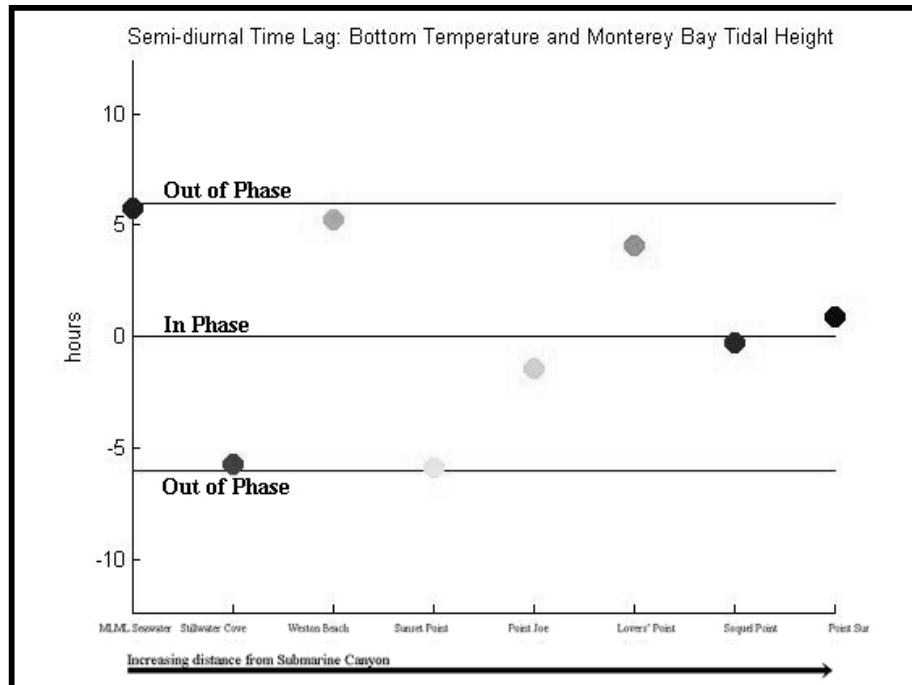


Figure 71: Semi-diurnal time lag between bottom temperature and Monterey Bay tide.

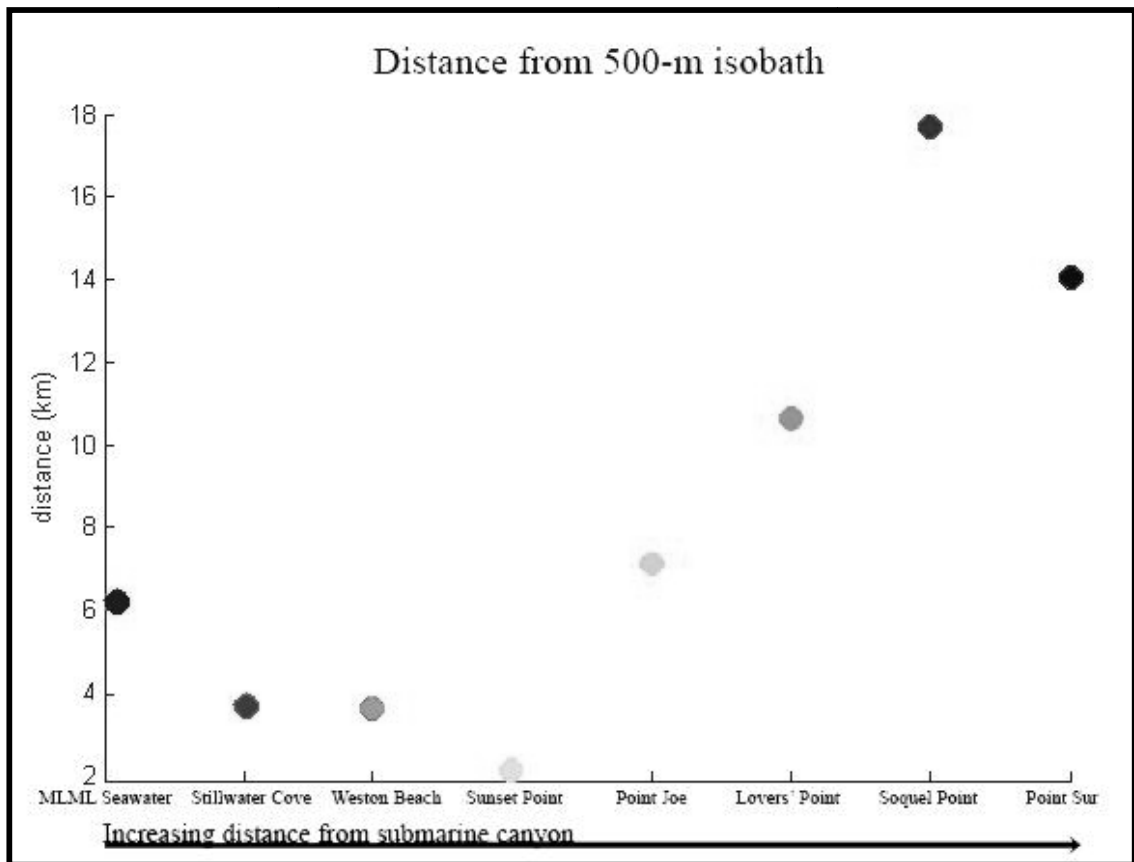


Figure 72: Mooring distance from the 500-m isobath.

4.3 Tidal flushing and stagnation in Stillwater Cove

The *M. pyrifera* population inside of Stillwater Cove exhibits unique temporal dynamics compared to the nearby Carmel Bay (Donnellan, 2004). Donnellan (2004) found that over the course of five years, the Stillwater Cove *M. pyrifera* canopy declined 2 to 3 months before canopies at Sunset Point and Carmel Point. This diminishment in the kelp canopy at Stillwater Cove began during August, while canopies in outer Carmel Bay declined during November and December. A long residence time for nutrients in Stillwater Cove might facilitate nutrient depletion by the cove's ecosystem. Stillwater Cove also experienced substantial nitrate delivery from internal waves during stratified summer conditions. The concerning issue may be that the Stillwater Cove ecosystem was overloaded with nutrients or terrestrial pollutants that are subsequently trapped by the cove's slow circulation and semi-enclosed basin. If Stillwater Cove was experiencing strong tidal currents outside the cove, is water from the inside of the cove being advected outward into Carmel Bay? What are the seasonal tidal and sub-tidal diurnal excursion distances? Is Stillwater Cove continually tidally flushed, or are there period of time when it may become stagnant? We will investigate tidal currents and develop a box model to assess this question. We know from the ADCP time series that tidal currents dominated over sub-tidal currents in terms of magnitude, and for the purposes of our model we will assume that tidal currents were the primary flushing mechanism for the cove. The seasonal *M. pyrifera* canopy inside the cove may also significantly dampen the currents and increase the residence time. Previous studies have shown that the drag in a kelp bed can be a factor of 10 times greater than that of a non-kelp area (Jackson and Winant,

1983; Jackson, 1997). Pescadero Rock may divide the cove into two cells, separating cross-circulation of the cove in the center. If currents outside the cove are weak, Stillwater Cove may function as an enclosed environment and would not be tidally flushed.

To estimate if there could be possible stagnation and subsequent nutrient overloading in Stillwater Cove, we used a simple two dimensional box model. The length of the mouth of Stillwater Cove (L_{cove}) is approximately 1000 m. The width of Stillwater Cove (W_{cove}) is approximately 500 m. Using a two dimensional box, the estimated entire surface area of the Stillwater Cove region was 500,000 m². We chose to use a smaller area for our model, focusing on the region of the cove constrained by Arrowhead Point. The size of this box is 950 m by 300 m, with a total surface area of 285,000 m². Arrowhead Point extends ~ 400 m outward from the beach in Stillwater Cove, and would block any horizontal circulation into or out of the cove. This box would consist of 285,000 individual 1 m² square water parcels, and we will assume that tidal currents are drawing water parcels out of the cove during half of the diurnal tidal cycle. We can visualize this process as the tidal currents removing an individual square water parcel from our box during each time interval. We will then assess whether the area exchanged by the tidal currents was a significant fraction of the total area (no stagnation), or a small portion (possible stagnation). If the tidal excursion distance was less than or equal to the length of the cove, no square water parcels would be “pulled” out of the cove by tidal currents (Fig 73). This would mean that no exchange between Stillwater Cove and Carmel Bay would occur and stagnation was likely.

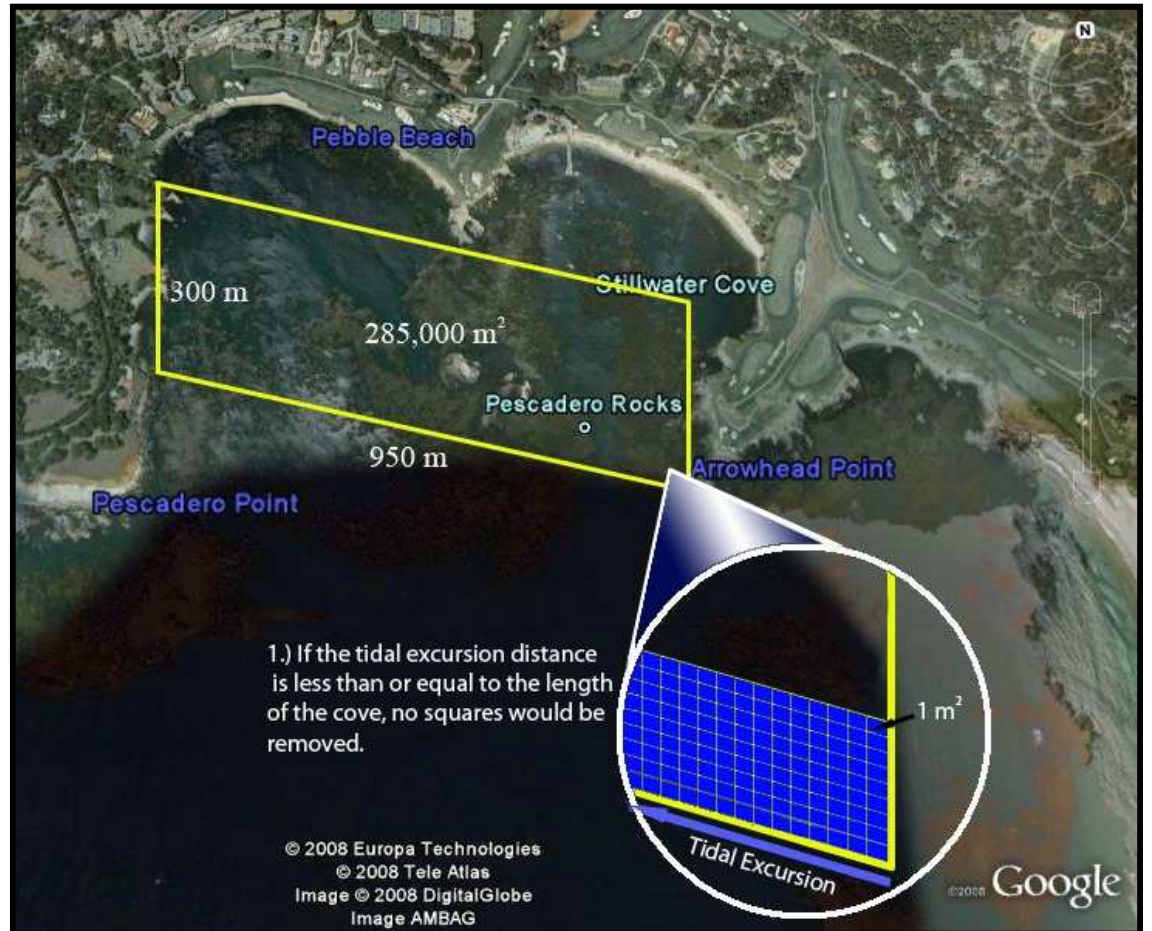


Figure 73: Stagnation scenario: tidal excursion distance is less than the length of the cove. No squares are removed from the box.

If the tidal excursion is longer than the length of the cove, tidal currents would remove square water parcels from the box (Fig 74). If a significant amount of square water parcels are removed from the box, the replacement of the removed squares due to conservation of mass may create significant circulation in the cove.

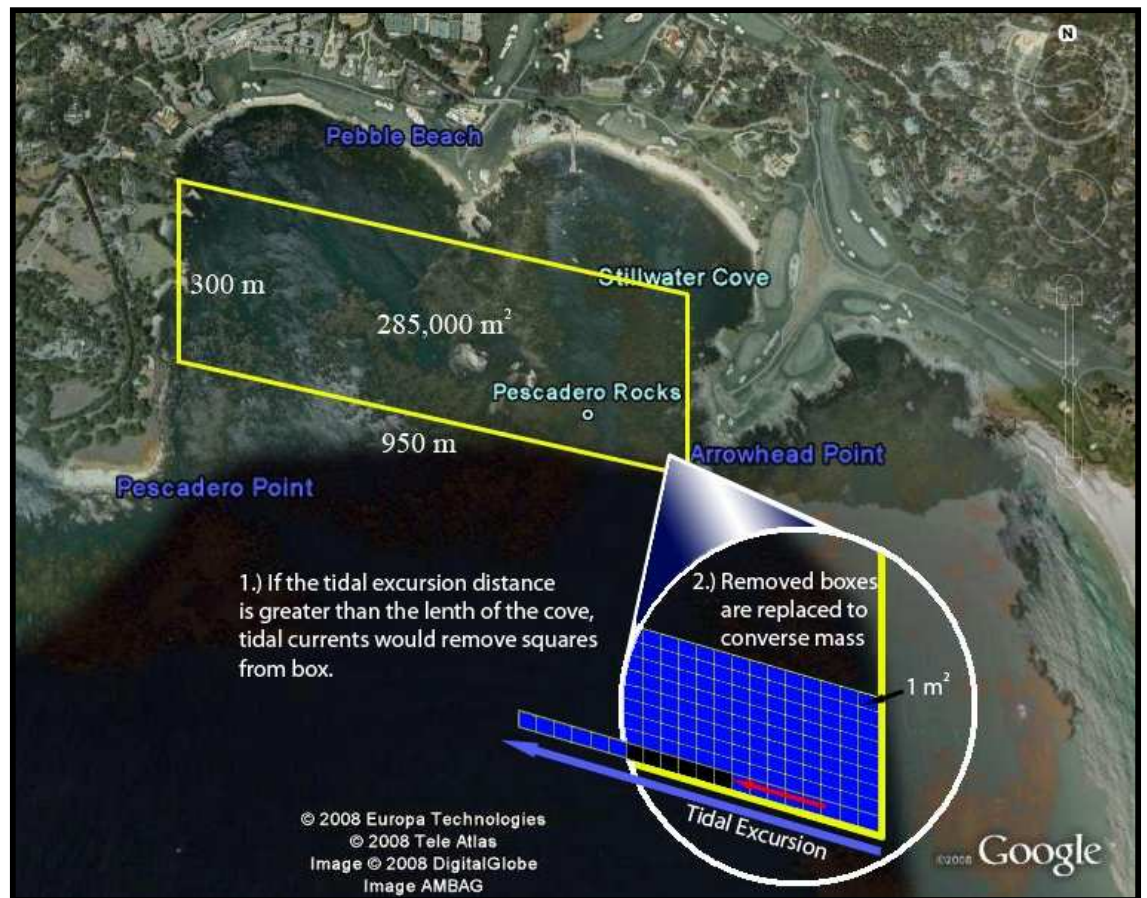


Figure 74: Non-stagnation scenario: tidal excursion distance is greater than the length of the cove. Squares are removed from the box.

If this process removes at least 50% of the box's square water parcels in 12 hours, we will assume that there would be significant mixing and that water inside the cove was not stagnant. This would imply a short residence time for nutrients circulating inside the cove, and significant tidal flushing of the cove's environment.

To estimate mean seasonal tidal velocities and excursion distances, currents were then averaged from near-surface to bottom depths, and a seasonal daily path length for the entire water column was calculated. The tidal daily path length for the entire water

column during summer was 1880 m, winter was 3241 m, and spring was 3300 m.

Dividing these path lengths in half provides us with an estimate of the tidal excursion distance over a diurnal period. The daily tidal excursion distances were: 940 m during summer, 1620 m for winter, and 1650 m for spring (Figure 75). The daily sub-tidal excursion distances were: 628 m during summer, 1152 m during winter, and 823 m during spring (Figure 76).



Figure 75: Stillwater Cove seasonal tidal excursion distances.



Figure 76: Stillwater Cove seasonal tidal excursion distances.

The mean seasonal diurnal tidal velocities are:

$$U_{summer} = 0.0217 \frac{m}{s} \quad (8)$$

$$U_{winter} = 0.0375 \frac{m}{s} \quad (9)$$

$$U_{spring} = 0.0382 \frac{m}{s} \quad (10)$$

Over half of a diurnal tidal excursion, tidal currents would remove:

$$\text{Mean seasonal tidal velocity} \times (1 \text{ m}^2) \times 43200 \text{ s} \quad (11)$$

$$U_{\text{summer removed}} = 0.0217 \frac{\text{m}^2}{\text{s}} \times 43200 \text{ s} = 937 \text{ m}^2 \quad (12)$$

$$U_{\text{winter removed}} = 0.0375 \frac{\text{m}^2}{\text{s}} \times 43200 \text{ s} = 1620 \text{ m}^2 \quad (13)$$

$$U_{\text{spring removed}} = 0.0382 \frac{\text{m}^2}{\text{s}} \times 43200 \text{ s} = 1650 \text{ m}^2 \quad (14)$$

These values were extremely small, with spring conditions having the largest removal of water parcels from our two dimensional box. During summer conditions, the tidal excursion distance was less than the length of the box and no exchange of water between Stillwater Cove and Carmel Bay would occur. Using the estimate for removal of square water parcels by spring tidal currents, only 0.0057% of the individual 1 m^2 water parcels would be removed from the box over a diurnal tidal excursion. To remove 50% of the box area and induce significant mixing in the cove, mean tidal currents would have to be 3.3 m/s over the entire tidal excursion. This value was far above any observed values from our Stillwater Cove ADCP time series. According to our model, this implied that stagnation was likely year-round in Stillwater Cove, and tidal currents would not be strong enough to cause significant exchange between the cove and Carmel Bay. The sub-

tidal excursion distances were even smaller than their tidal counterparts, and both spring and summer have excursion distances that are less than the length of the cove. If tidal currents were consistently 10 cm/s during the entire diurnal tidal cycle, it would take ~ 16 days to replace half the squares in the box and induce significant mixing in the cove. Figure 77 shows an estimate of the elapsed time before significant mixing would occur using a range of tidal current velocities.

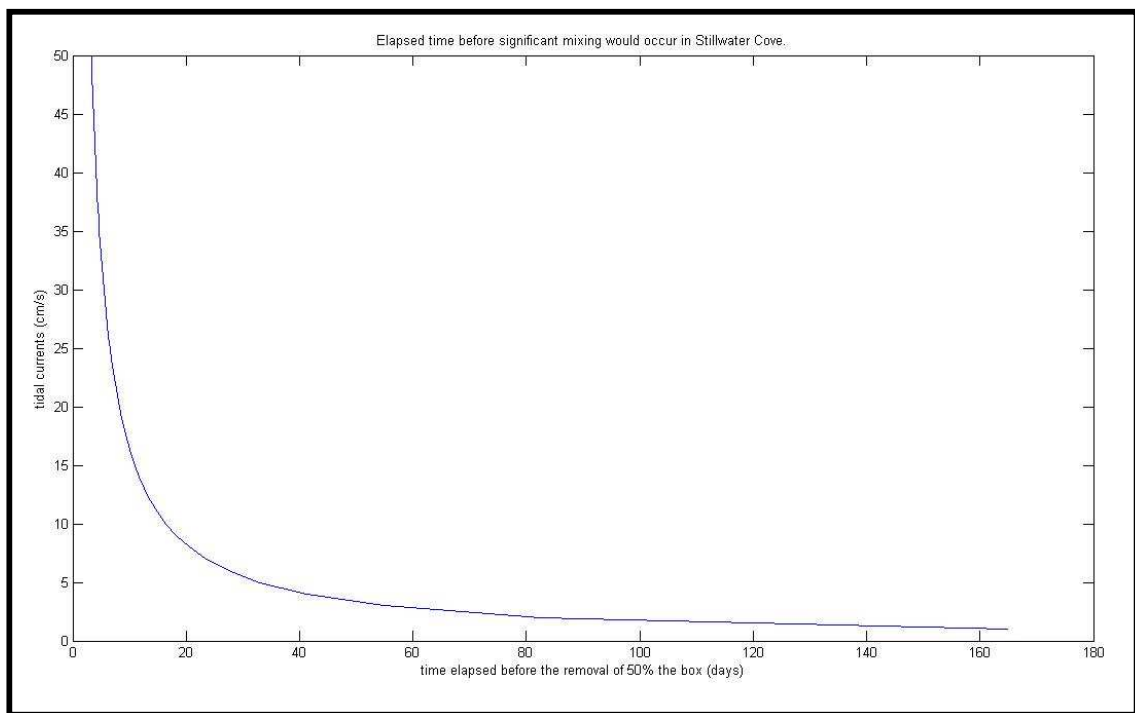


Figure 77: Elapsed time before significant mixing would occur.

Nutrients would be trapped by the cove's slow circulation and long residence time, and nutrient or pollutant overloading may be a significant concern for the near-shore ecosystem. Little exchange would occur between Carmel Bay and Stillwater Cove, and

the two may function as separate environments.

4.4 Implications for Cross-Shelf Nutrient Transport in Monterey Bay

The results of this project have important implications for understanding nutrient delivery via internal waves to near-shore regions. An underlying motivation for this project was to identify and describe the physical oceanographic processes that may deliver nutrients to near-shore ecosystems, specifically the *Macrocystis pyrifera* kelp population located in Carmel Bay. Knowledge of the physical processes surrounding the kelp ecosystem is essential in order to accurately describe nutrient delivery, spore dispersal, and overall kelp population dynamics. The transport of nutrients to shallow areas (< 20 m) is essential for the health of *M. pyrifera* (Jackson, 1977). The Monterey Bay National Marine Sanctuary contains many diverse ecosystems and habitats in regions that span from vast submarine canyons to the wide outer shelf. The estimated NO_3 contributions during summer conditions from the semi-diurnal and diurnal frequency bands mirror the plots of power spectral density. This shows that the developed nutrient model accurately represents the physical process. This model provides insight into the spatial variability of nutrient delivery via the internal tide across the greater Monterey Bay. Point Sur and Stillwater Cove have the highest percentage contributions from the wind frequency band, while Lovers' Point has the highest percentage contribution from the diurnal tidal band. Stillwater Cove is located farther inside the wind sheltered Carmel Bay than Weston Beach and Sunset Point, however; Stillwater Cove receives more NO_3 from the wind band than the two other locations. The Monterey Canyon head has the

highest percentage contribution from the semi-diurnal tidal band with Weston Beach in Carmel Bay having the second highest. Soquel Point received the least total NO_3 of all the mooring locations due to the lack of both internal waves and upwelling. Examining the total estimated NO_3 budget from all frequency bands during summer conditions, the MLML seawater system at the head of the Monterey Canyon received the largest total NO_3 contribution (Figure 69). This location received a small contribution from the wind band compared to other locations; however, the amplitude of internal waves at the head of the Monterey Canyon was extremely high. During stratified summer conditions, semi-diurnal internal waves increased NO_3 concentrations by up to $12 \mu\text{M}$ for periods of 8 hours. Diurnal internal waves increased NO_3 concentrations by up to $5 \mu\text{M}$ for periods of 6-7 hours. These internal waves were observed at the diurnal and semi-diurnal periods and harmonics during the entire summer time series. The consistent presence of these internal waves provided a massive amount of NO_3 to the head of the Monterey Canyon during summer conditions. The seawater system received almost twice as much total NO_3 as Point Sur. At the seawater system, the wind band contributed only 16% of the total NO_3 , while the tidal band at Point Sur contributed 15.5%. These locations represented the two extremes in terms of wind band versus tidal band contributions. This is an important result as it shows that the seasonal NO_3 contribution from internal waves in a submarine canyon can easily exceed the NO_3 contribution at an upwelling center. In Carmel Bay, the wind frequency band was the dominant mechanism for delivering NO_3 to the near-shore environment. In Stillwater Cove, internal waves contributed 36% of the total NO_3 , while upwelling contributed 64%. Nutrient delivery via upwelling plays a much larger role in

Carmel Bay than at the head of the Monterey Canyon. The head of the Monterey Canyon is located ~ 60 km from the upwelling center at Point Año Nuevo, while Stillwater Cove is only ~ 25 km from Point Sur. While internal waves were a significant contributor of NO_3 in Carmel Bay, the amplitude of the internal pulses was much smaller than their Monterey Canyon counterparts. Internal waves in Carmel Bay during stratified summer conditions increased NO_3 concentrations by up to 5 μM , half of the concentration increase observed at the seawater system. While Carmel Bay was within close proximity to a submarine canyon, the branch of the Carmel Canyon was far smaller and shallower than the Monterey Canyon. Vertical velocities at the head of the Monterey Canyon have been documented at 30 m/hr (McPhee-Shaw, 2004), twice the vertical excursion velocity observed in Carmel Canyon. Using the results from this project, we can show that near-shore ecosystems in the greater Monterey Bay that lie within close proximity to submarine canyons have an additional source of nutrients via internal waves. Figure 78 shows an interpolated map of the total nutrient budget across the Monterey Bay during summer conditions. In these regions, the semi-diurnal internal tide is greatly amplified and provides a consistent source of nutrient-rich cold bottom water. The importance of this dynamic has serious implication for cross-shelf nutrient transport, as internal waves in the head of the Monterey Canyon are a larger annual NO_3 contributor than upwelling at Point Sur. During periods of upwelling relaxation and decreased NO_3 levels in the water column, internal waves may sustain the near-shore ecosystem with essential nutrients. At locations where the shelf width increases greatly, far away from any major submarine canyon branches, this mechanism diminishes almost completely. Therefore, in

near-shore regions located within close proximity to submarine canyons, the bottom depths of the water column are continually being bathed with nutrient rich water during the rising semi-diurnal tide during stratified conditions. Kelp forests located in these near-shore regions would have a direct source of nitrate via this mechanism. Regions located further out the shelf, away from any major submarine canyons, would not have this delivery mechanism and their respective ecosystems may have to rely solely on upwelling as a dominant nutrient source.

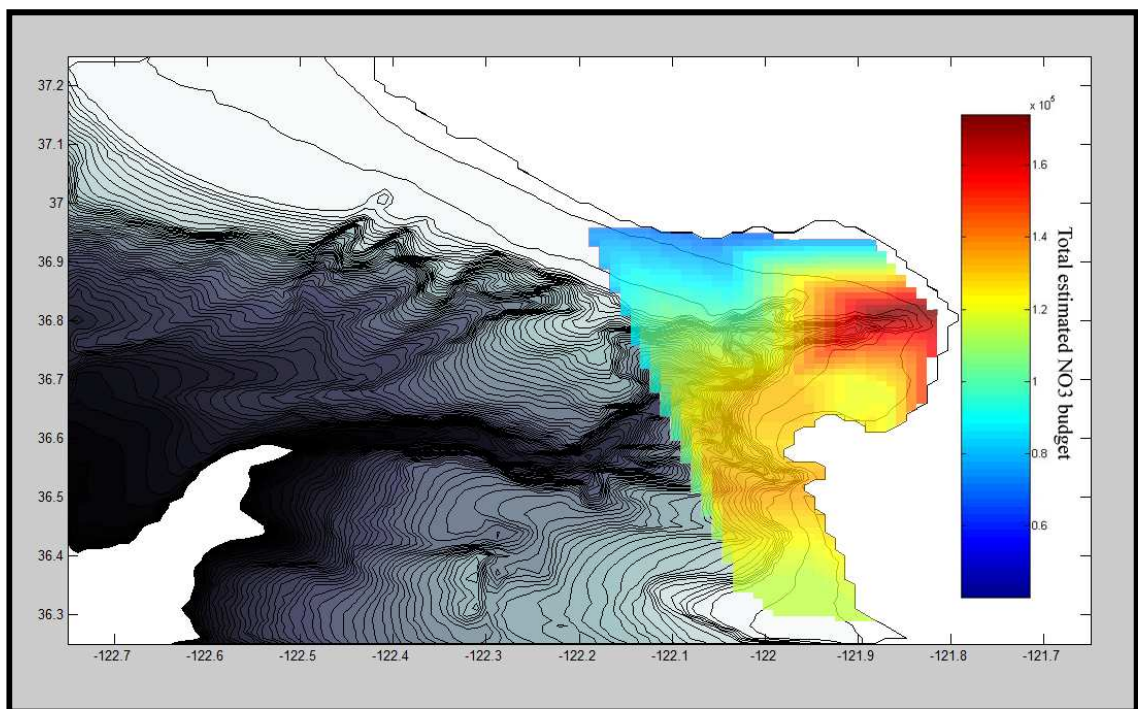


Figure 78: Spatially interpolated estimated NO₃ budget for the greater Monterey Bay.

6. REFERENCES

- Bassin, C., L. Washburn, M. Brzezinski, and E. McPhee-Shaw. 2005. Sub-mesoscale coastal eddies observed by high-frequency radar: A new mechanism for delivering nutrients to kelp forests in the Southern California Bight. *Geophysical Research Letters* 32: L12604, doi:10.1029/2005GL023017.
- Breaker, L.C., Broenkow, W.W., 1989. The circulation of Monterey Bay and related processes. Technical Publication 89-1, Moss Landing Marine Laboratories, California, p. 91.
- Broenkow, W.W and S. McKain. 1972. Tidal oscillations at the head of Monterey Submarine Canyon and their relation to oceanographic sampling and circulation of water in Monterey Bay. Moss Landing Marine Laboratories Technical Publication 72-5. 42 pp.
- Brown, J. 2001. A Review of Marine Zones in the Monterey Bay National Marine Sanctuary. Marine Sanctuaries Conservation Series MSD-01-2. U.S. Department of Commerce, National Oceanic and Atmospheric Administration, Marine Sanctuaries Division, Silver Spring, MD.
- Carter, G.S., M.C Gregg and R. Lien. 2004. Internal waves, solitary-like waves, and mixing on the Monterey Bay shelf. *Continental Shelf Research* 25: 1499-1520.
- Cazenave, F. 2008. Internal waves over the continental shelf in south Monterey Bay. Masters thesis. Moss Landing Marine Laboratories.
- Dayton, P. K. 1985. Ecology of kelp communities. *Annual Review of Ecology and Systematics* 16: 215-245.
- Donnellan, M. 2004. Spatial and temporal variability of kelp forest canopies in Central California. Masters Thesis. Moss Landing Marine Laboratories.
- Foster, M. 1982. The regulation of macroalgal associations in kelp forests. *Synthetic and Degradative Processes in Marine Macrophytes*. 185-205.
- Fram J.P., Stewart H.L., Brzezinski M.A., Gaylord B., Reed D.C., Williams S.L., MacIntyre S. 2008. Physical pathways and utilization of nitrate supply to the giant kelp, *Macrocystis pyrifera*. *Limnology and Oceanography*, 53 (4), pp. 1589-1603.
- Graham, W.M. and J.L. Largier, 1997. Upwelling shadows as nearshore retention sites: the example of northern Monterey Bay. *Continental Shelf Research* 17, 509-532.
- Heal the Bay, 2004. Monterey County Grades. Annual beach report card.

- Heard, J. A. 1992. A kinematic model of baroclinic tidal currents at the head of Monterey Submarine Canyon. M.S. thesis, Moss Landing Marine Laboratories. 59 pp.
- Hosegood, P. and H. van Haren, 2004. Near-bed solibores over the continental slope in the Faeroe-Shetland Channel. *Deep-Sea Research, II*, 51, 2943-2971.
- Kunze, E., L. K. Rosenfeld., G. S. Carter and M. C. Gregg. 2001. Internal waves in Monterey submarine canyon. *Journal of Physical Oceanography* 32: 1890-1913.
- Jachec, S. M., O.B Fringer., M. G. Gerritsen and R. L. Street. 2006. Numerical simulation of internal tides and the resulting energetics within Monterey Bay and the surrounding area. *Geophysical Research Letters* 33: L12605.
- Jackson, G. A. 1977. Nutrients and production of giant kelp, *Macrosystis pyrifera* , off Southern California. *Limnology and Oceanography* 22: 979-995.
- McPhee-Shaw, E.E., D.A. Siegel, L. Washburn , M.A. Brzezinski, J.L. Jones, A. Leydecker and J.M. Melack. 2007. Mechanisms for nutrient delivery to the inner shelf: Observations from the Santa Barbara Channel. *Limnology and Oceanography*, in press.
- Pebble Beach Company. 2004. DFM / PDP Draft environmental impact report.
- Parrett, C. and K.D. Cartier. 1990. Methods for estimating monthly streamflow characteristics at ungaged sites in western Montana. U.S. Geological Survey Water-Supply Paper 2365, 30p.
- Petruncio, E.T., L.K. Rosenfeld, and J.D. Paduan. 1998. Observations of the Internal Tide in Monterey Canyon. *Journal of Physical Oceanography* 28: 1873–1903.
- Rosenfeld, L.K., J.D. Paduan, E.T. Petruncio, and J.E. Goncalves, 1999. Numerical simulations and observations of the internal tide in a submarine canyon. *Proceedings, 'Aha Huliko'a Hawaiian Winter Workshop*, University of Hawaii at Manoa, January 19-22.
- Sassoubre, L. 2006. Chemical oceanography class project data. Moss Landing Marine Laboratories.
- Seymour, R.J., M.J. Tegner., P.K. Dayton and P.E. Parnell. 1998. Storm wave induced mortality of giant kelp, *Macrocystis pyrifera*, in Southern California. *Estuarine, Coastal, and Shelf Science* 28: 277-292.
- Shea, R.E. and W.W Broenkow. 1981. The role of internal tides in the nutrient

enrichment of Monterey Bay, California. *Estuarine, Coastal, and Shelf Science* 15: 57-66.

Storlazzi C.D., McManus M.A., Figurski J.D. 2003. Long-term, high-frequency current and temperature measurements along central California: insights into upwelling/relaxation and internal waves on the inner shelf. *Continental Shelf Research*, 23 (9), pp. 901-918.

Strickland, J.D.H., Parsons, T.R., 1972. A Practical Handbook of Seawater Analysis. Fisheries Research Board of Canada, Ottawa.

Wheeler P.A., and W. J. North. 1980. Effect of nitrogen supply on nitrogen content and growth rates of juvenile *Macrocystis pyrifera* (Phaeophyta) sporophytes. *Journal of Phycology* 16: 577-582.

Zimmerman, R and J.N Kramer. 1984. Episodic nutrient supply to a kelp forest ecosystem in Southern California. *Journal of Marine Research* 42: 591-604.